4.5 "Model Studies of LNG Vapor Cloud Dispersion with Water Spray Curtains," Meroney et al., 1983, 1984, and Heskestad et al., 1985

Experiment Configuration:

A series of model tests were funded by Factory Mutual Research, Inc. and the Gas Research Institute to evaluate the ability of water spray curtains to reduce concentrations around an LNG spill below flammability limits. Water sprays are not expected to remove natural gas from LNG spill clouds. The objective of the water spray is to entrain air and dilute the cloud below the flammability limit. Thus, these experiments do not simulate the potential for HF reduction due to water-spray induced deposition. Since the desire was to determine concentration reductions immediately downwind of the spray curtain measurements were only made out to equivalent distances of 390 m from the release point. One series of measurements were also made to validate the simulation methodology using field data from the CO2/water spray tests performed by Moodie et al. (1981) at a scale ratio of 1:28.9. Carbon dioxide was released from a point source upwind of an array of water spray nozzles (Figure 4.5-1). Both ground level and vertical profiles of concentration were taken.

Most of the measurements were made over a 1:100 scale model of a 60 m x 60 m bunded spill area (Figure 4.5-2). Many different arrangements of water spray release points, nozzle orientations, nozzle sizes were considered (Figure 4.5-3). Vapor barrier fences varied in height from 4 to 16 m. A small (S), medium (M), and large (L) tank were situated within the bunded area during some tests (Figure 4.5-4). Tank diameters ranged from 22 to 36 m, and tank heights ranged from 23 to 28 m. LNG boiloff rate (3000 to 21,400 cubic meters/sec gas) and wind speed (1.7 to 8 m/sec) were also varied.

These data have been extensively examined previously to evaluate the optimum performance of a water spray curtain (Heskestad et al., 1983) or to calibrate a numerical dispersion model (Meroney and Neff, 1985.) This review will focus on the various vertical profiles measured, the effects of discharge on barrier influence on the dense gas cloud, and the relative reductions in peak concentration seen downwind of various size tanks.

Results of Comparison:

Consideration of data from Meroney, Neff and Heskestad (1984) showed that peak concentrations were reduced to values of 0.21 some 5 m downwind of the water curtains modeled, then the ratio began to rise at farther distances downwind (Figure 4.5-5). A vertical concentration profile measured along the centerline at a distance of 18.3 m reveals that the water spray re-distributed the mass of the plume upward and reduced peak concentrations by 75 % (Figure 4.5-6).

A water spray system was found to reduce peak centerline concentration ratios to 0.1; however, a tank placed within the spill area tended to lift the gas into the upper separation cavity downwind of the tank. Thus, aerodynamic turbulence pre-mixed the gas to significant

heights, even before the cloud reached the water spray curtain. Figure 4.5-7 shows that concentration ratios with the tanks present increase from 0.2 to 0.8.

Figures 4.5-8 to 4.5-11 display centerline vertical concentration profiles with and without a water spray activated for the conditions of bund alone, small tank, medium tank, and large tank. Without water spray or tank the dense plume remains below a height of 10 m, but the tanks mix the gas up to a height of 20 or 30 m. The water spray curtain then distributes the cloud to heights above 30 m.

Increased water flow through the spray nozzles tends to increase the entrainment velocity, w_e. Figure 4.5-12 summarizes the net effect of increasing water discharge for all data disregarding nozzle or spray arrangement. Water flow rate appears to dominate dilution; whereas nozzle number, size and orientation produce only second order effects.

The increased entrainment associated with larger water discharge rates leads to deeper, well-mixed plumes downwind of the spray curtain (Figures 4.5-13 and 4.5-14).

Conclusions:

Water spray curtains were found to dilute dense gas clouds by factors ranging from 3 to 50. Large tanks and fences result in increased mechanical mixing which dilutes the dense gas before it reaches the water curtain; hence, effectiveness of the curtain decreases. Nonetheless, the combined effect of tank and water spray curtain on air entrainment was more than the enhanced mixing induced by either object alone. Water spray curtains mix dense gas clouds to considerable heights as a result of their entrainment of air into the gas cloud. Water spray curtain effectiveness increases directly with the rate water is discharged through the curtain.

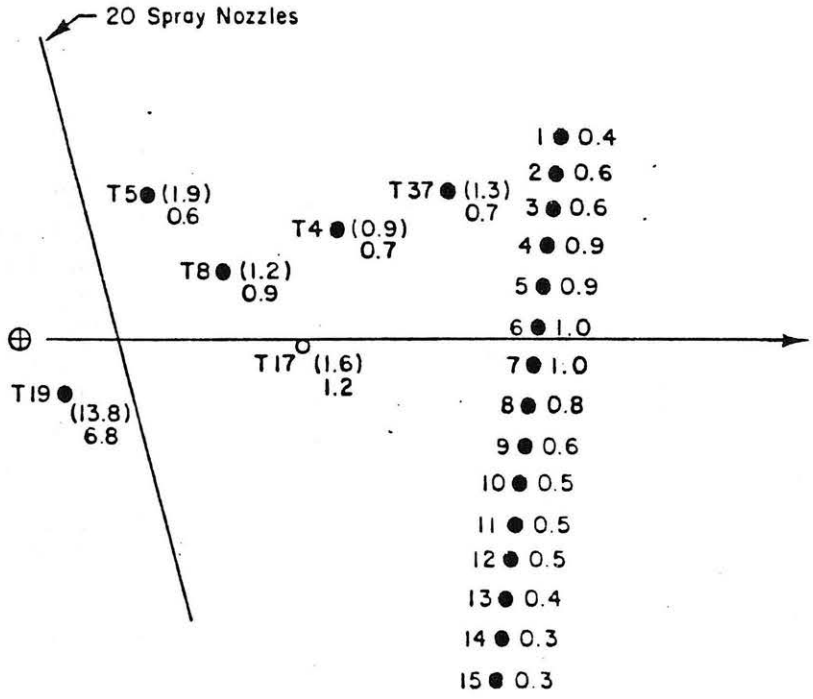

Fig. 4.5-1 Experimental Configuration and Measurement Grid, Health and Safety Executive CO2/Water Spray Trial No. 46

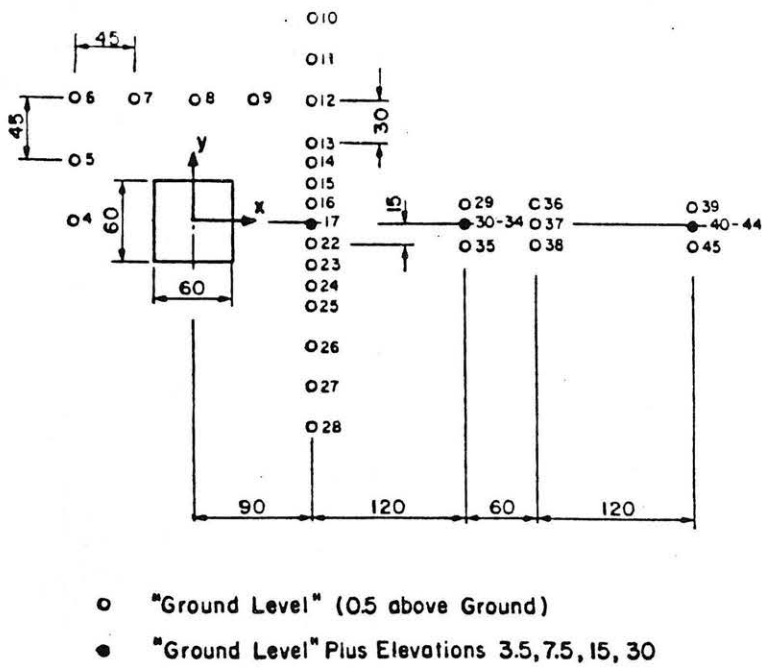

Fig. 4.5-2 Experimental Configuration and Measurement Grid, Generic Bunded Spill Area

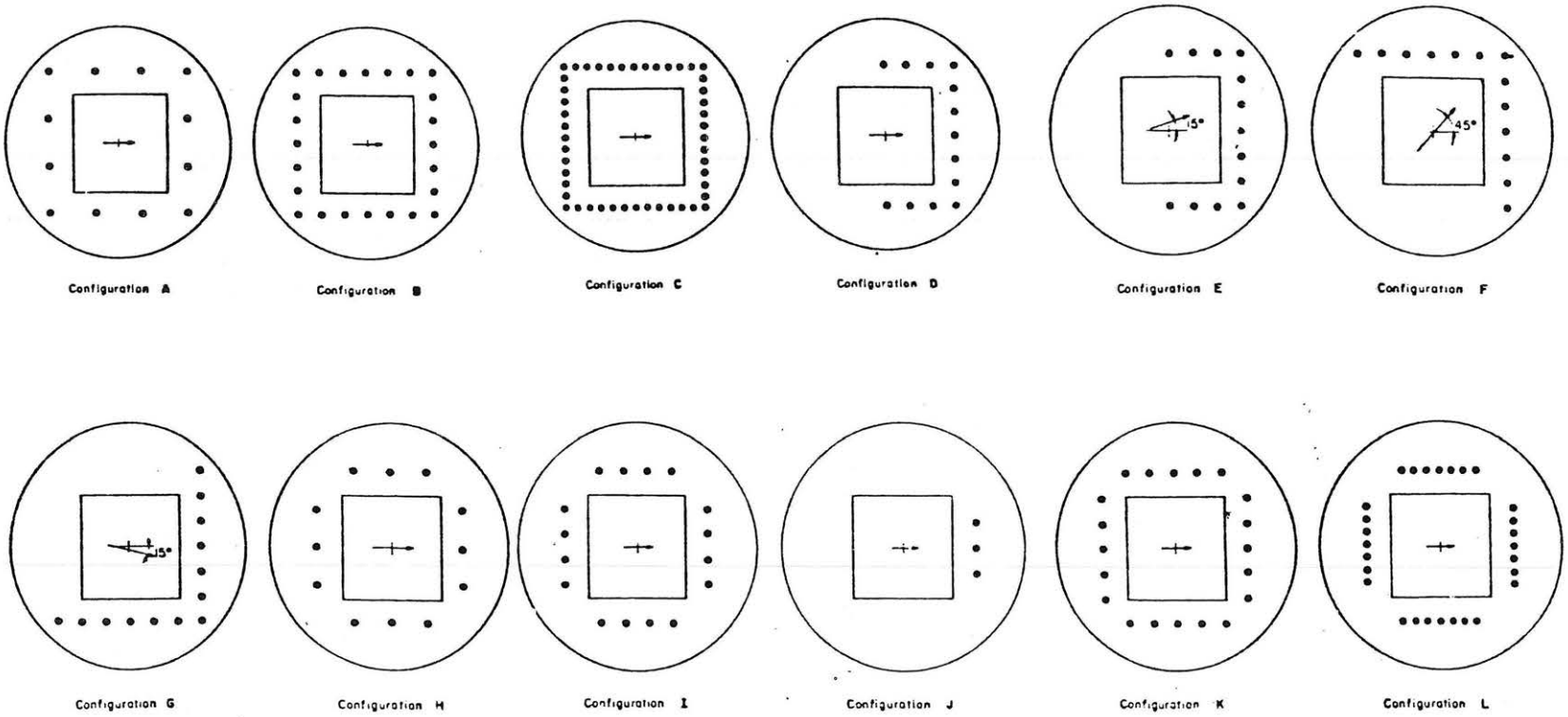

Fig. 4.5-3 Water Spray Configurations for Generic Bunded Spill Area

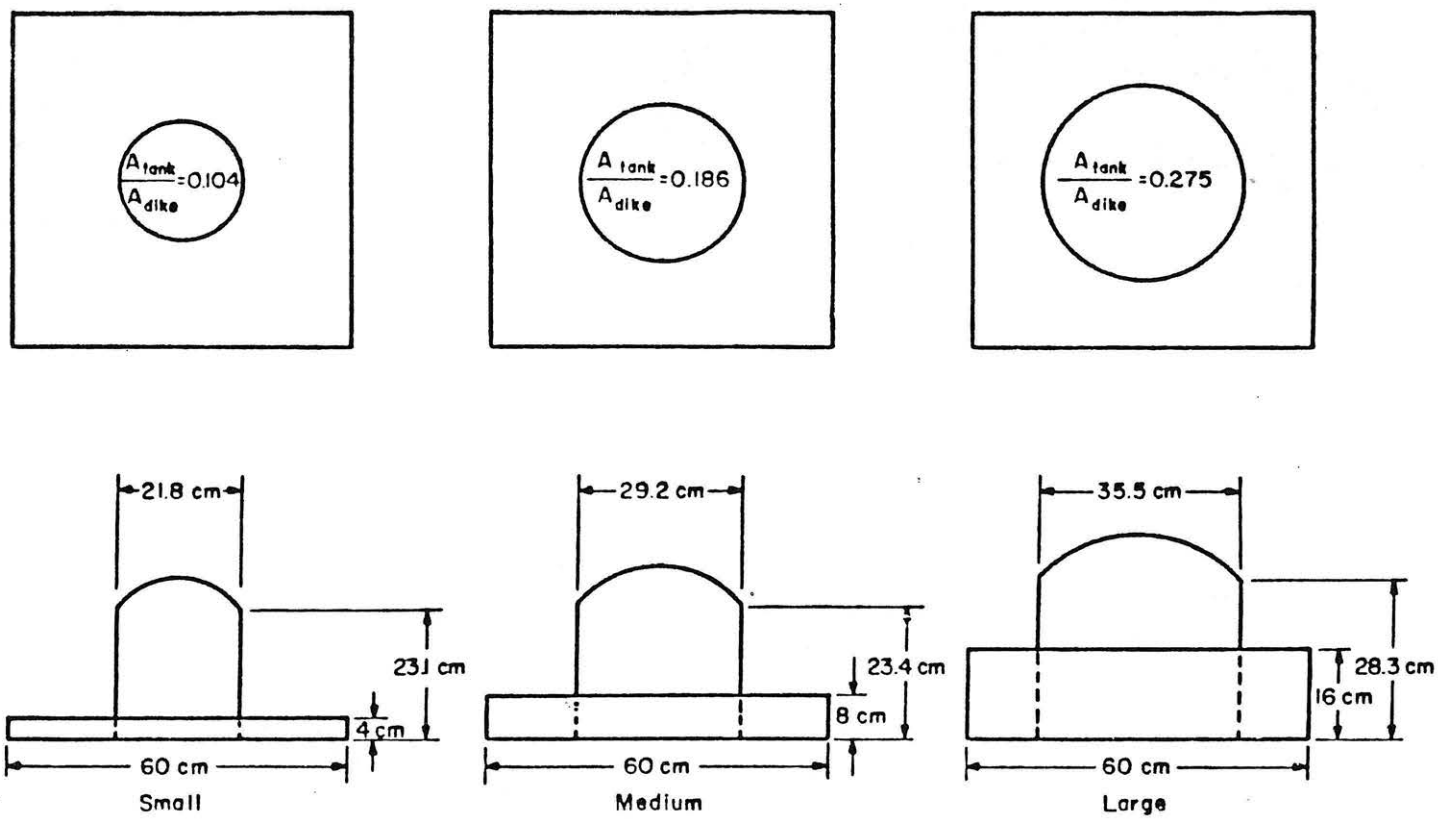

Fig. 4.5-4 Tank and Fence Configurations for Generic Bunded Spill Area

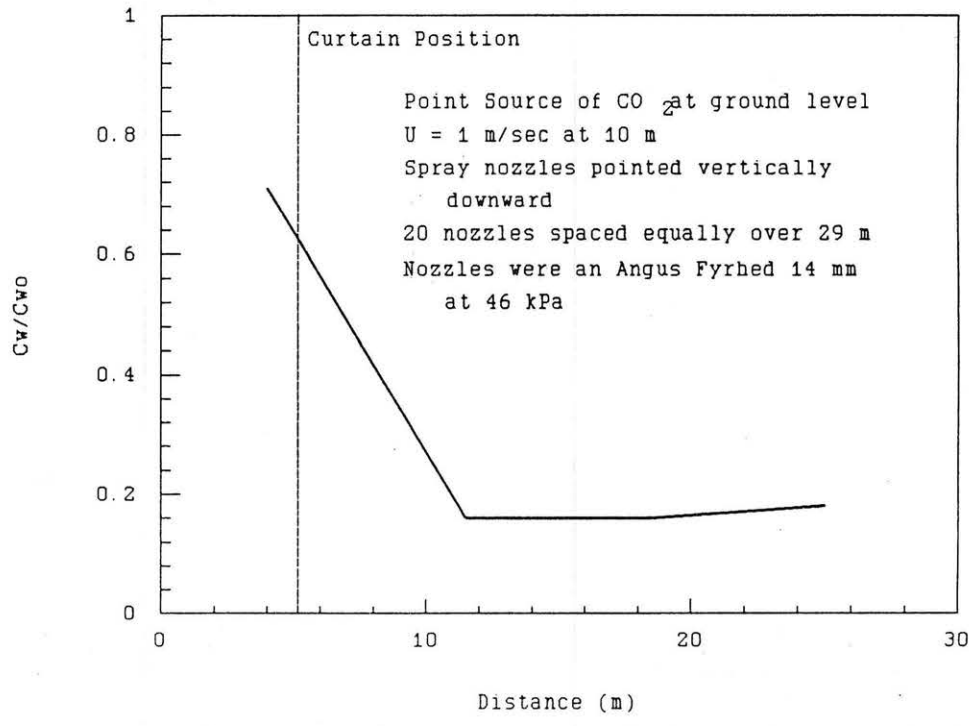

Fig. 4.5-5 Peak Concentration Ratio vs Downwind Distance, HSE Trial No. 46

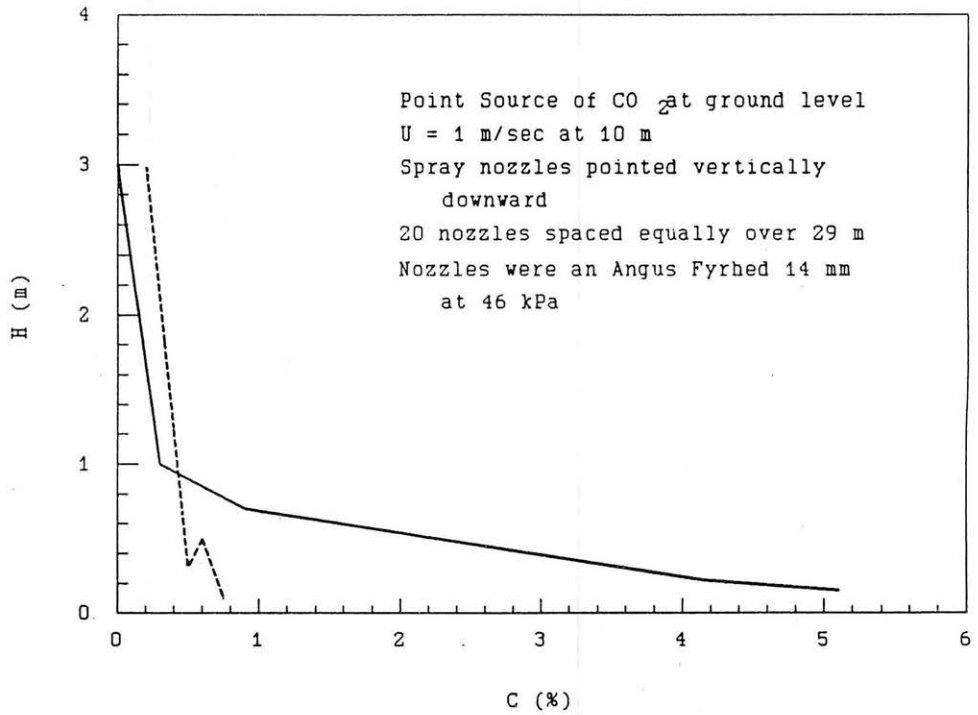

Fig. 4.5-6 Vertical Concentration Profiles at X = 18.3 m, HSE Trial No. 46

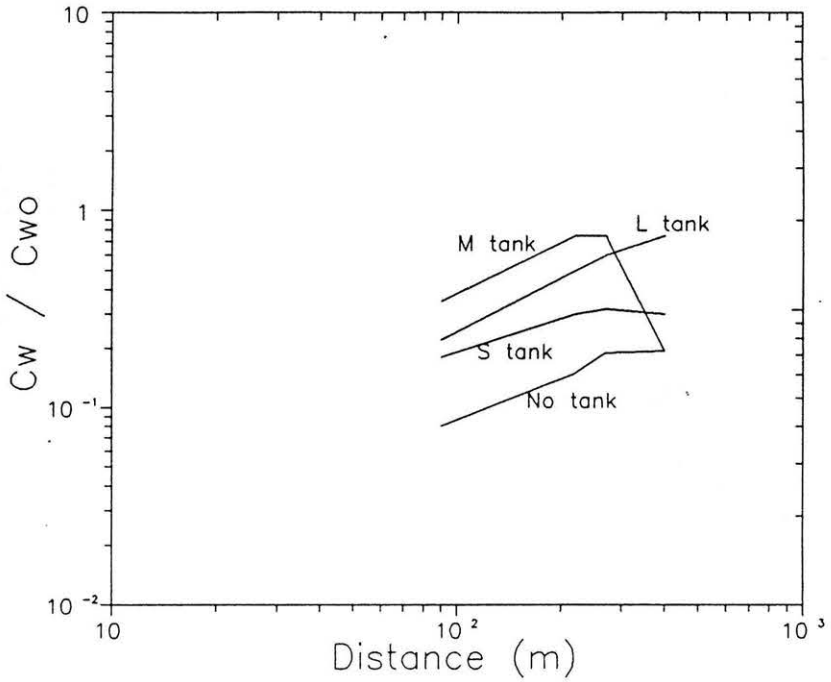

Fig. 4.5-7 Peak Concentration Ratio vs Downwind Distance, Water Spray together with Small, Medium and Large Tank Obstacles

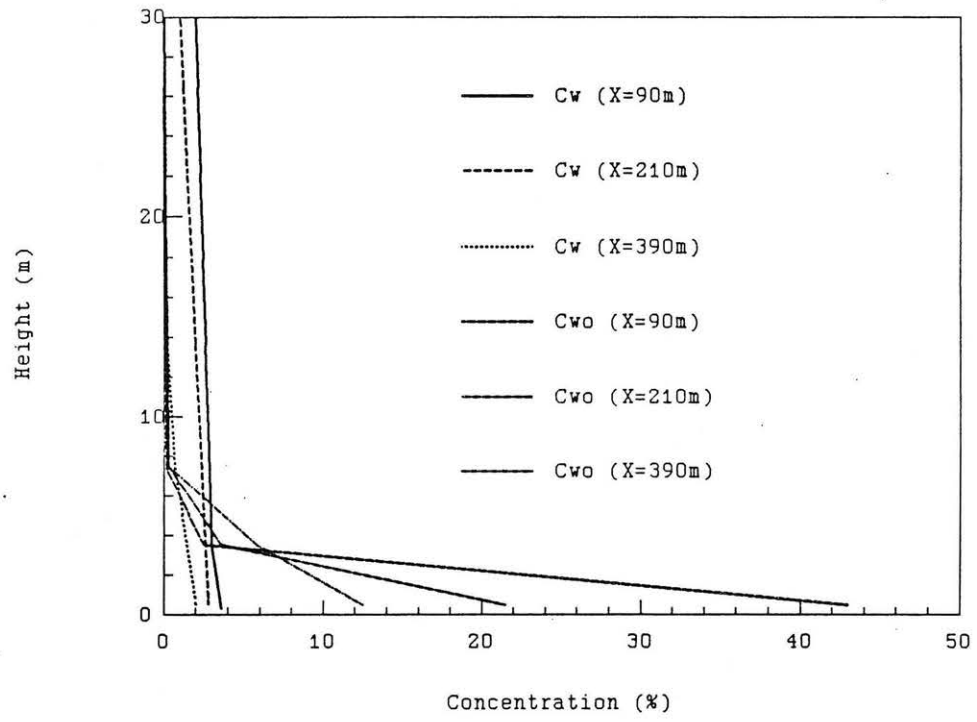

Fig. 4.5-8 Vertical Concentration Profiles, No Tank

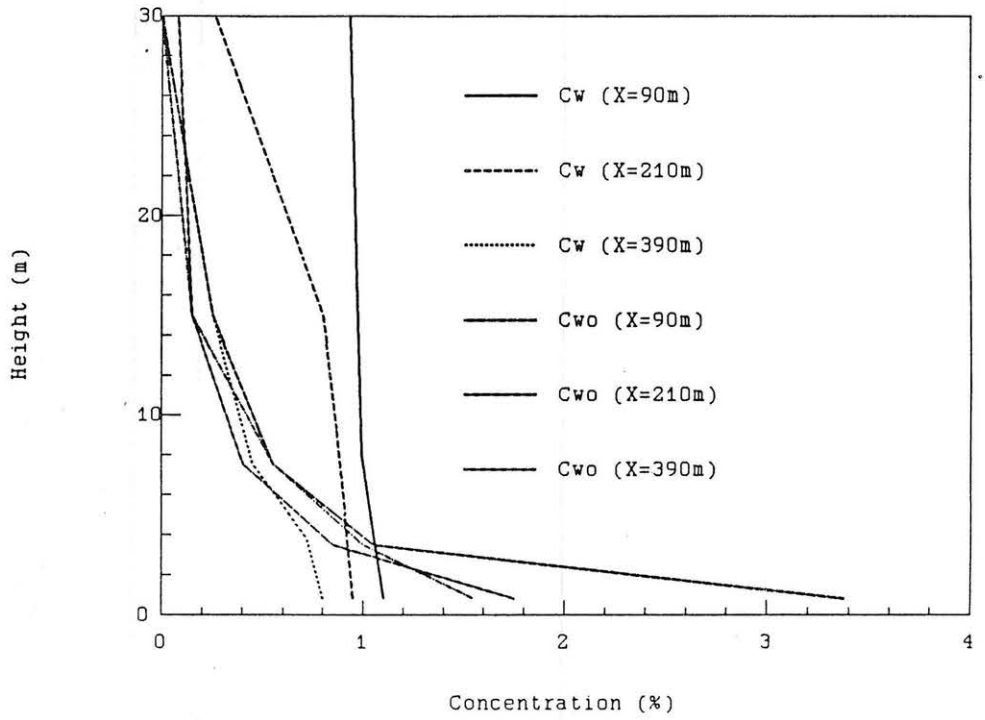

Fig. 4.5-9 Vertical Concentration Profiles, Small Tank

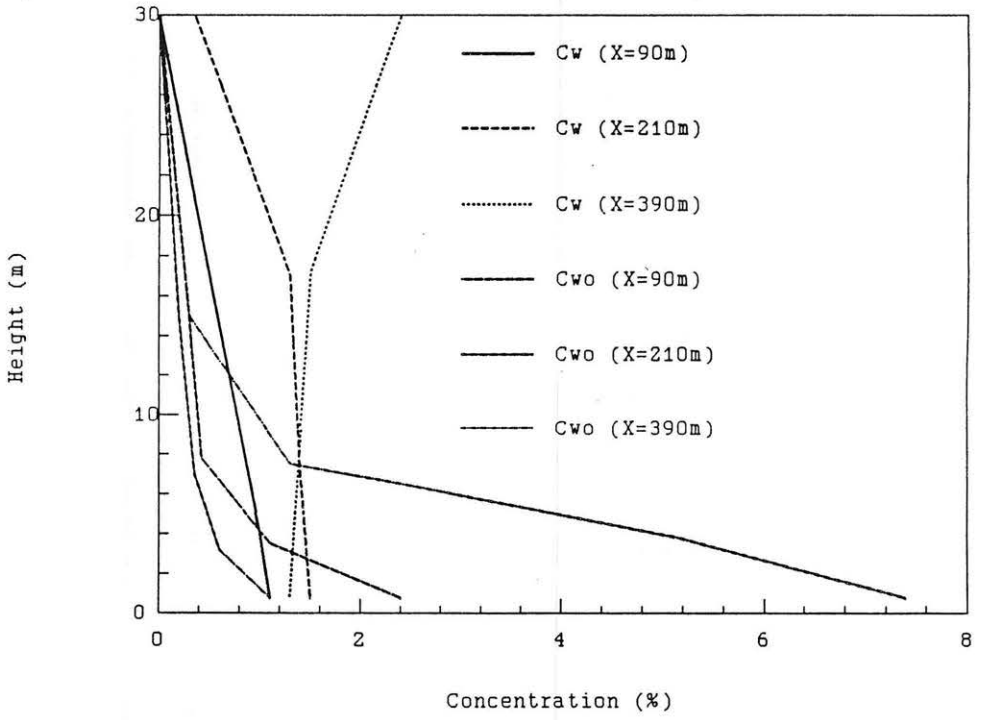

Fig. 4.5-10 Vertical Concentration Profiles, Medium Tank

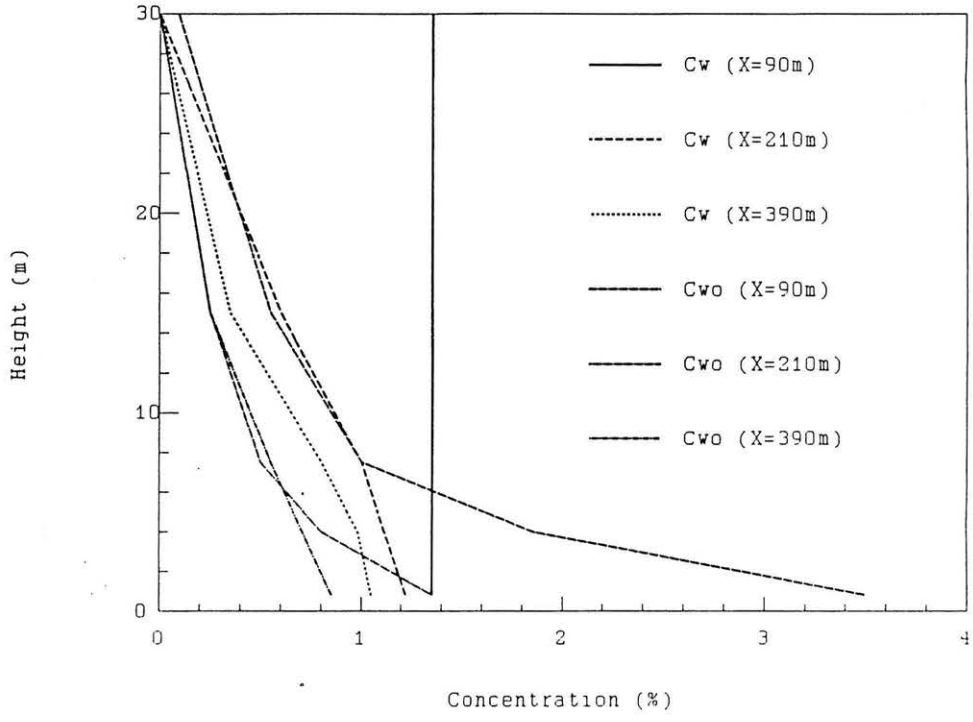

Fig. 4.5-11 Vertical Concentration Profiles, Large Tank

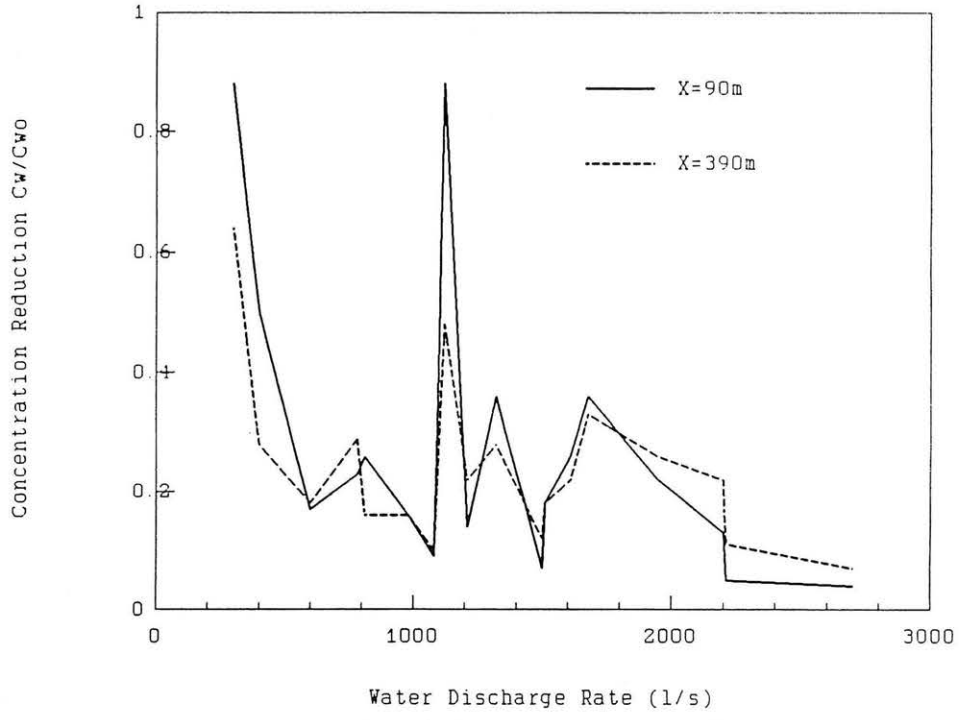

Fig. 4.5-12 Peak Concentration vs Total Water Spray Discharge Rate

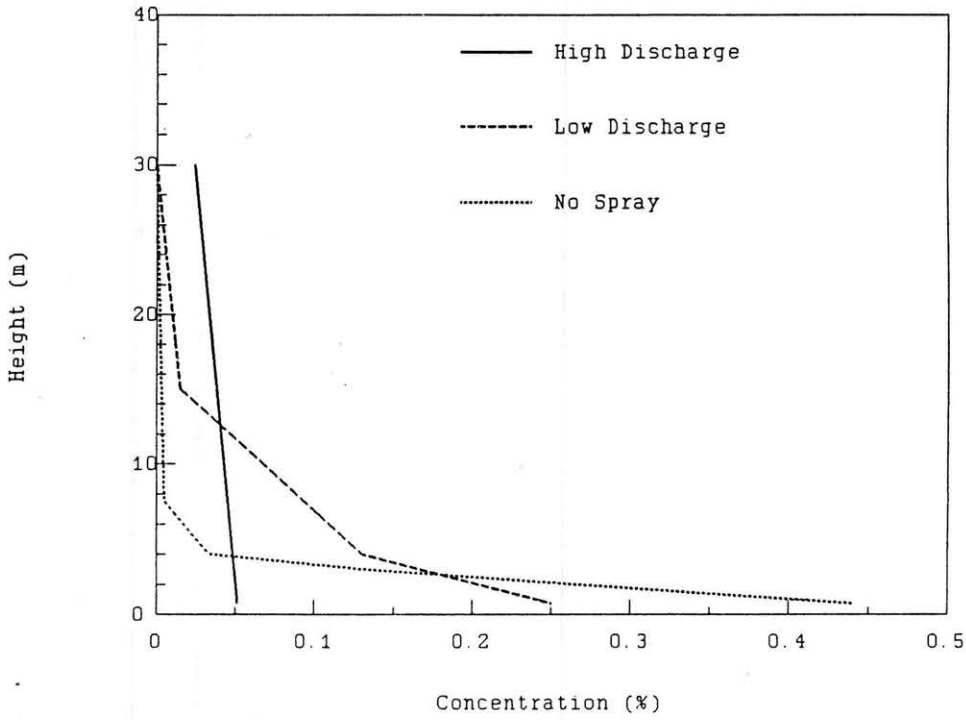

Fig. 4.5-13 Vertical Concentration Profiles at X = 90 m for Various Water Spray Discharge Rates

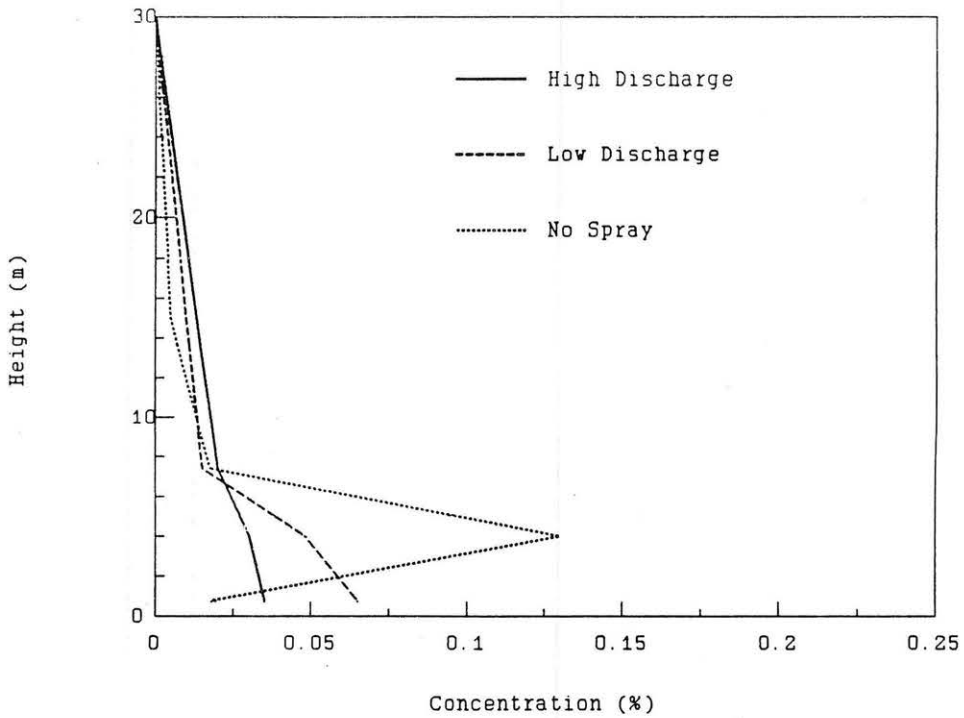

Fig. 4.5-14 Vertical Concentration Profiles at X = 390 m for Various Water Spray Discharge Rates

4.6 "Large Scale Field Trials on Dense Vapor Dispersion," McQuaid and Roebuck, 1984

Experiment Configuration:

In 1976 the Health and Safety Executive (HSE) initiated a program of research on the atmospheric dispersion of heavy gases. The principal theme of the experimental part of the program was the study of the dispersion of fixed-volume clouds. The clouds were initially placed at atmospheric pressure and temperature in a ground-level container which was then suddenly removed. The Thorney Island Heavy Gas Dispersion Trials (HGDT) project was the large-scale constituent of their program, and it was the subject of the report by McQuaid and Roebuck (1984).

The HGDT project as originally planned was limited to experiments on clouds dispersing over uniform, unobstructed ground. After these experiments had commenced, a second series of experiments were performed in which the effects of several types of obstruction were studied. The former experimental program was designated Phase I and the later instantaneous spills were designated Phase II and the later continuous spills designated Phase III.

Figure 4.6-1 indicates the measurement domain about the test location. Figures 4.6-2 display the alternative arrangements of solid fences (5 m), porous fences (10 m), buildings (9 m square), and vapor barrier enclosures (2.4 m x 26 m x 54 m studied.)

Since each field trial was performed at a unique combination of spill rate, meteorology, and obstruction conditions, no two tests were really carried out at identical conditions. Nonetheless, the data were stratified by Froude number and volume release conditions to identify pairs of data suitable for comparison. Seven sets of data pairs from Phase I and II were identified. Only three sets of data pairs (or triplets) were found in the Phase III series suitable for comparison. Table 4.6-1 summarizes the characteristics of the spill sets selected for comparison. The peak concentration, time of arrival, time of peak concentration arrival, and time of departure for each near cloud centerline measurement station were measured on figures provided by HSE. Base line drift of the measuring instrumentation was removed from the figures, and arrival and departure time was defined as the time at which concentrations reached 5% of their peak values.

Results of Comparison:

In the following figures Y represents downwind distance, the release location was always at Y = 200 m and the solid and porous fences were always located at Y = 250 m. During the continuous gas tests the wind approached either along or perpendicular to the longer fence dimension. Note that clouds are delayed by the barriers for time ratios greater than one and accelerated at ratios lower than one.

During the tests for instantaneous spills upwind of the 5 m solid fence it was found that the peak concentration ratios decreased from 0.4 to 0.1 downwind of the fence then slowly increased beyond 400 m (30 fence heights) (Figure 4.6-3). Cloud arrival, peak arrival and cloud departure times changed from +20 to -40%, +50 to +200%, and +50 to +400 % immediately downwind of the fence (0 to 40 fence heights downwind). But farther downwind the cloud arrival, peak arrival and cloud departure times were -40 to -60%, 0 to -40%, and 0 to -10% of their no fence values (Figures 4.6-4 to 4.6-6). Apparently the lower wind speeds directly in the wake of the fences initially slow cloud movement, but beyond the wake region the deeper cloud is advected with higher average wind speeds.

During the tests for instantaneous spills upwind of the 10 m porous fences it was found that the peak concentration ratios increased at the fence line (1.2 to 3.3), but then the ratio fell to levels near 0.2 at about 15 fence heights downwind (Figure 4.6-7). Rottman et al. (1985) suggested that a gravity current might actually decrease its height passing through a porous barrier, which would explain the increased cloud concentrations detected locally. Farther downwind the turbulence generated by the fence increases entrainment levels and results in reduced concentration ratios. Cloud arrival, peak arrival and cloud departure times appear delayed in the wake region of the porous fences, but further downwind the ratios approach a magnitude near one (Figures 4.6-8 to 4.6-10).

The presence of a 9 m square building downwind of a spill site appears to perturb the instantaneous gas cloud much like the presence of a fence barrier. Enhanced mixing of the plume resulting in a more dilute and larger cloud produces reduced peak concentration ratios (0.1 to 0.4), and reduced arrival, peak arrival and cloud departure time ratios. If the building is not directly downwind dilution can occur but time ratios quickly return to one. An upwind building situated to one side of the spill will also result in plume dilution and negligible changes in time ratios.

A vapor barrier enclosure that surrounds a continuous source of dense gas appeared to <u>increase</u> peak concentration ratios directly downwind of the enclosure (2.2 to 8.0). Farther downwind peak concentration ratios decreased (0.3 to 2.0) (Figure 4.6-11). One explanation for the increased peak concentration ratios is associated with the tendency for the enclosure to restrain the initial upwind and lateral spreading of a dense cloud. A narrower cloud will produce higher centerline concentrations. The enclosures also seem to loft a small amount of gas to heights at which increased wind speeds advect the gas faster downwind; thus, one notes reduced arrival times in two of the three sets of comparisons (i.e. 0.1 to 0.2), but the third case produced peculiarly large arrival time ratios (1 to 9?). Nonetheless, peak arrival and departure time ratios ranged between 0.5 to 1.5 for all three data sets (See typical Figures 4.6-12 to 4.6-14).

Conclusions:

The HGDT tests at Thorney Island provides tantalizing glimpses of the physics of plume dynamics downstream of a variety of obstacles. As expected normal meteorological variability produces perturbations in measurements which are often confusing as they are educational. Nonetheless, a few conclusions may be made from the comparison exercise.

@ Solid barrier fences reduce ground level concentrations measured downwind of instantaneous spills of dense gas. The additional mixing produced by the fence appears to have reduced effect beyond the wake region (30 fence heights).

@ Solid barrier fences initially delay the cloud movement through the wake region, but the cloud actually arrives earlier farther downstream.

@ Porous barriers may increase concentrations directly downstream of the fence; however, farther downstream peak concentrations are reduced.

@ Small buildings perturb a dense cloud much like a solid fence when placed directly downwind of the spill. Buildings placed off centerline from the cloud trajectory have minimal effects on time ratios.

@ Enclosures placed around continuous sources of dense gas may increase concentrations downwind of the enclosure. Farther downstream the peak concentration ratios remained near one.

Table 4.6-1 Spill and Meteorological Conditions During Thorney Island Trials

INSTANTANEOUS RELEASES

TRIAL NO.	S.G.	U10 m/s	VOL m^3	H m	(X)f m	uM m/s	Zo mm	Fr	uM/U10	Zo/VOL^(1/3) m10-4	H/VOL^(1/3)	(X)f/VOL^(1/3)	V/L^3
16	1.68	4.8	1580	-	-	.17	20	1.42	.04	17.17	-	-	1.58
20	1.92	5.7	1920	5	50	.46	20	1.65	.08	16.09	.40	4.02	1.92
7	1.78	3.2	2000	-	-	.07	2	.34	.02	1.59	-	-	2.00
21	2.02	3.9	2050	5	50	.41	20	.47	.11	15.74	.39	3.94	2.05
8	1.70	2.4	2000	-	-	0	2	.16	0	1.59	-	-	2.00
22	4.20	5.9	1400	5	50	.12	2	.59	.02	1.79	.45	4.47	1.40
19	2.12	6.4	2100	-	-	.48	20	1.87	.08	15.62	-	-	2.10
23	1.80	5.8	N/A	10	50	N/A	N/A	N/A	N/A	N/A	N/A	N/A	N/A
13	1.96	7.5	1950	-	-	.51	20	3.59	.07	16.01	-	-	1.95
24	2.03	7	N/A	10	50	.4	150	N/A	N/A	N/A	N/A	N/A	N/A
9	1.73	1.7	2000	-	-	.03	2	.05	.02	1.59	-	-	2.00
26	2.00	1.9	1970	9	50	.24	2	.06	.13	1.60	.72	3.99	1.97
15	1.41	5.4	2100	-	-	.37	2	3.06	.07	1.56	-	-	2.10
28	2.00	9	1850	9	50	.3	2	6.06	.03	1.63	.73	4.07	1.85
11	2.00	5.1	2100	-	-	N/A	N/A	1.06	N/A	N/A	-	-	2.10
29	2.00	5.6	1950	9	27	.25	2	1.43	.04	1.60	.72	2.16	1.95

CONTINUOUS RELEASES

TRIAL NO.	S.G.	U10 m/s	VOL m^3	RATE(Q) m^3/min	H m	W m	L m	uM m/s	Zo mm	Fr	uM/U10	Zo/VOL^(1/3) m10-4	Q/(U10mL^2) m10-2
46	2.00	3.4	1690	260	0	0	0	N/A	N/A	.12	N/A	N/A	1.27
33	1.63	2.5	1870	340	2.4	26	54	.15	10.00	.10	.06	8.12	2.27
49	1.60	2.4	1907	260	2.4	54	26	N/A	N/A	.10	N/A	N/A	1.81
45	2.00	2.3	1972	260	0	0	0	N/A	N/A	.05	N/A	N/A	1.88
43	1.55	1.5	1899	265	2.4	26	54	N/A	N/A	.07	N/A	N/A	2.94
50	1.58	1.6	1800	270	2.4	54	26	N/A	N/A	.07	N/A	N/A	2.81
38	1.60	3.8	1867	280	0	0	0	N/A	N/A	.25	N/A	N/A	1.23
37	1.60	3.4	1891	255	2.4	26	54	.39	10.00	.20	.11	8.09	1.25

TRIAL NO.	Fr	VOL/(HxWxL)	H/VOL^(1/3)	W/VOL^(1/3)	L/VOL^(1/3)
46	9.26	-	0	0	0
33	4.47	.55	.19	2.11	4.38
49	5.43	.57	.19	4.35	2.10
45	2.87	-	0	0	0
43	2.56	.56	.19	2.10	4.36
50	2.44	.53	.20	4.44	2.14
38	20.00	-	0	0	0
37	15.73	.56	.19	2.10	4.37

Table 4.6-1 Obstacle Configurations During Thorney Island Trials

INSTANTANEOUS RELEASES

TRIAL NO.	WIND DIR.(DEG)	Fr	CONFIGURATION
16	-14.3	.35	UNOBSTRUCTED
20	-6.5	.36	5M WALL AT 50M
7	45.3	.14	UNOBSTRUCTED
21	-6.1	.15	5M WALL AT 50M
8	-15.8	.09	UNOBSTRUCTED
22	-7.6	.11	5M WALL AT 50M
19	30.2	.37	UNOBSTRUCTED
23	28.6	.43	2M10M POROUS FENCE AT 50M
13	30.8	.57	UNOBSTRUCTED
24	28.8	.46	4M10M POROUS FENCE AT 50M
9	-26.9	.05	UNOBSTRUCTED
26	5	.04	9M SQUARE BLDG, 50M DOWN RANGE
15	.8	.72	UNOBSTRUCTED
28	41.9	.82	9M SQUARE BLDG, 50M AT 45 DOWN RANGE
11	69.6	.28	UNOBSTRUCTED
29	27	.32	9M SQUARE BLDG, 27M AT 30 UP RANGE

CONTINUOUS RELEASES

TRIAL NO.	WIND DIR.(DEG)	Fr	CONFIGURATION
46	76.6	.12	UNOBSTRUCTED
33	1.8	.13	2.4M FENCE LONGITUDINAL
49	1.2	.11	2.4M FENCE TRANSVERSE
45	-34.5	.05	UNOBSTRUCTED
43	10	.08	2.4M FENCE LONGITUDINAL
50	42.9	.08	2.4M FENCE TRANSVERSE
38	-25.1	.25	UNOBSTRUCTED
37	-26.5	.17	2.4M FENCE LONGITUDINAL

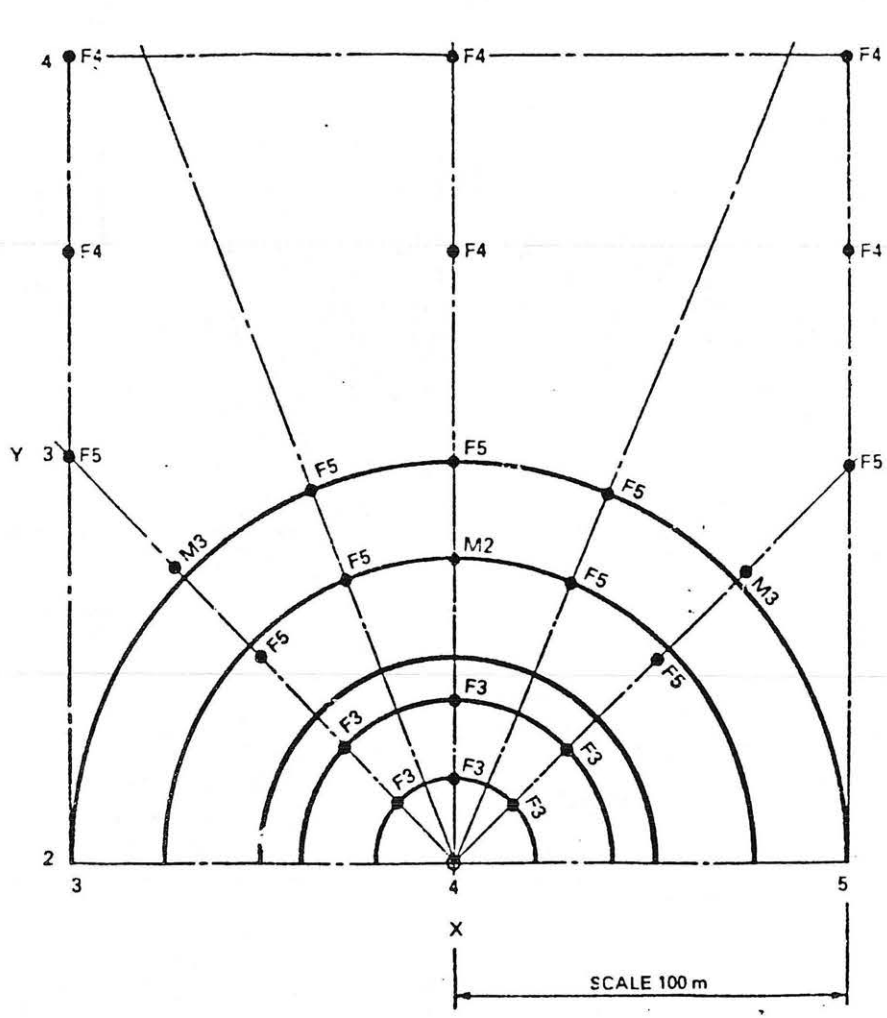

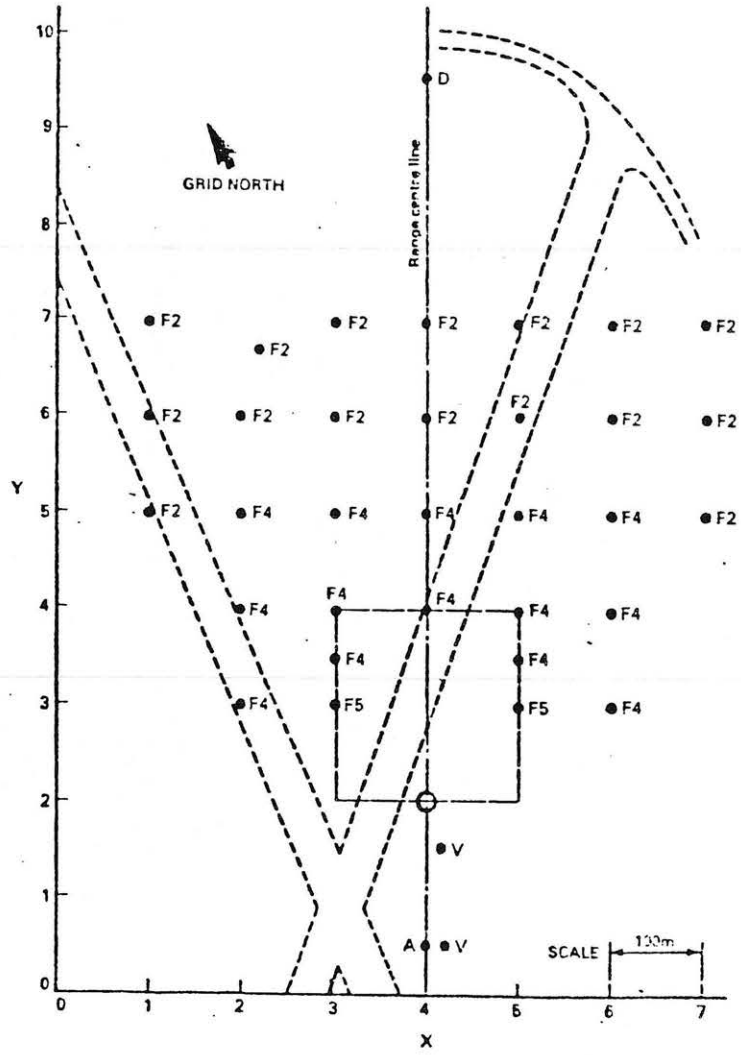

Fig. 4.6-1 Spill Configuration and Measurement Grid, Thorney Island Trials

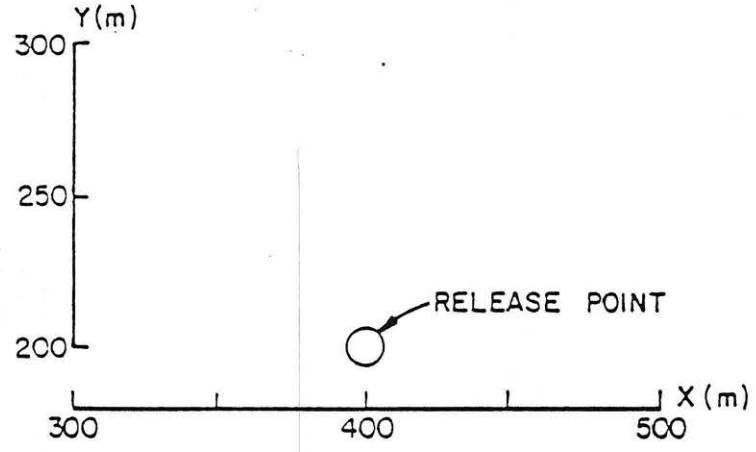

(a)

Trials 1 - 19

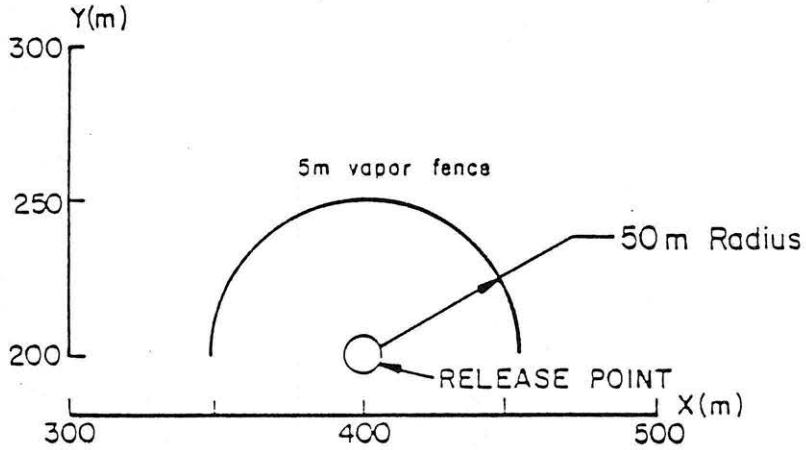

(b)

Trials 20, 21, 22, 25

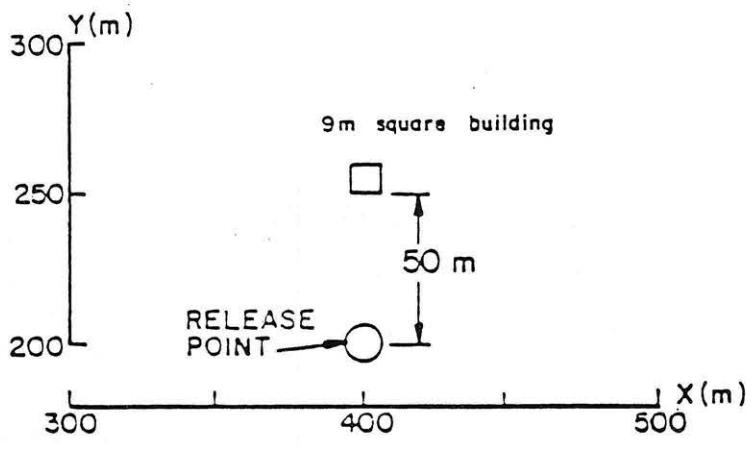

(c)

Trials 26, 27

Fig. 4.6-2 Obstacle Configurations During Thorney Island Trials

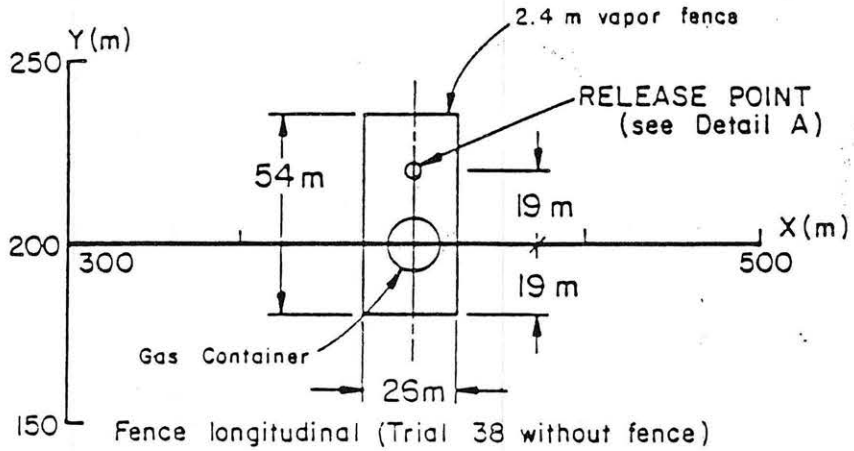

(a)

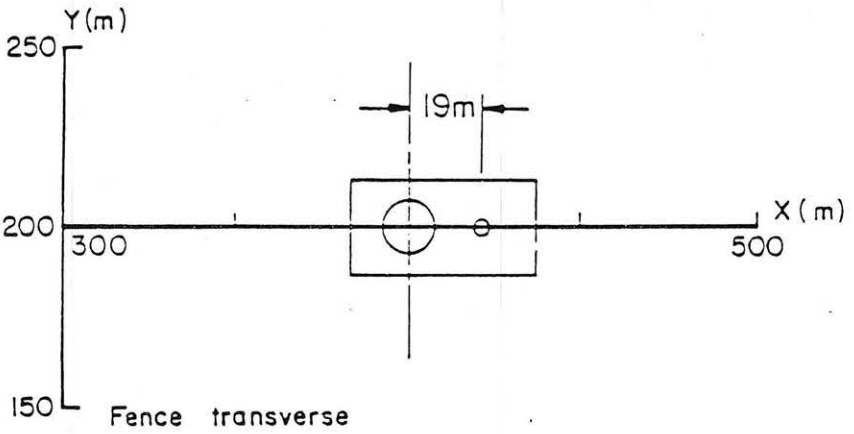

(b)

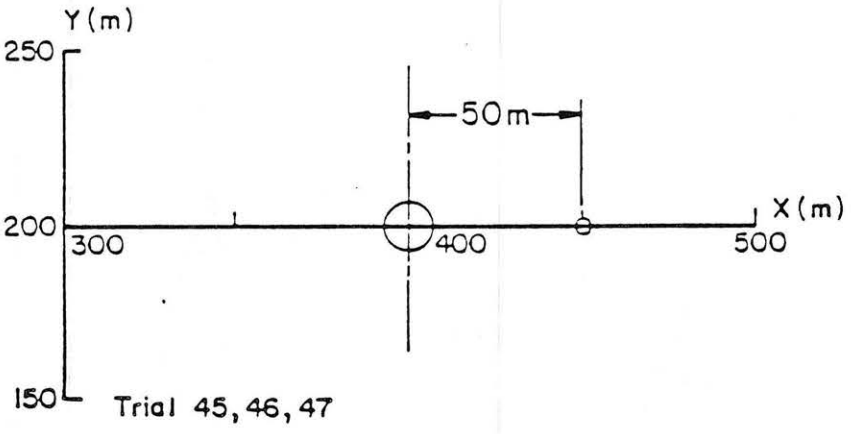

(c)

Fig. 4.6-2 Obstacle Arrangements, Phases II and III, Thorney Island Trials

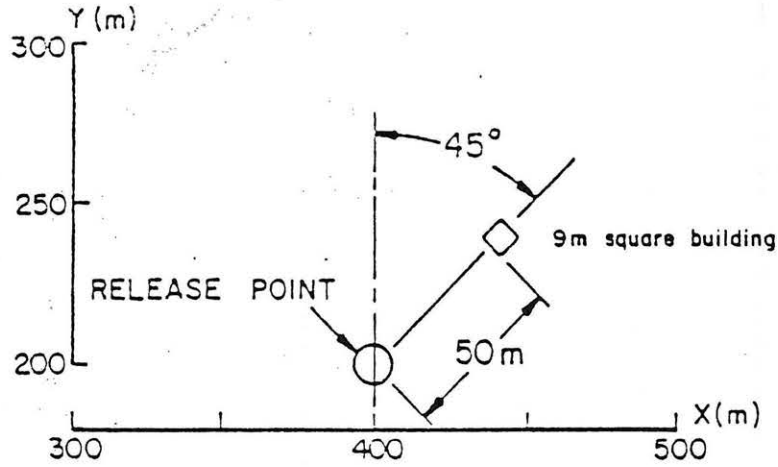

Trial 28

(d)

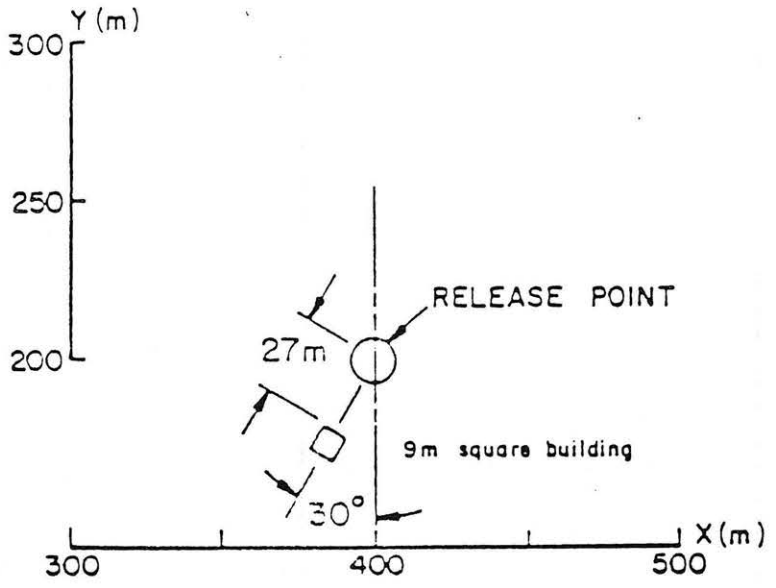

Trial 29

(e)

Fig. 4.6-2 Obstacle Arrangements, Phases II and III, Thorney Island Trials

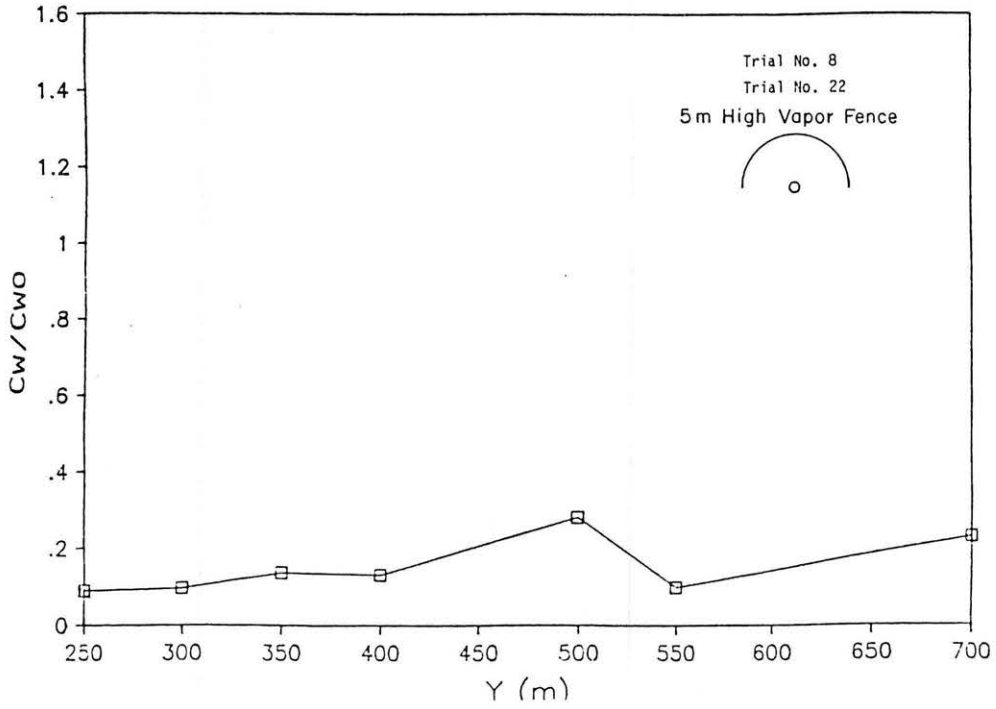

Fig. 4.6-3 Peak Concentration Ratio vs Downwind Distance, Thorney Island Trials 8 and 22

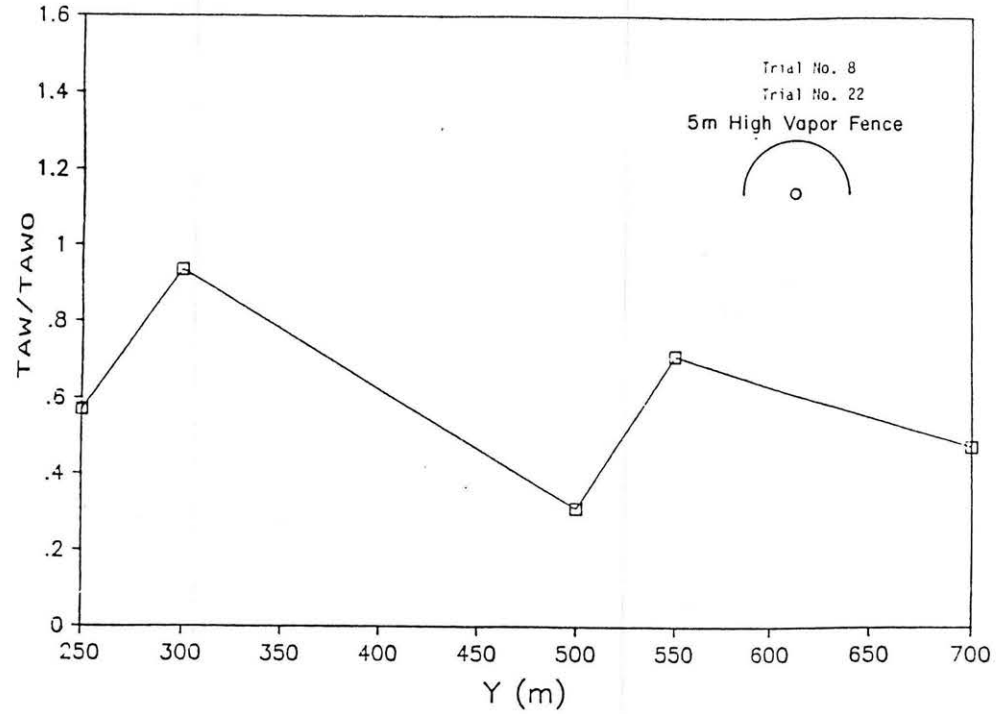

Fig. 4.6-4 Arrival Time Ratio vs Downwind Distance, Thorney Island Trials 8 and 22

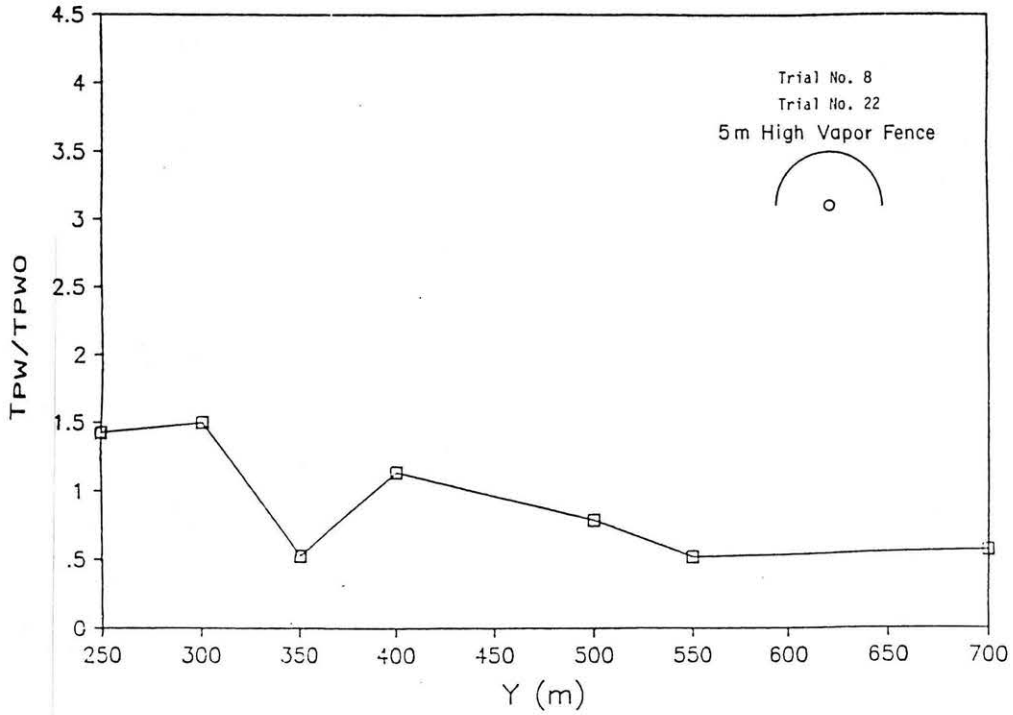

Fig. 4.6-5 Peak Arrival Time Ratio vs. Downwind Distance,. Thorney Island Trials 8 and 22

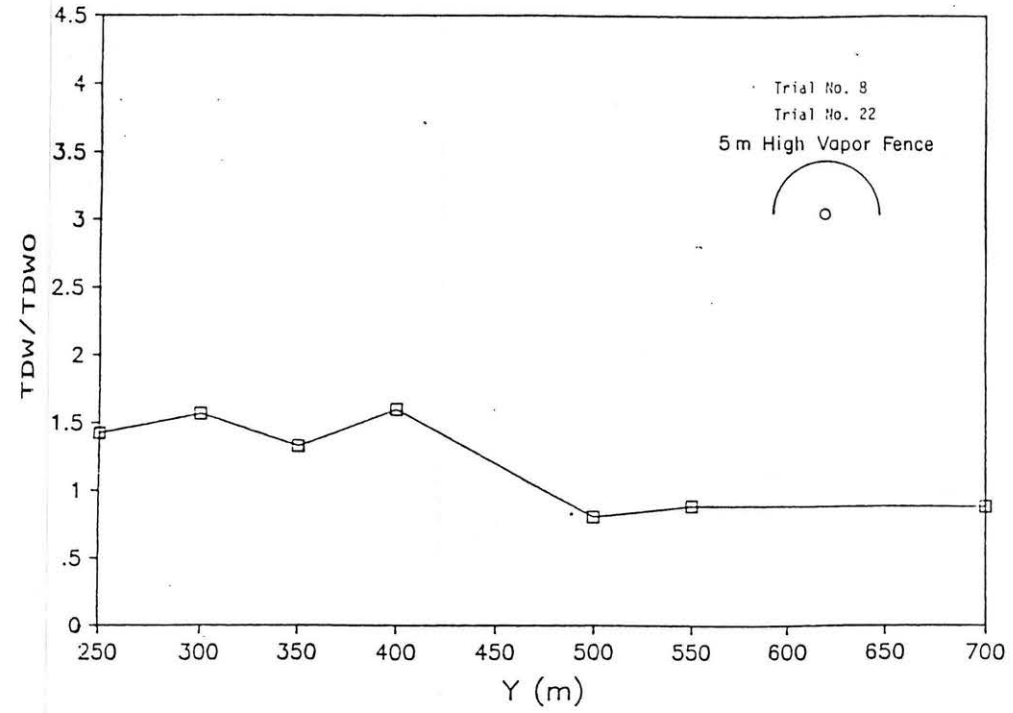

Fig. 4.6-6 Departure Time Ratio vs. Downwind Distance, Thorney Island Trials 8 and 22

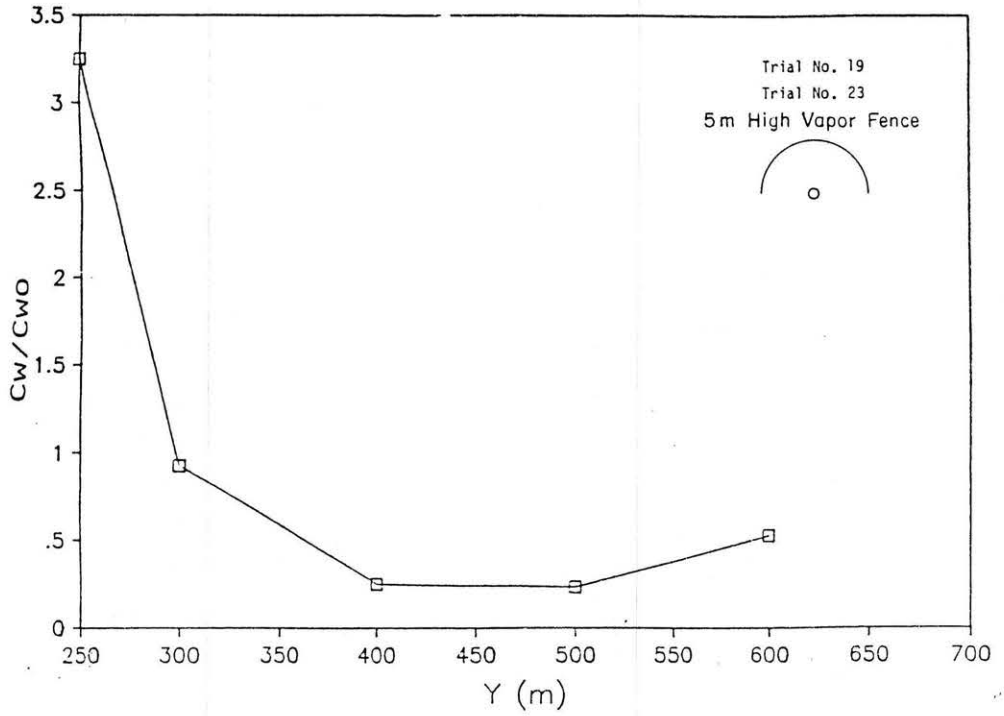

Fig. 4.6-7 Peak Concentration Ratio vs. Downwind Distance, Thorney Island Trials 19 and 23

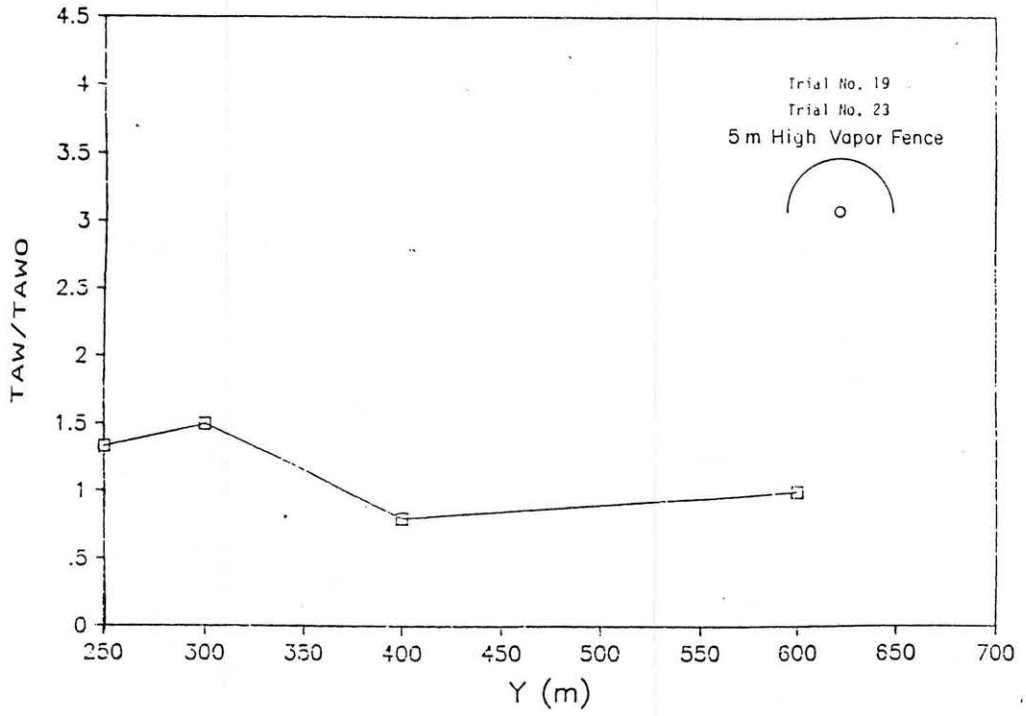

Fig. 4.6-8 Arrival Time Ratio vs. Downwind Distance, Thorney Island Trials 19 and 23

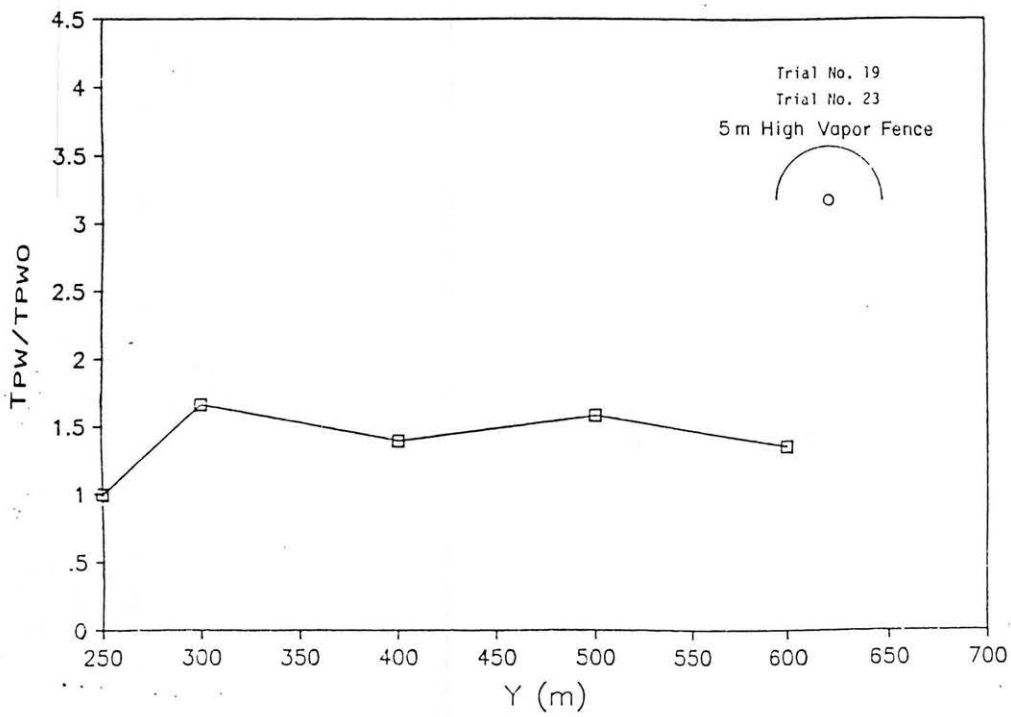

Fig. 4.6-9 Peak Arrival Time Ratio vs. Downwind Distance, Thorney Island Trials 19 and 23

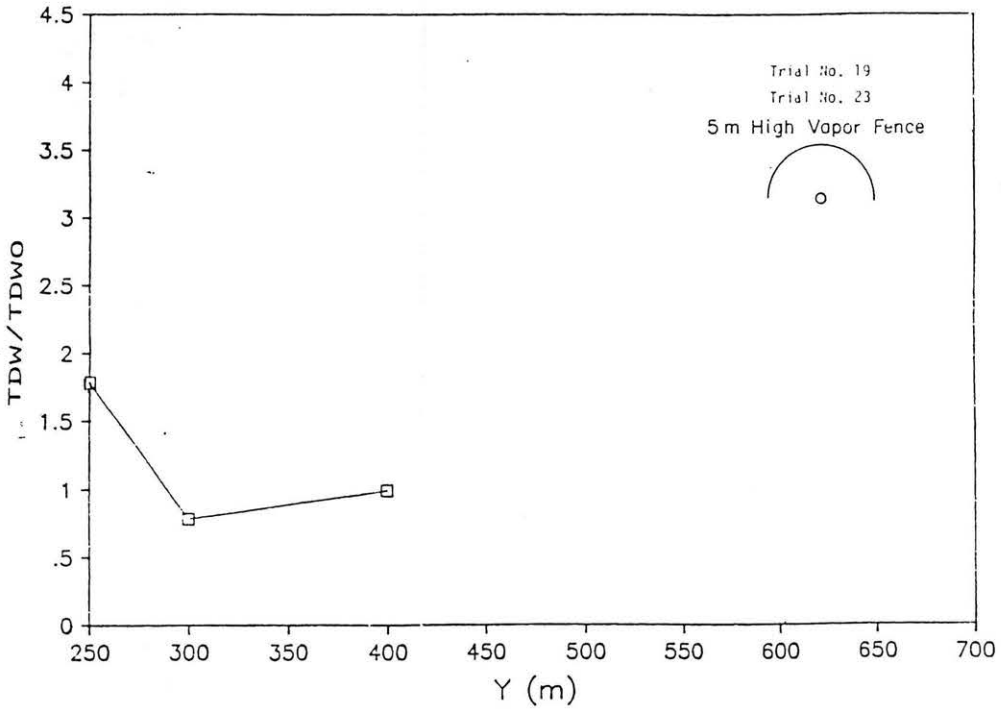

Fig. 4.6-10 Departure Time Ratio vs. Downwind Distance, Thorney Island Tirals 19 and 23

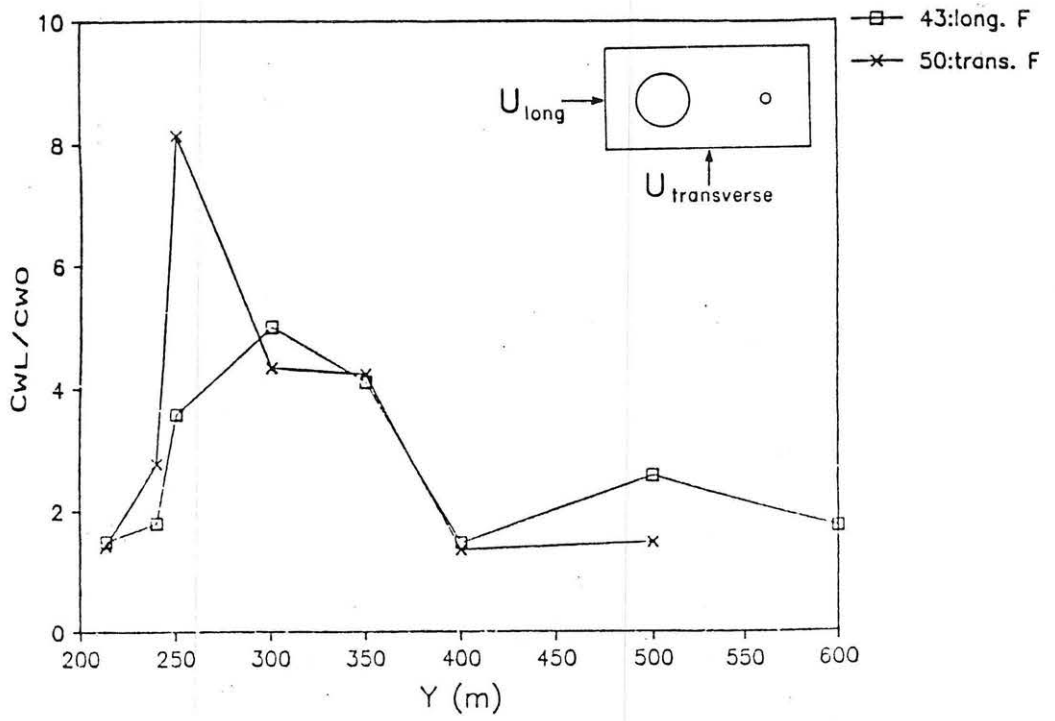

Fig. 4.6-11 Peak Concentration Ratio vs. Downwind Distance, Thorney Island Trials 43, 45 and 50

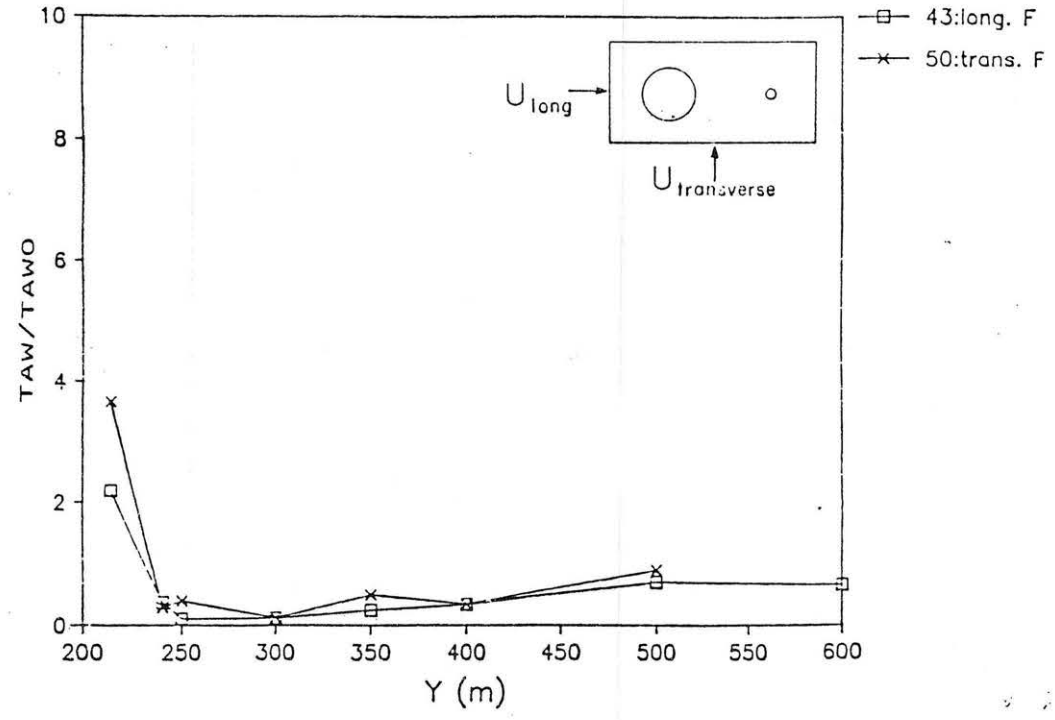

Fig. 4.6-12 Arrival Time Ratio vs. Downwind Distance, Thorney Island Trials 43, 45 and 50

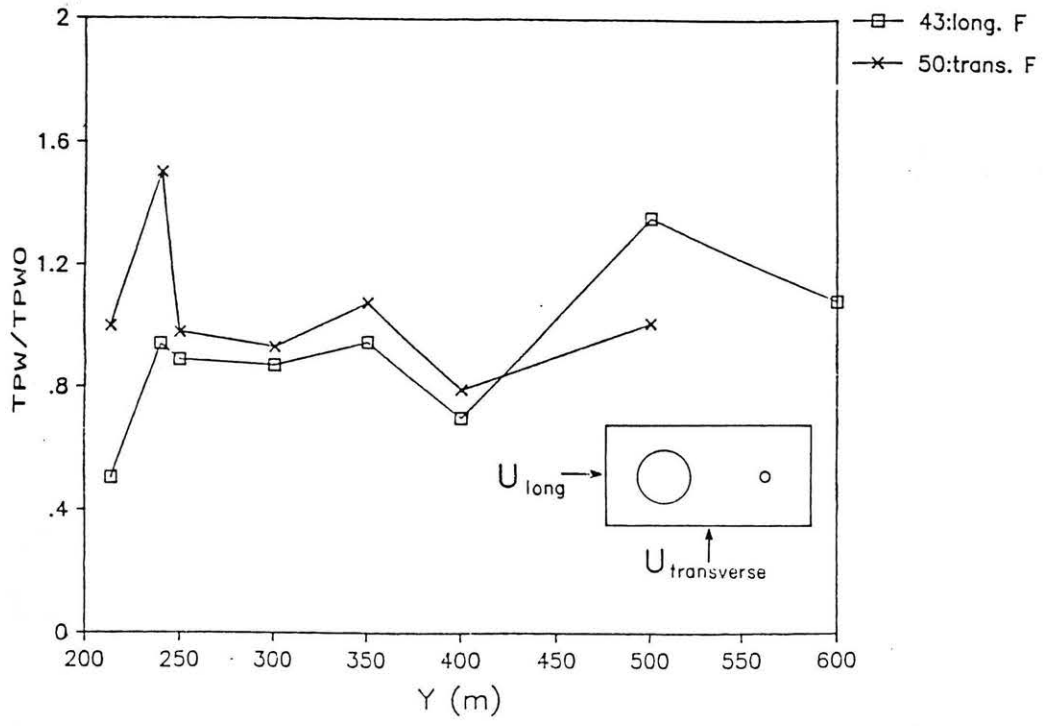

Fig. 4.6-13 Peak Arrival Time Ratio vs. Downwind Distance, Thorney Island Trials 43, 45 and 50

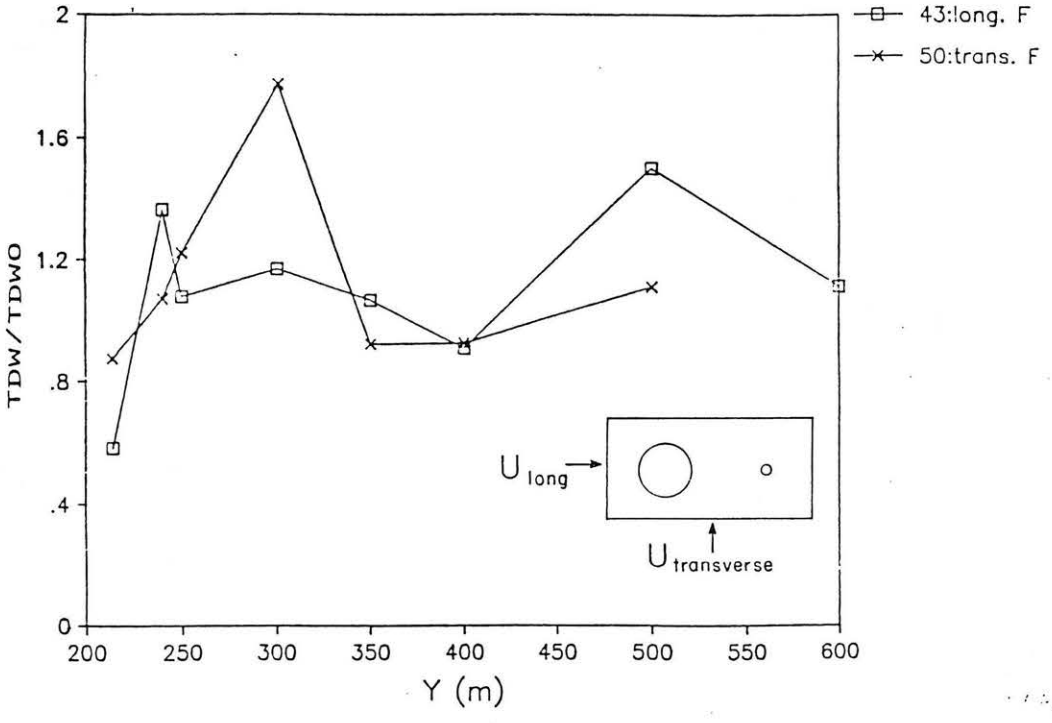

Fig. 4.6-14 Departure Time Ratio vs. Downwind Distance, Thorney Island Tirals 43, 45 and 50

4.7 "Wind Tunnel Modeling of the Thorney Island Heavy Gas Dispersion Trials," Davies and Inman, 1986

Experiment Configuration:

The purpose of the Davies and Inman (1986) wind-tunnel tests was to obtain a large data base of laboratory simulations over a range of model scales typical of those used in hazard studies on prototype installations. Scales ranging from 1:40 to 1:250 were used to simulate 34 trials from the Thorney Island HGDT project. A total of 86 laboratory cases were produced. Typically, 10 repetitions of each wind tunnel run were required to map the concentration field for each simulation and to provide point to point comparisons with the 10 to 20 "ground level" (0.4 m high) sensors used during the field trials.

The instantaneous spill cases of the HGDT project were simulated at scales of 1:40, 1:100, and 1:150 using a collapsing wall type container to simulate the prototype collapsing bag. A large grid of sensor locations were used in the laboratory to enable concentration contours to be prepared from the laboratory measurements. Concentration measurements were made in the laboratory with low-volume hot-wire aspirated katherometers. These instruments permitted measurement of concentration time series at each sensor location.

Davies and Inman provided some comparisons between their laboratory measurements and the Thorney Island field results. This report examines the data further by the Surface Pattern Comparison technique described by Meroney (1986b, 1987). The emphasis here is to analyze the results to establish the level of confidence which can be placed in laboratory simulations.

During the field study there were a large number of uncontrolled or poorly specified variables, which have effects on the resultant concentration field, that are not completely accounted for by either a physical or numerical model. The full-scale wind field is typically nonstationary, the source conditions are only approximately known, and the modeling method itself introduces errors. The Surface Pattern Comparison method estimates how much the predicted concentration contour pattern must be shifted in space to cover all of the observed values. This is done by comparing observed and calculated patterns over increments of decreasing spatial resolution. The result of such a comparison is knowledge of what percentage of observed concentrations are contained within increased areas of spatial resolution as specified by their angular displacement observed from the release location, delta theta.

Results of Comparison:

Table 4.7-1 lists the prototype and model conditions considered by Davies and Inman. The peak concentration contours at ground level measured at full scale and during the laboratory simulation are plotted together in the Davies and Inman report. These data were used to produce Figures 4.7-1 to 4.7-3 and Table 4.7-2. Figure 4.7-1 shows a typical plot

of f-N, the percentage of field data predicted within a factor of N by the laboratory data, versus angular displacement, a measure of spatial resolution. All trials were regrouped for comparison as follows:

1. Unobstructed instantaneous releases (Figure 4.7-2c),
2. Instantaneous releases with wall or building (Figure 4.7-2d),
3. Continuous releases with fence enclosures (Figures 4.7-3a to 4.7-3c),
4. Unobstructed continuous releases (Figure 4.7-3d).

Scale ratios of 40, 100, 150, and 250 are denoted by ##/a, ##/b, ##/c, and ##/d, respectively on these figures.

Most laboratory scientists expect that as model scale ratio, LSR, increases the quality of the physical simulation may decrease. This decrease results from mismatch in turbulence size and strength, exaggerated dispersion due to microscopic transport, and mismatch between buoyancy and inertial forces in the model. Thus, one expects some evidence that the quality of simulation decreases as one changes model scale from 1:40 to 1:250 (from cases a to d). It would be valuable if one could quantify the loss of accuracy as a function of model scale.

Unfortunately, close inspection of the data reveals no consistent pattern of error variability with model scale. Tests 42a, b, c, and d; tests 8b and c, tests 38a, b, c, and d show the expected decline in model reliability. Yet tests 49a, b, and c; tests 30a, b, and c; tests 33 a, b, and c show the opposite trend! Other tests display an irregular rise and fall of accuracy with scale ratio. At this time it is not known whether this is evidence of normal statistical variability, experimental errors, or fallacies in the similarity theories.

On a positive note, most of the data compared within a factor of one for angular displacements of 15 to 20 degrees. Similar comparisons between field data and many numerical models require angular displacements exceeding 45 degrees. Also results from continuous spill experiments appear to compare somewhat better than the instantaneous spill experiments.

Conclusions:

Laboratory simulation of dense gas behavior near obstructions appear to be reliable in the sense that predicted concentration contours do not require major modifications to reproduce field data. Based on this Surface Pattern Comparison analysis no limitations could be placed on the largest model scales which might be used to simulate dense cloud behavior.

Table 4.7-1 Prototype and Model Conditions Compared from Thorney Island Field and Model Tests by Davies and Inman

INSTANTANEOUS RELEASES

TRIAL CONFIGURATION/NO.	SCALE RATIO	(SPECIFIC GRAVITY)f	(SPECIFIC GRAVITY)m	U10,f m/s	U10,m m/s	VOL. m3	RATE m3/min	D cm2/s	(Ri)B	(Po/Ri)m	(Re)m	(Rom)m	PASQUILL STABILITY
UI/06	100.00	1.70	1.70	2.40	.24	2000.00	-	.08	15.50	269.00	1679.89	7.73	D
UI/08	150.00	1.70	1.70	2.40	.20	2000.00	-	.08	15.50	146.00	914.42	6.51	E
UI/12	100.00	2.30	2.30	2.60	.26	1950.00	-	.08	24.70	184.00	1804.59	8.37	E
UI/12	150.00	2.30	2.30	2.60	.21	1950.00	-	.08	24.70	100.00	982.30	6.84	E
UI/17	40.00	4.20	4.20	5.30	.84	1700.00	-	.08	12.50	2502.00	13890.88	26.98	D/E
UI/17	100.00	4.20	4.20	5.30	.53	1700.00	-	.08	12.50	633.00	3514.14	17.07	D/E
UI/17	150.00	4.20	4.20	5.30	.43	1700.00	-	.08	12.50	345.00	1912.46	13.93	D/E
UI/19	100.00	2.10	2.10	6.60	.66	2100.00	-	.08	3.50	3556.00	4635.46	21.25	D/E
UI/19	150.00	2.10	2.10	6.60	.54	2100.00	-	.08	3.50	1936.00	2555.88	17.35	D/E
SW-50/20	100.00	1.90	1.90	5.60	.56	1920.00	-	.08	3.50	2655.00	3866.78	18.03	C/D
SW-50/20	150.00	1.90	1.90	5.60	.46	1920.00	-	.08	3.50	1445.00	2104.81	14.72	C/D
SW-50/21	100.00	2.00	2.00	3.90	.39	2050.00	-	.08	9.00	807.00	2752.39	12.56	D/E
SW-50/21	150.00	2.00	2.00	3.90	.32	2050.00	-	.08	9.00	439.00	1498.21	10.25	D/E
SW-50/22	150.00	4.20	4.20	6.00	.49	1400.00	-	.08	7.80	500.00	2029.79	15.77	D/E
90-50/28	100.00	2.00	2.00	9.00	.90	1950.00	-	.08	1.50	9918.00	6130.01	28.98	D
90-50/28	150.00	2.00	2.00	9.00	.73	1950.00	-	.08	1.50	5399.00	3341.11	23.66	D
90-27/29	100.00	2.00	2.00	5.50	.55	1950.00	-	.08	4.10	2264.00	3817.41	17.71	D
90-27/29	150.00	2.00	2.00	5.50	.45	1950.00	-	.08	4.10	1232.00	2077.93	14.46	D
UI/34	40.00	1.80	1.80	1.40	.22	2110.00	-	.08	60.40	184.00	3943.30	7.13	F

CONTINUOUS RELEASES

TRIAL CONFIGURATION/NO.	SCALE RATIO	(SPECIFIC GRAVITY)f	(SPECIFIC GRAVITY)m	U10,f m/s	U10,m m/s	VOL. m3	RATE m3/min	D cm2/s	(Ri)B	(Po/Ri)m	(Re)m	(Rom)m	PASQUILL STABILITY
FL/30	40.00	1.40	1.40	4.30	.68	1603.00	260.00	.08	.20	10700	947.94	21.89	E
FL/30	100.00	1.40	1.40	4.30	.43	1603.00	260.00	.08	.20	2700	239.81	13.85	E
FL/30	150.00	1.40	1.40	4.30	.35	1603.00	260.00	.08	.20	1500	130.54	11.31	E
FL/30	250.00	1.40	1.40	4.30	.27	1603.00	260.00	.08	.20	700	60.67	8.76	E
FL/33	40.00	1.60	2.50	2.80	.70	1870.00	340.00	.08	1.20	5100	1383.09	22.54	D/E
FL/33	100.00	1.60	2.50	2.80	.44	1870.00	340.00	.08	1.20	800	349.90	14.26	D/E
FL/33	150.00	1.60	2.50	2.80	.36	1870.00	340.00	.08	1.20	400	190.46	11.64	D/E
FL/33	250.00	1.60	2.50	2.80	.28	1870.00	340.00	.08	1.20	200	88.52	9.02	D/E
FL/36	40.00	1.60	2.00	2.40	.49	1963.00	310.00	.08	1.60	1600	998.33	15.77	F/G
FL/36	100.00	1.60	2.00	2.40	.31	1963.00	310.00	.08	1.60	400	252.56	9.98	F/G
FL/36	150.00	1.60	2.00	2.40	.25	1963.00	310.00	.08	1.60	200	137.48	8.15	F/G
FL/37	40.00	1.60	1.60	3.20	.51	1891.00	255.00	.08	.70	2900	809.85	16.29	E
FL/37	100.00	1.60	1.60	3.20	.32	1891.00	255.00	.08	.70	700	204.88	10.30	E
FL/37	150.00	1.60	1.60	3.20	.26	1891.00	255.00	.08	.70	400	111.52	8.41	E
FL/37	250.00	1.60	1.60	3.20	.20	1891.00	255.00	.08	.70	200	51.83	6.52	E
UC/38	40.00	1.60	1.60	3.80	.60	1867.00	280.00	.08	.50	4900	924.77	19.35	F
UC/38	100.00	1.60	1.60	3.80	.38	1867.00	280.00	.08	.50	1200	233.95	12.24	F
UC/38	150.00	1.60	1.60	3.80	.31	1867.00	280.00	.08	.50	700	127.35	9.99	F
UC/38	250.00	1.60	1.60	3.80	.24	1867.00	280.00	.08	.50	300	59.19	7.74	F
FL/39	40.00	1.40	1.40	5.80	.92	1808.00	350.00	.08	.10	26200	1277.35	29.53	D
FL/39	100.00	1.40	1.40	5.80	.58	1808.00	350.00	.08	.10	6600	323.15	18.68	D
FL/39	150.00	1.40	1.40	5.80	.47	1808.00	350.00	.08	.10	3600	175.90	15.25	D
FL/39	250.00	1.40	1.40	5.80	.37	1808.00	350.00	.08	.10	1700	81.75	11.81	D
FL/40	40.00	1.20	1.20	3.10	.49	1860.00	310.00	.18	.20	5400	878.87	15.78	D
FL/40	100.00	1.20	1.20	3.10	.31	1860.00	310.00	.18	.20	900	222.34	9.98	D
FL/40	150.00	1.20	1.20	3.10	.25	1860.00	310.00	.18	.20	500	121.03	8.15	D
FL/40	250.00	1.20	1.20	3.10	.20	1860.00	310.00	.18	.20	200	56.25	6.31	D
FL/42	40.00	1.60	1.60	3.40	.54	1973.00	185.00	.08	.50	3500	711.03	17.31	D
FL/42	100.00	1.60	1.60	3.40	.34	1973.00	185.00	.08	.50	900	179.88	10.94	D
FL/42	150.00	1.60	1.60	3.40	.28	1973.00	185.00	.08	.50	500	97.91	8.94	D
FL/42	250.00	1.60	1.60	3.40	.22	1973.00	185.00	.08	.50	200	45.61	6.92	D
FL/43	40.00	1.30	2.00	1.50	.43	1899.00	265.00	.08	2.50	1100	1031.98	15.94	F
FL/43	100.00	1.30	2.00	1.50	.27	1899.00	265.00	.08	2.50	300	261.07	8.82	F
FL/43	150.00	1.30	2.00	1.50	.22	1899.00	265.00	.08	2.50	200	142.11	7.20	F
UC/45	40.00	2.00	2.00	2.30	.36	1972.00	260.00	.08	2.60	700	693.29	11.71	E/F
UC/45	100.00	2.00	2.00	2.30	.23	1972.00	260.00	.08	2.60	200	175.59	7.41	E/F
UC/46	40.00	2.00	2.00	3.30	.52	1490.00	260.00	.08	1.00	1900	830.43	16.80	D
UC/46	100.00	2.00	2.00	3.30	.33	1490.00	260.00	.08	1.00	500	210.09	10.63	D
UC/46	150.00	2.00	2.00	3.30	.27	1490.00	260.00	.08	1.00	300	114.36	8.68	D
UC/46	250.00	2.00	2.00	3.30	.21	1490.00	260.00	.08	1.00	100	53.15	6.72	D
UC/47	40.00	2.00	2.00	1.50	.24	1930.00	250.00	.08	7.90	200	549.01	7.64	F
FT/49	40.00	1.60	2.50	2.50	.63	1907.00	260.00	.08	1.30	2200	1142.45	20.13	F
FT/49	100.00	1.60	2.50	2.50	.40	1907.00	260.00	.08	1.30	600	289.12	12.73	F
FT/49	150.00	1.60	2.50	2.50	.32	1907.00	260.00	.08	1.30	300	157.58	10.59	F
FT/49	250.00	1.60	2.50	2.50	.25	1907.00	260.00	.08	1.30	100	75.14	8.05	F
FT/50	40.00	1.40	2.00	1.74	.44	1800.00	270.00	.08	2.10	1100	971.60	14.01	F
FT/50	100.00	1.40	2.00	1.74	.28	1800.00	270.00	.08	2.10	300	245.80	8.86	F
FT/50	150.00	1.40	2.00	1.74	.22	1800.00	270.00	.08	2.10	200	133.80	7.23	F

Table 4.7-2 Summary of Surface Pattern Comparison Results for Thorney Island Trials

Configuration	Date	Trial Configuration/No.	Scale Ratio	(Density Ratio)F	(Density Ratio)M	Points Compared	Intercept of Theta, Degrees f-1	f-2	f-5
Thorney Island Field ( ) Model (1985)									
		UI/08	100	1.7	1.7	6	10	7.5	
		UI/08	150	1.7	1.7	7	27.5	7.5	
		UI/12	100	2.3	2.3	8	25	15	
		UI/12	150	2.3	2.3	8	15	12.5	
		UI/17	40	4.2	4.2	7	50	30	
		UI/17	100	4.2	4.2	8	32.5	15	
		UI/17	150	4.2	4.2	8	27.5	7.5	
		UI/19	100	2.1	2.1	10	20	7.5	
		UI/19	150	2.1	2.1	10	20	10	
		5W-50/20	100	1.9	1.9	6	15	5	
		5W-50/20	150	1.9	1.9	5	10	5	
		5W-50/21	100	2	2	5	20		
		5W-50/21	150	2	2	12	22.5	12.5	
		5W-50/22	150	4.2	4.2	6	25	17.5	
		9B-50/28	100	2	2	7	15	7.5	
		9B-50/28	150	2	2	6	15	10	
		9B-27/29	100	2	2	9	20	12.5	
		9B-27/29	150	2	2	8	27.5	12.5	
		FL/30	40	1.4	1.4	6	22.5	12.5	
		FL/30	100	1.4	1.4	6	40		
		FL/30	150	1.4	1.4	4	12.5	5	
		FL/30	250	1.4	1.4	4	17.5		
		FL/33	40	1.6	2.5	6	25		
		FL/33	100	1.6	2.5	6	17.5	12.5	
		FL/33	150	1.6	2.5	6	15	10	
		FL/33	250	1.6	2.5	6	25	12.5	
		UI/34	40	1.8	1.8	8	22.5		
		FL/36	40	1.6	2	9	30	7.5	
		FL/36	100	1.6	2	11	15	7.5	
		FL/36	150	1.6	2	10	30		
		FL/37	40	1.6	1.6	4	7.5	7.5	
		FL/37	100	1.6	1.6	4	22.5	0	
		FL/37	150	1.6	1.6	4	17.5	2.5	
		FL/37	250	1.6	1.6	4	15	0	
		UC/38	40	1.6	1.6	7	20	7.5	
		UC/38	100	1.6	1.6	8	25	10	
		UC/38	150	1.6	1.6	11	30	22.5	
		UC/38	250	1.6	1.6	10	27.5	15	
		FL/39	40	1.4	1.4	6	22.5	7.5	
		FL/39	100	1.4	1.4	6	20	10	
		FL/39	150	1.4	1.4	6	22.5	10	
		FL/39	250	1.4	1.4	6	17.5	5	
		FL/40	40	1.2	1.2	5	7.5	7.5	
		FL/40	100	1.2	1.2	7	15	0	
		FL/40	150	1.2	1.2	7	7.5	2.5	
		FL/40	250	1.2	1.2	6	10	10	
		FL/42	40	1.6	1.6	5	5	0	
		FL/42	100	1.6	1.6	5	7.5	0	
		FL/42	150	1.6	1.6	5	15	15	
		FL/42	250	1.6	1.6	5	12.5	7.5	
		FL/43	40	1.3	2	8		5	5
		FL/43	100	1.3	2	12		20	7.5
		FL/43	150	1.3	2	12		20	10
		UC/45	40	2	2	7	15	12.5	
		UC/45	100	2	2	14	22.5	15	10
		UC/46	40	2	2	5	22.5	5	
		UC/46	100	2	2	6	10	10	
		UC/46	150	2	2	6	17.5	10	
		UC/46	250	2	2	6	27.5	10	
		UC/47	40	2	2	15		15	2.5
		FT/49	40	1.6	2.5	14	20	2.5	2.5
		FT/49	100	1.6	2.5	14	27.5	10	
		FT/49	150	1.6	2.5	14	25	10	
		FT/49	250	1.6	2.5	15	27.5	10	
		FT/50	40	1.4	2	32.5	30	15	
		FT/50	100	1.4	2	17	32.5	20	
		FT/50	150	1.4	2	18	35	10	

UI = Unobstructed instantaneous release
5W-50 = 5m wall at 50m
9B-50 = 9m square bldg, 50m at 45 degree down range
9B-27 = 9m square bldg, 27m at 30 degree up range
FL = Fence longitudinal
UC = Unobstructed continuous release
FT = Fence traverse

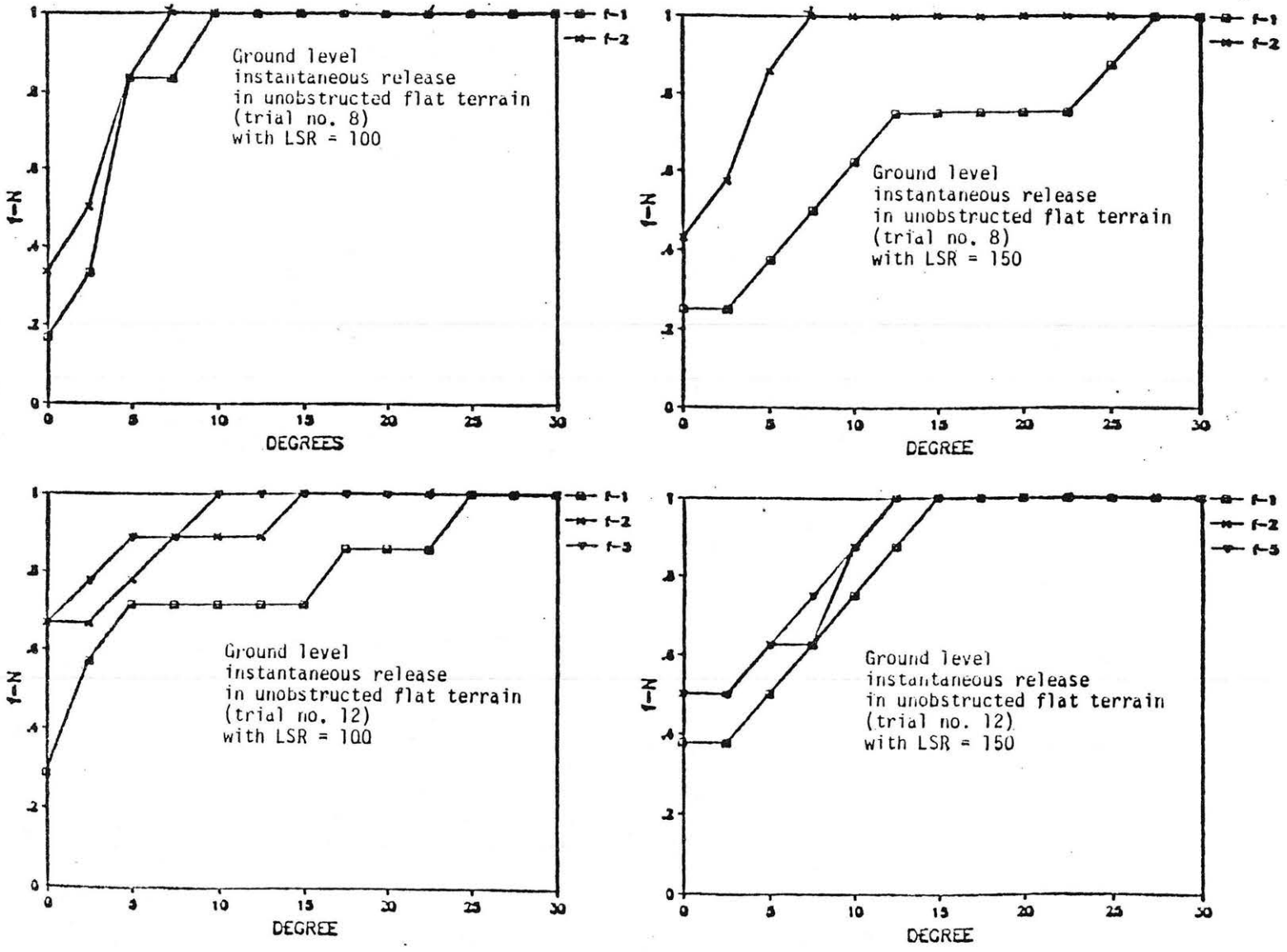

Fig. 4.7-1 Surface Pattern Comparison Results, f-N vs. Angular Displacement

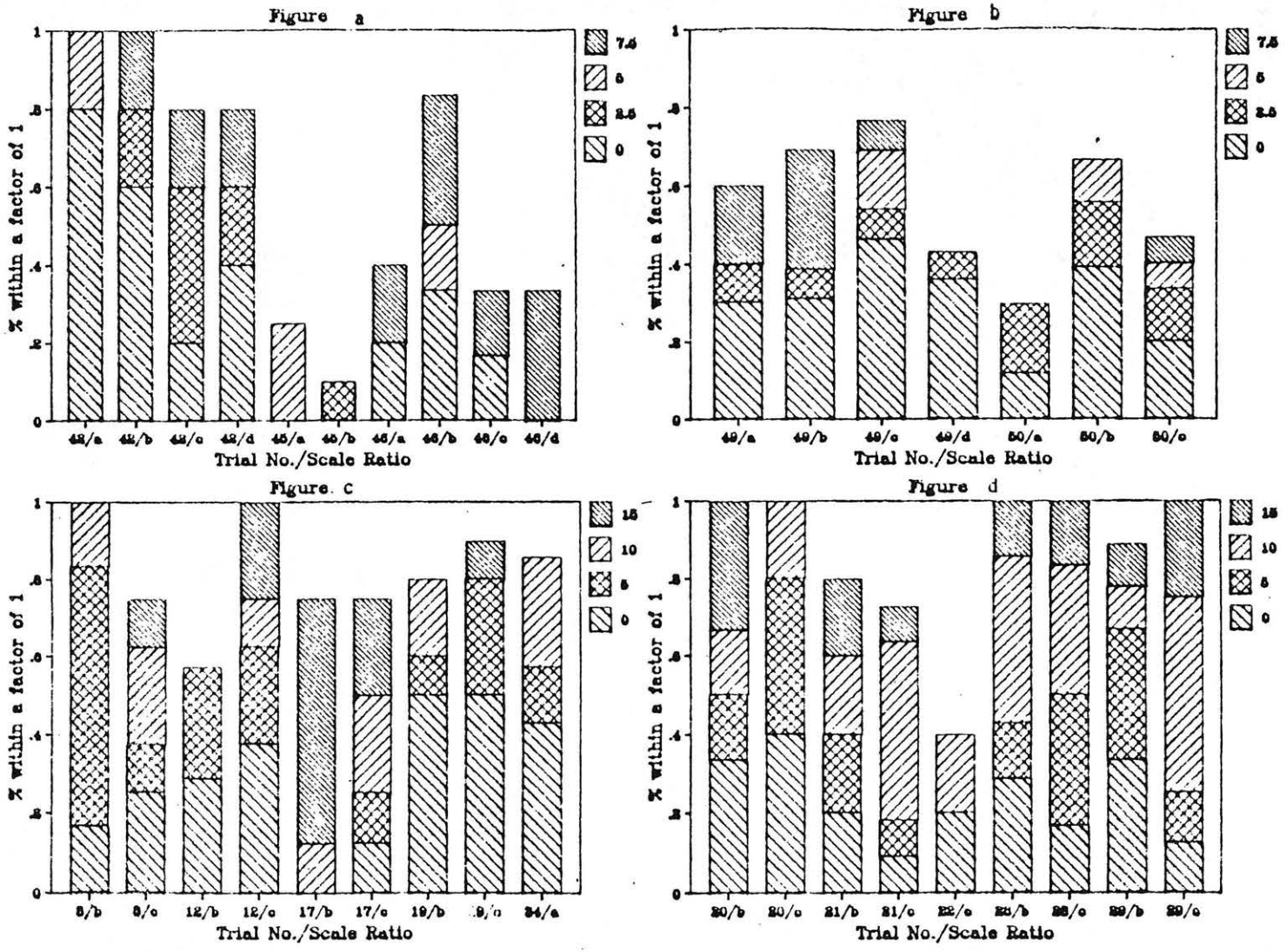

Fig. 4.7-2 Surface Pattern Comparison Results, Bar Charts of f-N vs. Angular Displacement

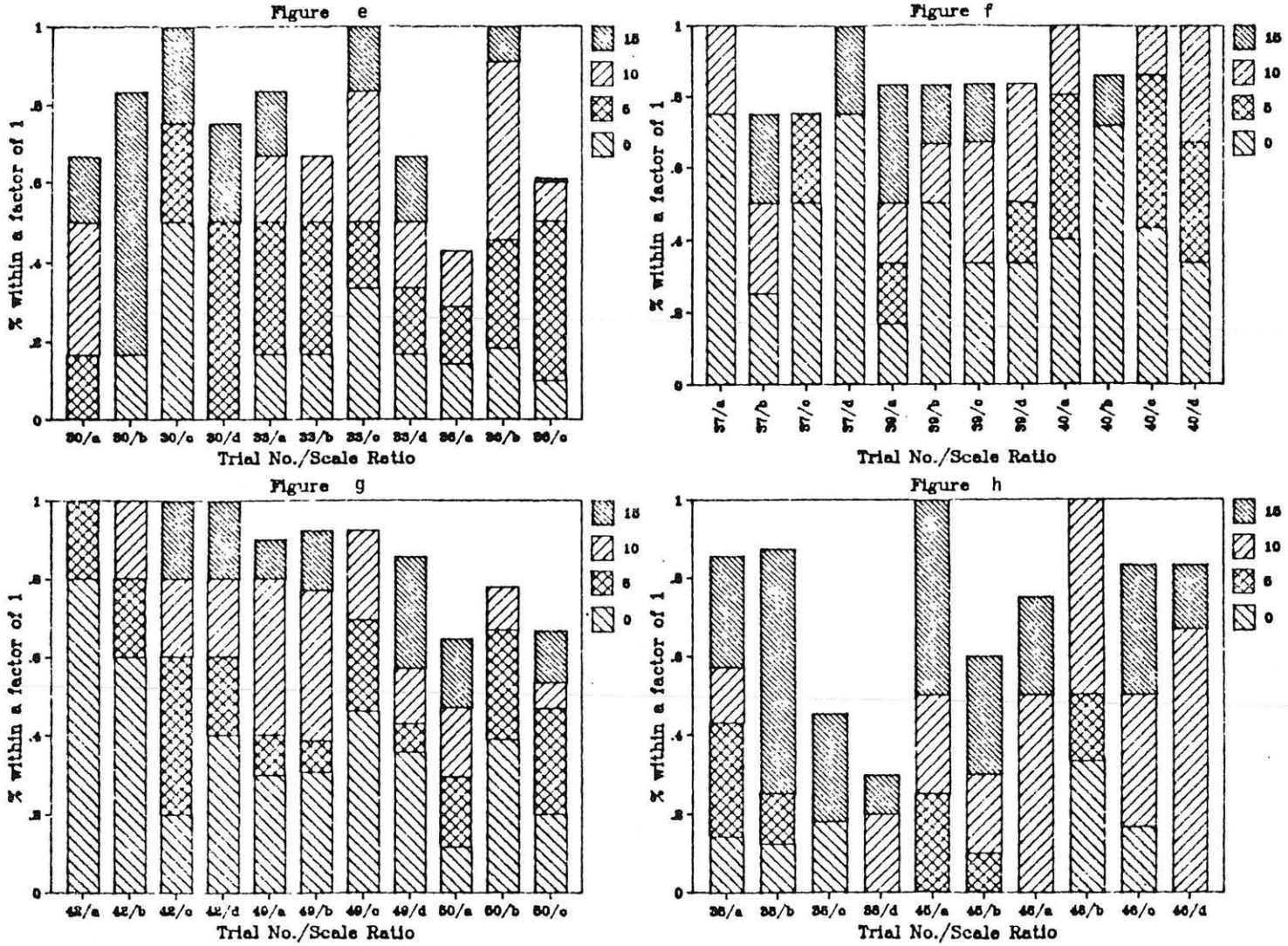

Fig. 4.7-3 Surface Pattern Comparison Results, Bar Charts of f-N vs. Angular Displacement

4.8 "LNG Vapor Barrier and Obstacle Evaluation: Wind-tunnel Prefield Test Results," Neff and Meroney, 1986

Experiment Configuration:

The experiments described by Meroney and Neff (1986) were performed to provide planning information to design the instrumentation grid used during the Falcon LNG Spill tests. The Falcon test series were performed by Lawrence Livermore National Laboratory during the summer of 1987 at the DOE Liquefied Gaseous Fuels Test Facility at Frenchman's Flats, Nevada. The pre-field laboratory tests were run at a model scale of 1:100 for a range of spill rates (10, 20, and 40 cubic meters/min of LNG), total spill volumes (50, 70 and 100 cubic meters of LNG), wind speeds (2, 3.5, and 5 m/sec), and four spill arrangements (no enclosure, 9.4 m fence only, and 9.4 or 14.1 m vortex generator added). A total of 17 tests were completed using a rake of aspirated hot-wire katherometer probes to obtain multiple replications of concentration times series at each measurement location.

The measurement grid included cross-wind sections at 15, 75, 200 and 400 m downwind with vertical profiles from ground level to a height of 28 m. Only a wind direction along the long axis of the enclosure was considered. The fence enclosure geometry and measurement grid are shown in Figures 4.8-1 and 4.8-2.

Results of Comparison:

Figure 4.8-3 considers the centerline variation of the peak concentration ratios for the fence enclosure alone and the two vortex generator additions. Notice that the peak ratio drops to a minimum value at 75 m, but thereafter all cases behave in a similar fashion and increase slowly with downstream distance. Apparently an upwind vortex generator acts to dilute gases before they pass over the downwind fence; hence, the tests with vortex generator installed produced minimum peak concentration ratios at 15 m rather than 75 m.

Figures 4.8-4 to 4.8-6 present arrival time, peak arrival time, and departure time ratios for the same conditions displayed on Figure 4.8-3. Cloud advection times are from 1.5 to 4 times larger than the no enclosure case in the immediate wake of the enclosure;however, by the time the cloud reaches 300 to 400 meters downwind, time ratios are reduced to one or less. This behavior is consistent with that observed for data from the Thorney Island tests discussed in Chapter 4.6.

Given a fence enclosure with a 14.1 m vortex generator upwind of the spill area and an LNG spill rate of 40 cubic meters/min then Figure 4.8-7 presents the influence of increase in total spill volume on peak concentration. Doubling the total spill volume appears to double ground level peak concentrations. Yet an increase in spill volume has less systematic effect on peak arrival time in Figure 4.8-8.

Similarly, Figure 4.8-9 shows that increasing spill rate while holding spill volume constant may increase peak concentrations, but the

perturbations are much smaller. Increased spill rate produces only minor variations in peak concentration arrival time on Figure 4.8-10.

Figures 4.8-11 to 4.8-14 display vertical profiles of concentration, arrival, peak arrival, and departure times for a section 15 m downstream of the downwind enclosure fence. The fence clearly mixes the cloud to greater heights, and a peak in the concentration profile occurs just above fence height (13 m). The fence also delays the arrival and departure of the cloud in the wake region, but the cloud appears first near fence height.

By the time the cloud reaches 75 m downstream of the fence, the concentrations and arrival, peak arrival, and departure times are essentially constant with height as noted on Figures 4.8-15 to 4.8-18. Measurements at stations farther downstream look similar to the 75 m data sets, except that concentrations are less and times are larger.

Figures 4.8-19 to 4.8-22 and 4.8-23 to 4.8-26 display crosswind profiles of ground level concentrations and cloud times at distance of 15 and 75 m downstream of the fence, respectively. Lateral profiles for the no-enclosure release condition extend to significantly greater lateral distances than the enclosure conditions. Visual observations of the model and field enclosure spills revealed strong three dimensionality in the cloud. Longitudinal vortices generated at enclosure corners appeared to draw the cloud over the fence first at the corners. Nonetheless, concentration and cloud time data show a strong two-dimensionality in the cloud wake.

Multilinear Regression by ANOVA of Pre-Falcon Wind Tunnel Data:

Since the pre-Falcon data set were the most complete, reliable, and comprehensive available, the SAS-PC statistical package was used to estimate coefficients in a multilinear regression on the data. The ANOVA procedure was applied to the logarithmic form of simple power law formula, i.e.:

$$(1 - C_w/C_{wo}) = (A*Fr^a*\underline{V}^b*(Vol/L_c^3)^c*(H/L_c)^d*(x/L_c)^e),$$

$$(Ta_w/Ta_{wo} - 1) = (\quad " \quad),$$

$$(Tpa_w/Tpa_{wo} - 1) = (\quad " \quad), \text{ and}$$

$$(Tda_w/Tda_{wo} - 1) = (\quad " \quad),$$

where subscripts w and wo indicate measurements with and without the enclosure present. The coefficients A, a, b, c, d, and e were determined by the ANOVA procedure. Both Forward, Backward, and Maximizing versions of the multilinear regression procedures were employed. The regression was applied to data from Runs 1, 3, 4, 7, 8, 9, 13, 10, 16, and 17 from the Neff and Meroney data set. Data were always normalized by a no-enclosure reference value taken under the same spill rate and wind speed conditions.

The regression procedure revealed that inclusion of the Froude number term did not reduce the variance of the prediction equation significantly. This probably occurs because all data points are normalized by data with the same Froude number magnitude. The dominant terms were found to be volume spill rate and total volume spilled. The optimum expressions were determined to be:

$$(1 - C_w/Cwo) = (1.56\underline{V}^{0.051}*(Vol/L_c^3)^{-0.163}*(H/L_c)^{0.040}*(x/L_c)^{-0.035}),$$

$$(Ta_w/Ta_{wo} - 1) = (0.103*\underline{V}^{-1.035}*(Vol/L_c^3)^{0.681}*(H/L_c)^{0.212}*(x/L_c)^{-0.181}),$$

$$(Tpa_w/Tpa_{wo} - 1) = (0.027*\underline{V}^{0.438}*(Vol/L_c^3)^{1.267}*(H/L_c)^{-0.264}*(x/L_c)^{-0.275}), \text{ and}$$

$$(Tda_w/Tda_{wo} - 1) = (0.142*Fr^{-0.450}*(Vol/L_c^3)^{0.230}*(H/L_c)^{1.332}*(x/L_c)^{-0.419}).$$

These relations are the best four-variable expressions determinable by the ANOVA approach. Notice the analysis presumes all time ratio data is greater than one and all peak concentration ratio data is less than one.

Presuming a correct expression has been derived by the ANOVA procedure the peak concentration ratio formula was used to prepare Figures 4.8-27 and 4.8-28. A range of conditions were selected that might be encountered during an HF release. The first figure predicts peak concentration ratios versus downwind distance for a fixed spill rate and increasing spill volume. The second figure predicts peak concentration ratios versus downwind distance for a fixed spill volume and increasing spill rate. The second figure does not seem physically realistic, since, intuitively, a fence should be very efficient at low spill rates. Examination of the original data set reveals that the variations with spill rate are themselves irregular; hence, the unusual behavior in the final regression expression.

Conclusions:

Since each measurement was repeated several times during the pre-Falcon experiment, it is possible to focus on trends that occur with confidence. A fence enclosure around a transient dense gas spill will reduce downwind concentrations, reduce the lateral extent of the cloud near the source, and delay the arrival, peak arrival and departure of the cloud at downwind measurement stations. An increase in total spill volume released or spill rate is expected to increase peak concentrations. Vertical profiles along the plume centerline reveal a maximum in plume concentrations very near the fence, but further downwind the cloud is well mixed in the vertical.

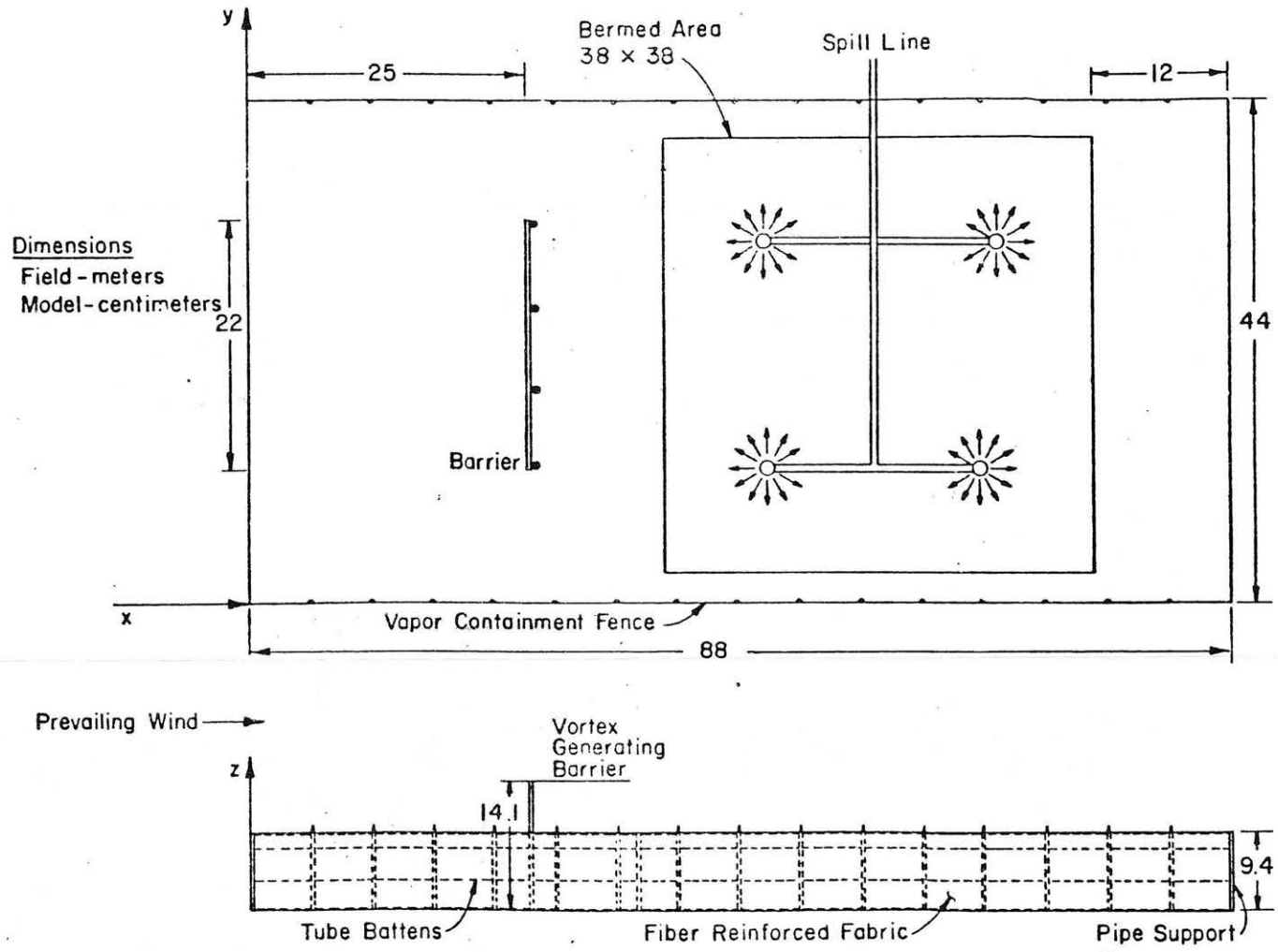

Figure 4.8-1 Fence Enclosure Geometry, Pre-Falcon Wind-tunnel Tests

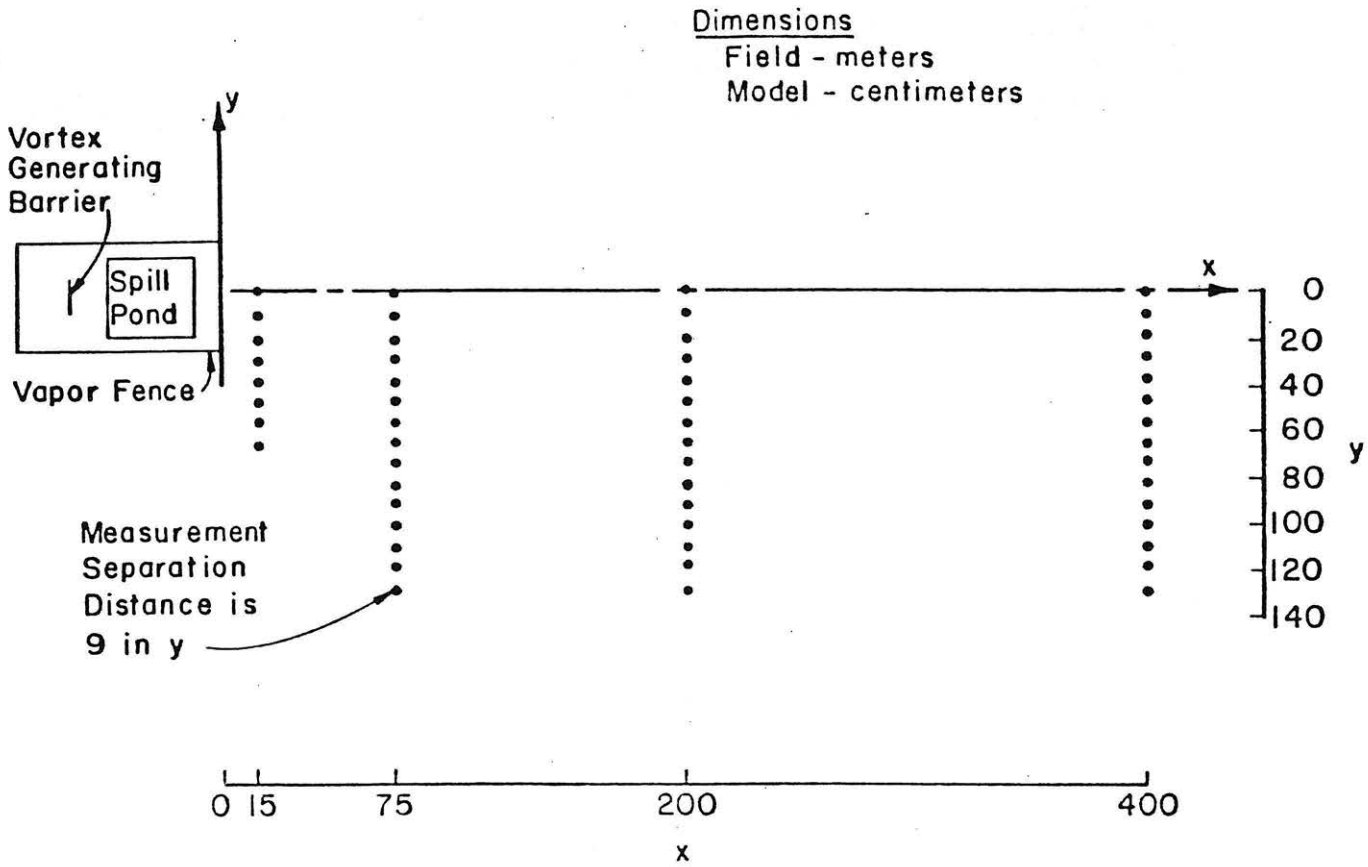

Figure 4.8-2 Measurement Grid, Pre-Falcon Wind-tunnel Tests

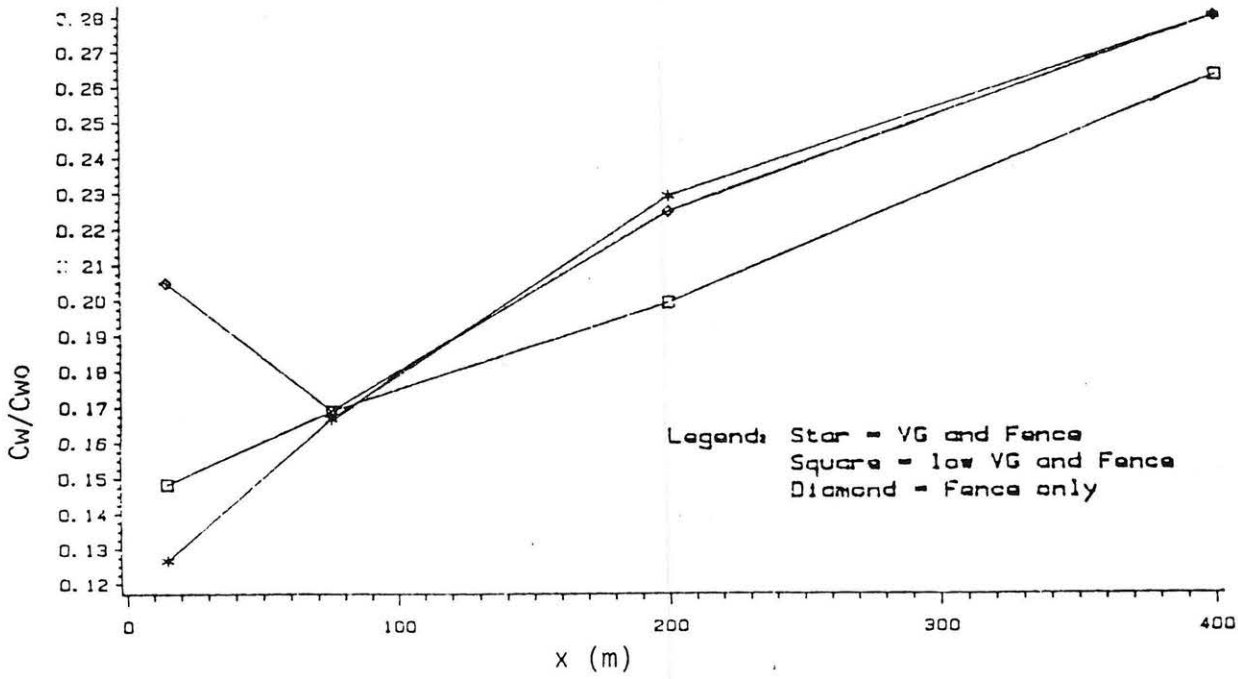

Figure 4.8-3 Peak Concentration Ratio vs. Downwind Distance, $V = 100\ m^3$, $Q = 40\ m^3/min$ LNG, Various Enclosure Arrangements

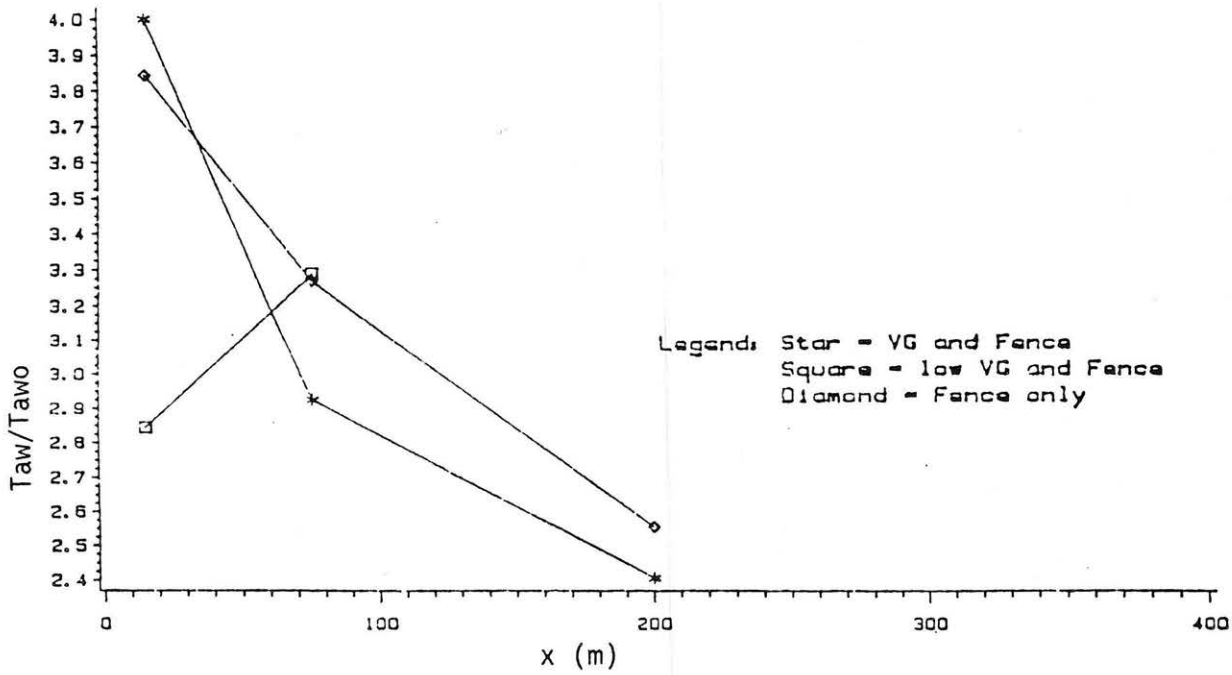

Figure 4.8-4 Arrival Time Ratio vs. Downwind Distance, $V = 100\ m^3$, $Q = 40\ m^3/min$ LNG, Various Enclosure Arrangements

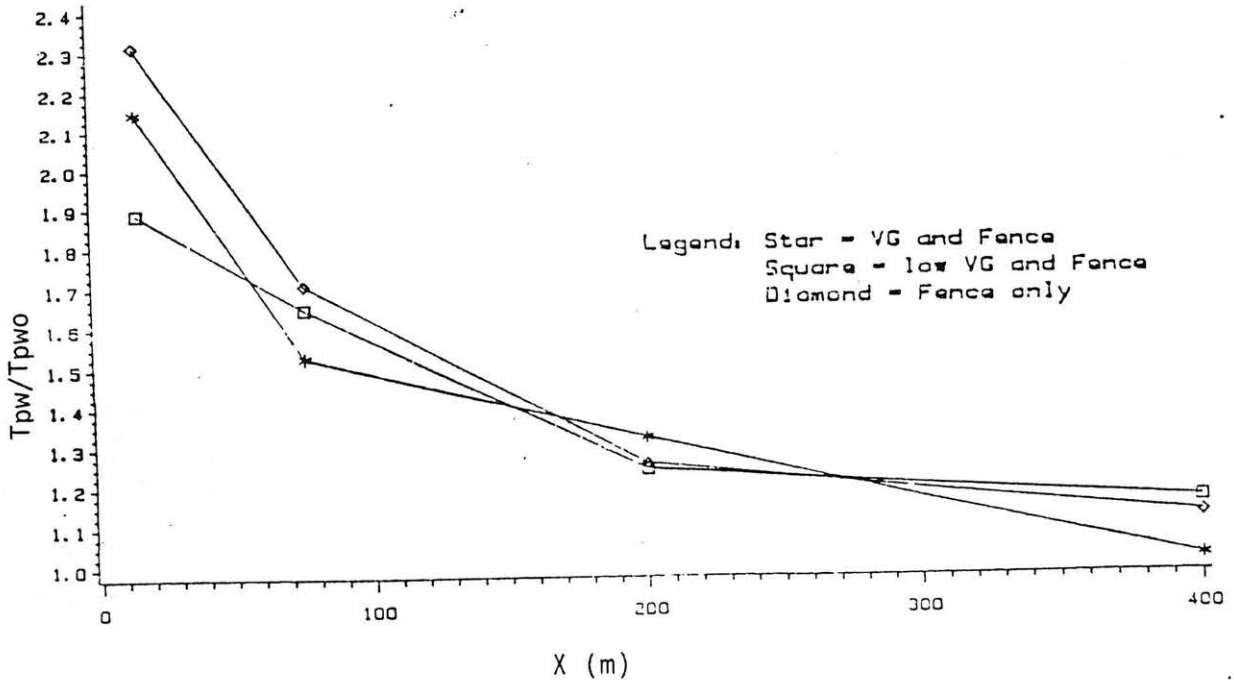

Figure 4.8-5 Peak Arrival Time Ratio vs. Downwind Distance, $V = 100\ m^3$, $Q = 40\ m^3/min$ LNG, Various Enclosure Arrangements

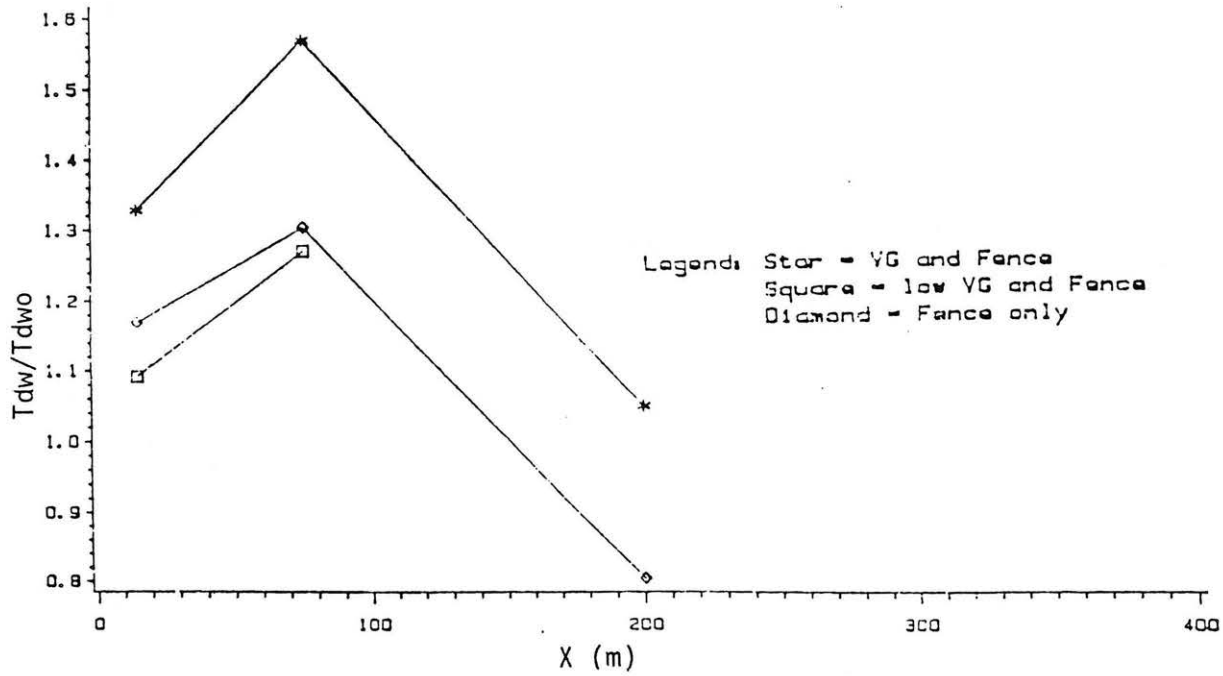

Figure 4.8-6 Departure Time Ratio vs. Downwind Distance, $V = 100\ m^3$, $Q = 40\ m^3/min$ LNG, Various Enclosure Arrangements

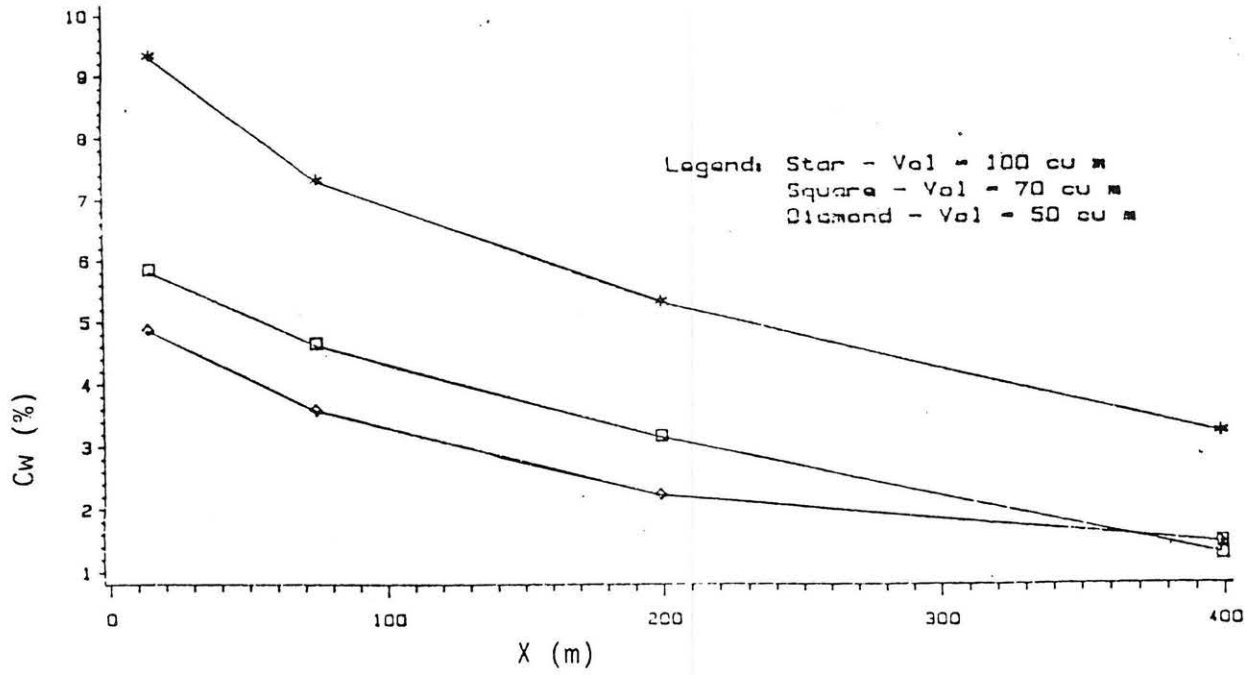

Figure 4.8-7 Peak Concentration vs. Downwind Distance, 14.1 m Vortex Generator and Fence, Q = 40 m^3/min LNG, Various Total Spill Volumes

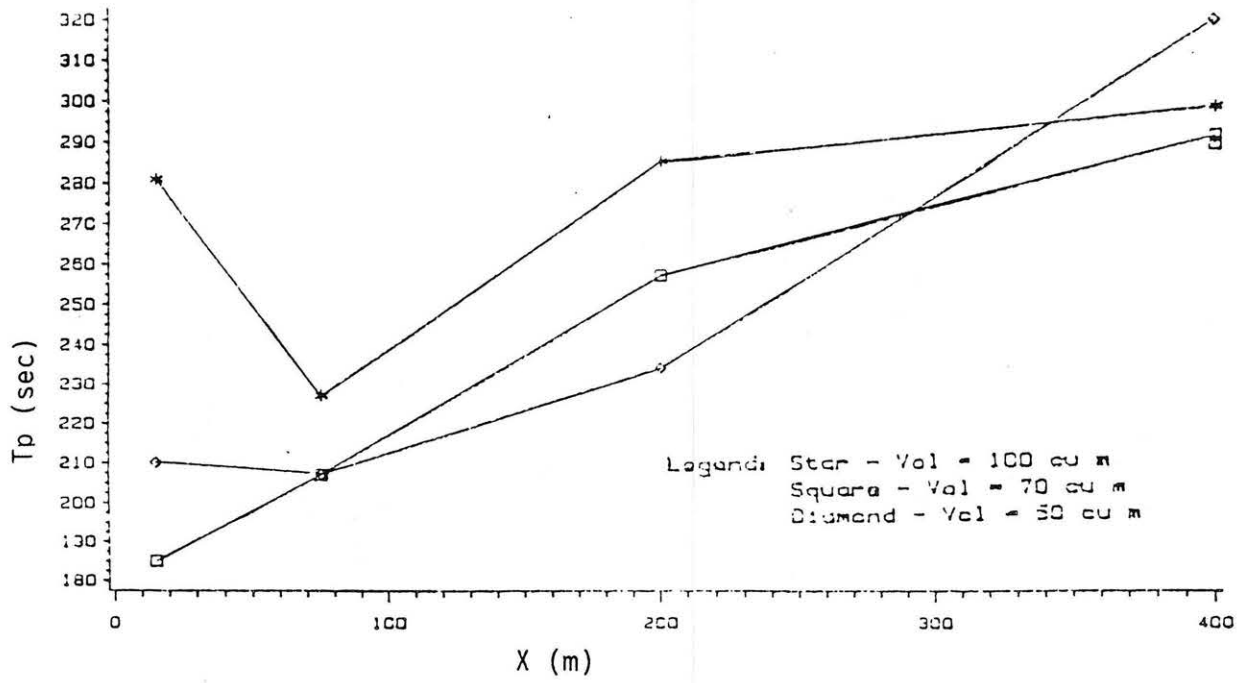

Figure 4.8-8 Arrival Time vs. Downwind Distance, 14.1 m Vortex Generator and Fence, Q = 40 m^3/min LNG, Various Total Spill Volumes

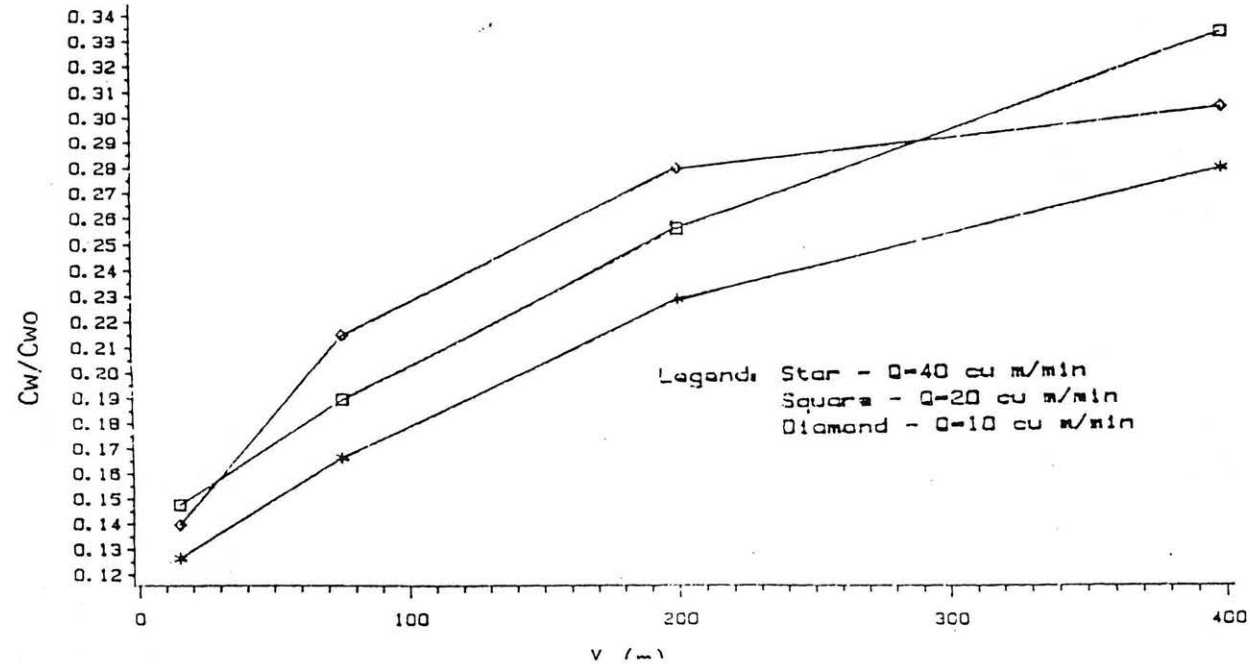

Fig. 4.8-9 Peak Concentration Ratio vs. Downwind Distance, 14.1 m Vortex Generator and Fence, V = 100 m^3 LNG, Various Spill Rates

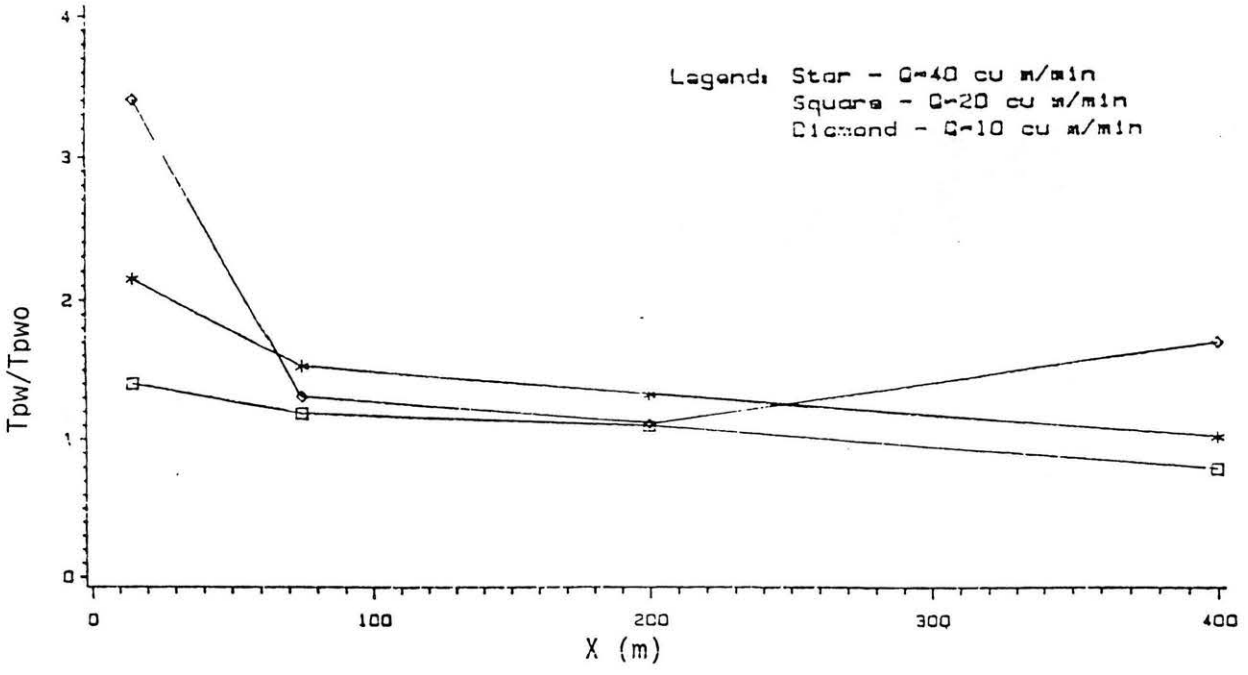

Fig. 4.8-10 Peak Time Ratio vs. Downwind Distance, 14.1 m Vortex Generator and Fence, V = 100 m^3 LNG, Various Spill Rates

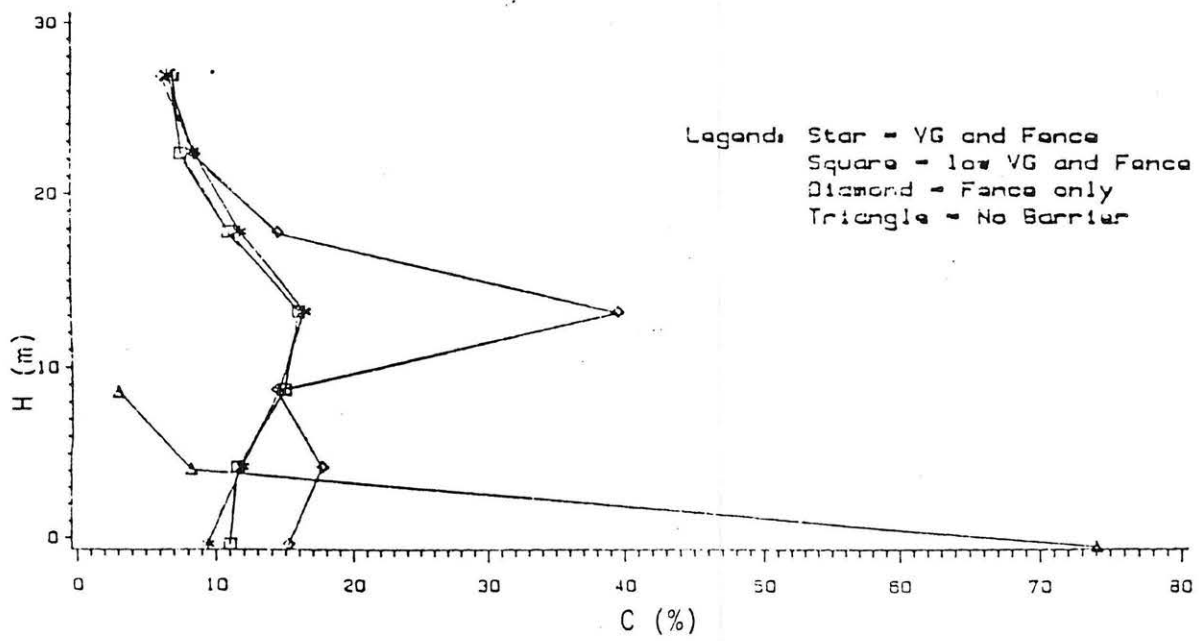

Figure 4.8-11 Peak Concentration vs. Height at X = 15 m, V = 100 m^3, Q = 40 m^3/min LNG, Various Enclosure Arrangements

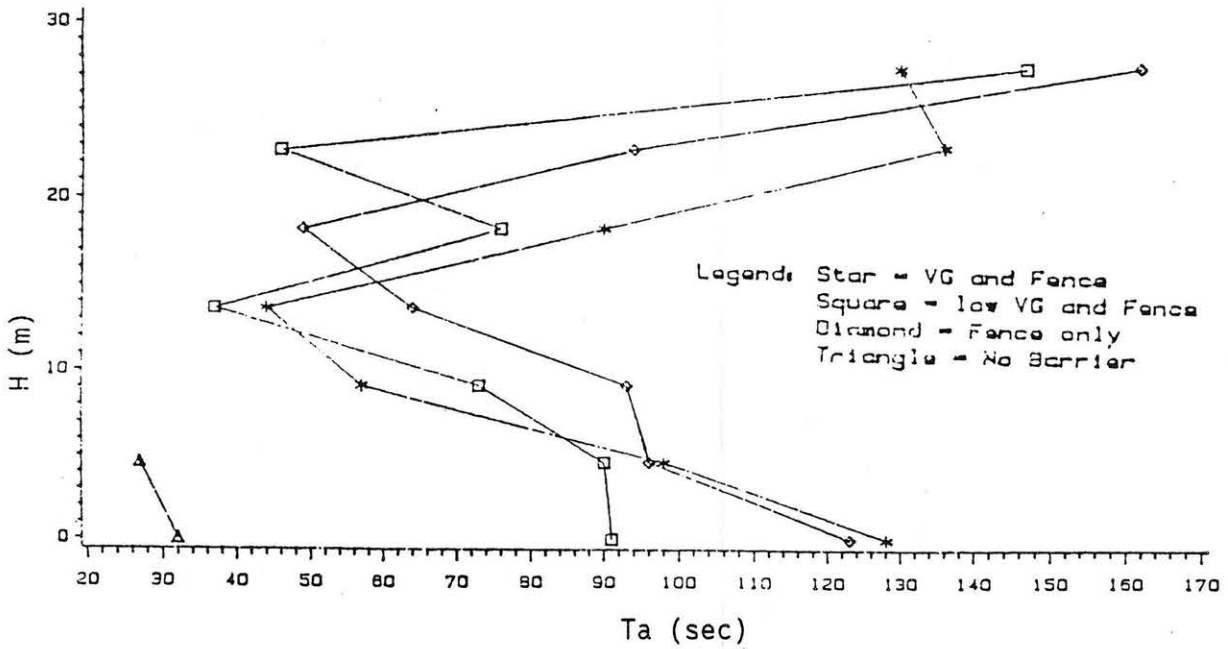

Figure 4.8-12 Arrival Time vs. Height at X = 15 m, V = 100 m^3, Q = 40 m^3/min LNG, Various Enclosure Arrangements

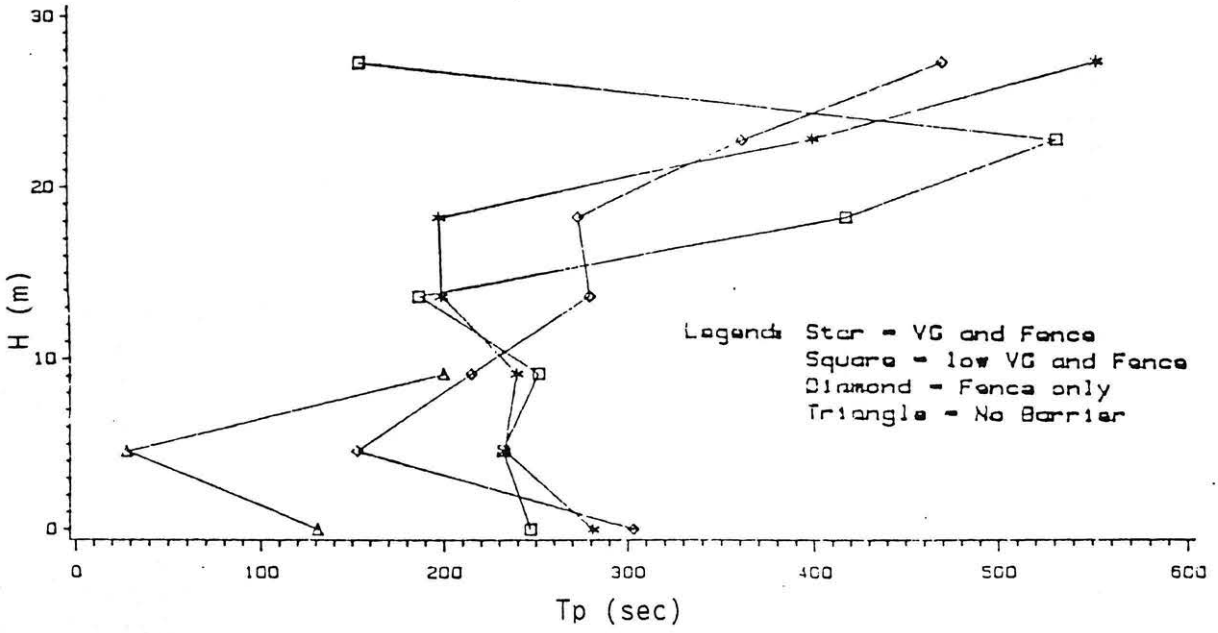

Figure 4.8-13 Peak Arrival Time vs. Height at X = 15 m, V = 100 m^3, Q = 40 m^3/min LNG, Various Enclosure Arrangements

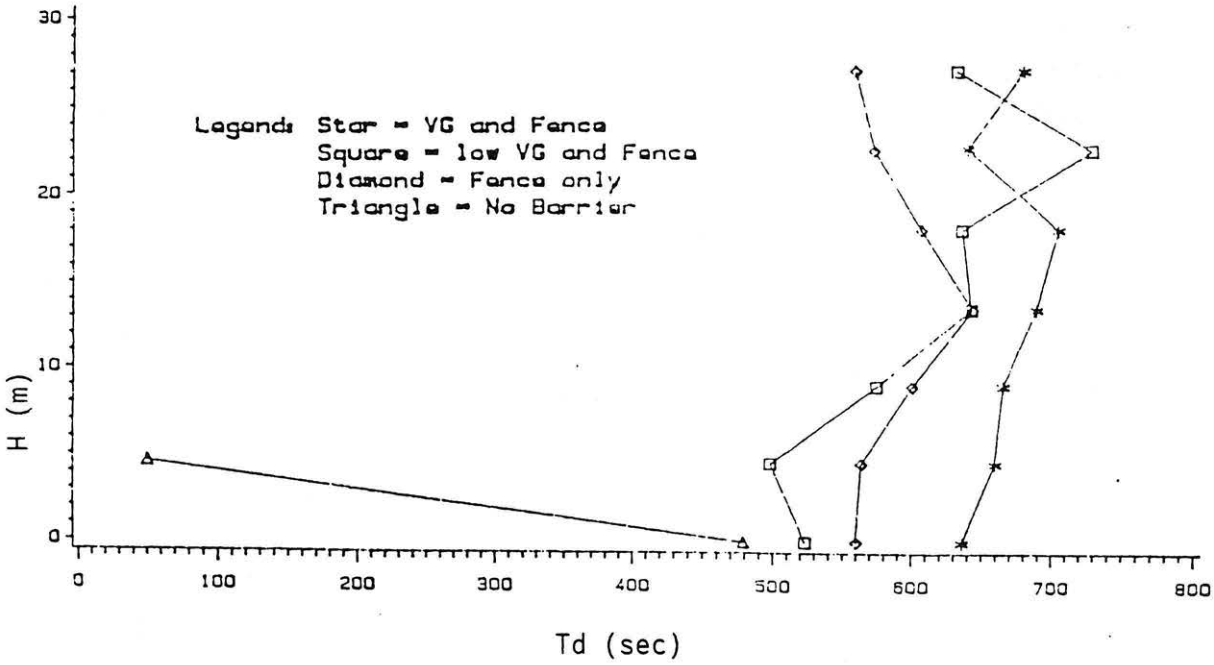

Figure 4.8-14 Departure Time vs. Height, at X = 15 m, V = 100 m^3, Q = 40 m^3/min LNG, Various Enclosure Arrangements

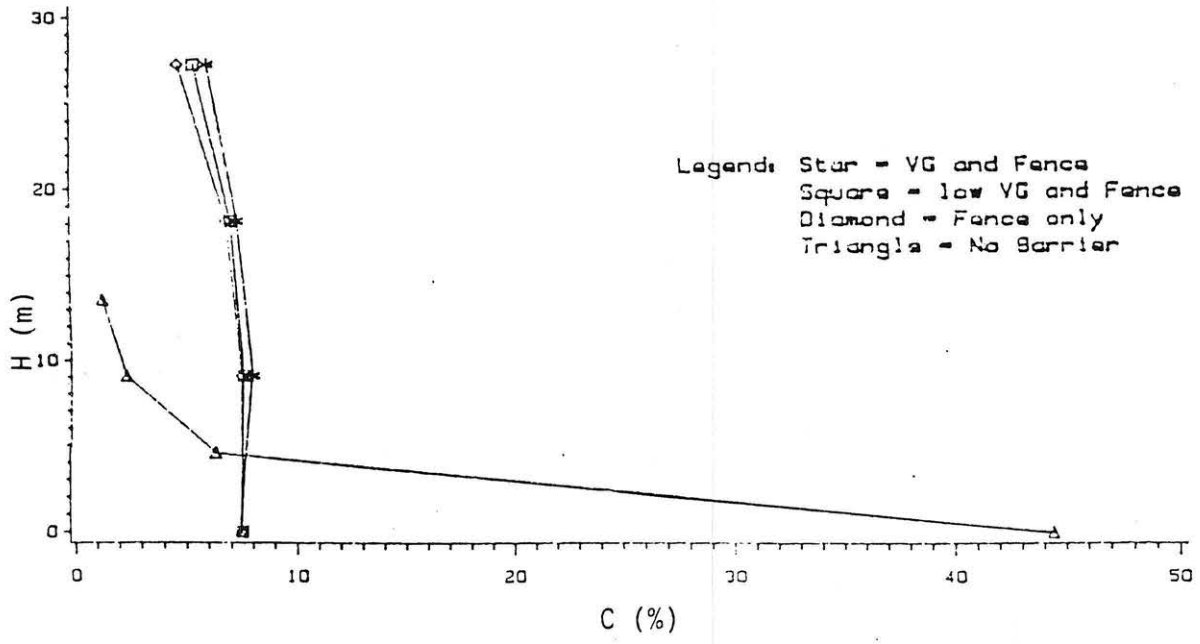

Figure 4.8-15 Peak Concentration vs. Height at X = 75 m, V = 100 m^3, Q = 40 m^3/min LNG, Various Enclosure Arrangements

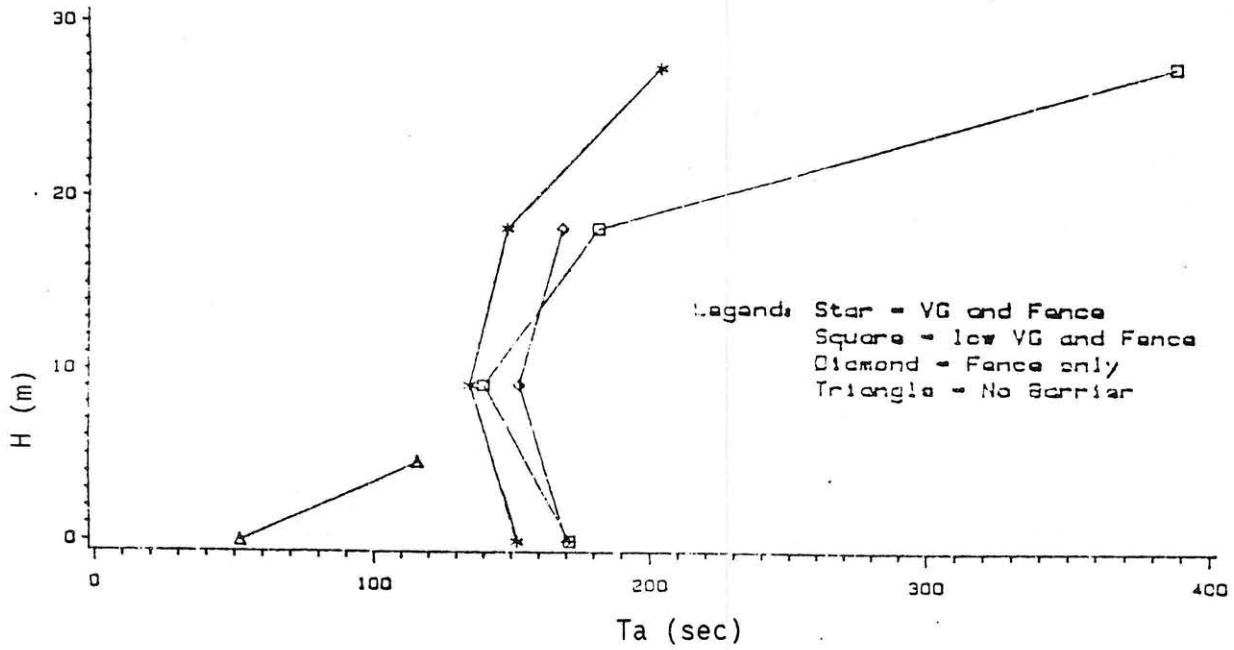

Figure 4.8-16 Arrival Time vs. Height at X = 75 m, V = 100 m^3, Q = 40 m^3/min LNG, Various Enclosure Arrangements

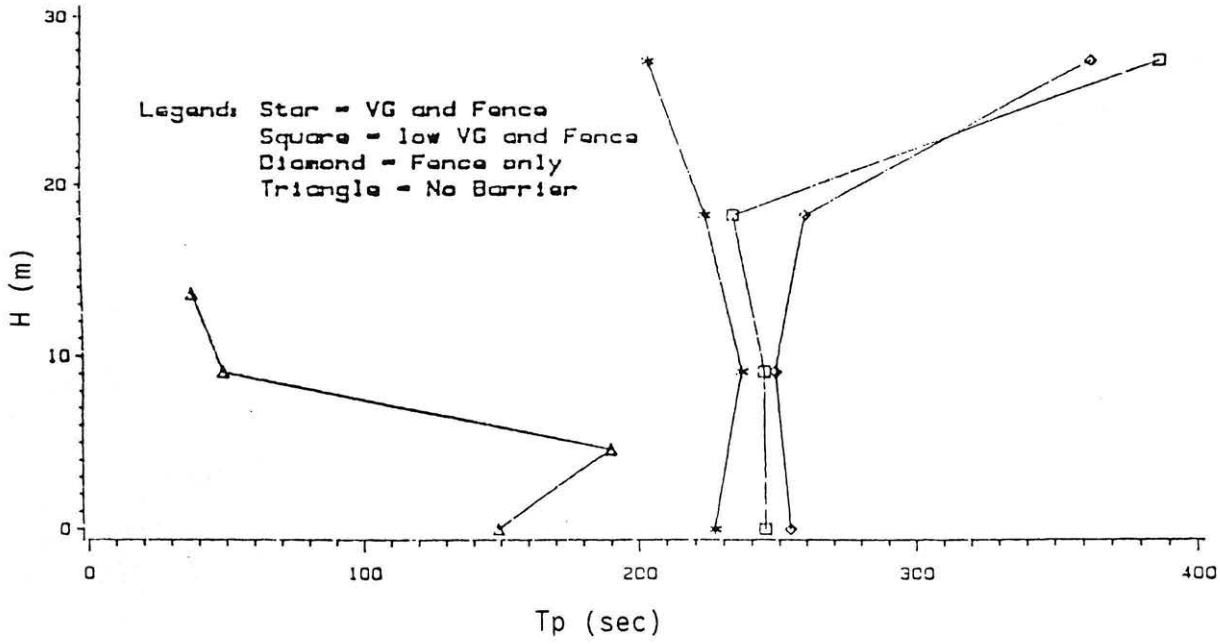

Figure 4.8-17 Peak Arrival Time vs. Height at X = 75 m, V = 100 m^3, Q = 40 m^3/min LNG, Various Enclosure Arrangements

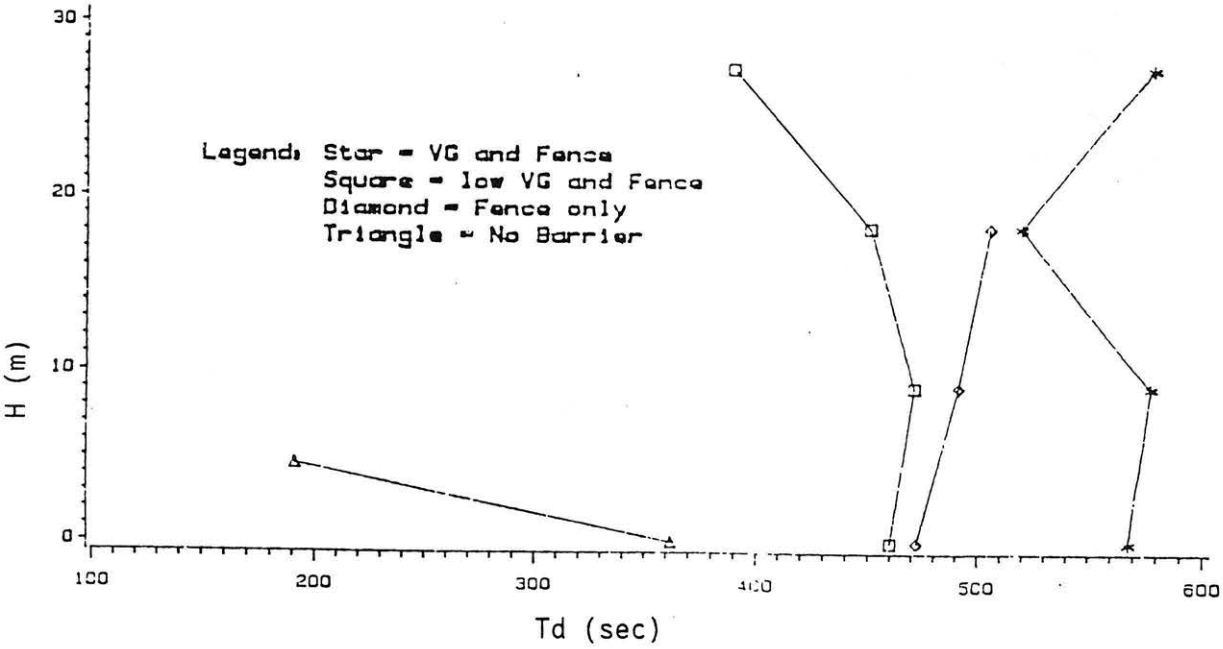

Figure 4.8-18 Departure Time vs. Height at X = 75 m, V = 100 m^3, Q = 40 m^3/min LNG, Various Enclosure Arrangements

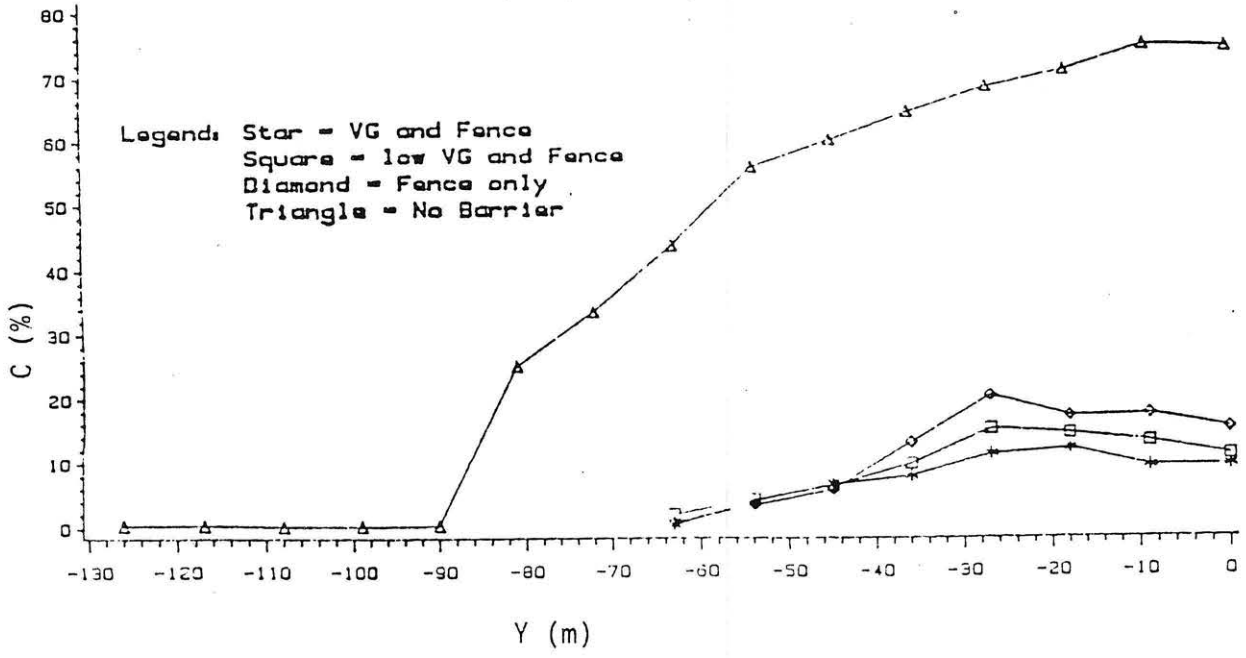

Figure 4.8-19 Peak Concentration vs Crosswind Distance at X = 15 m, V = 100 m^3, Q = 40 m^3/min LNG, Various Enclosure Arrangements

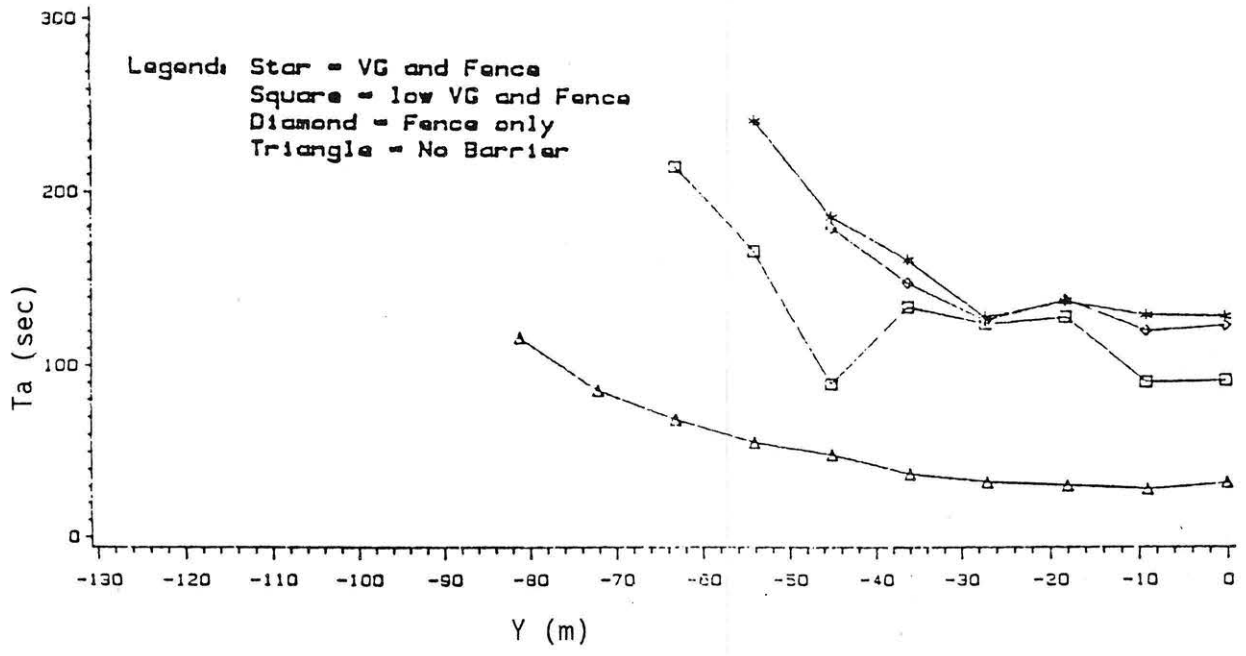

Figure 4.8-20 Arrival Time vs Crosswind Distance at X = 15 m, V = 100 m^3, Q = 40 m^3/min LNG, Various Enclosure Arrangements

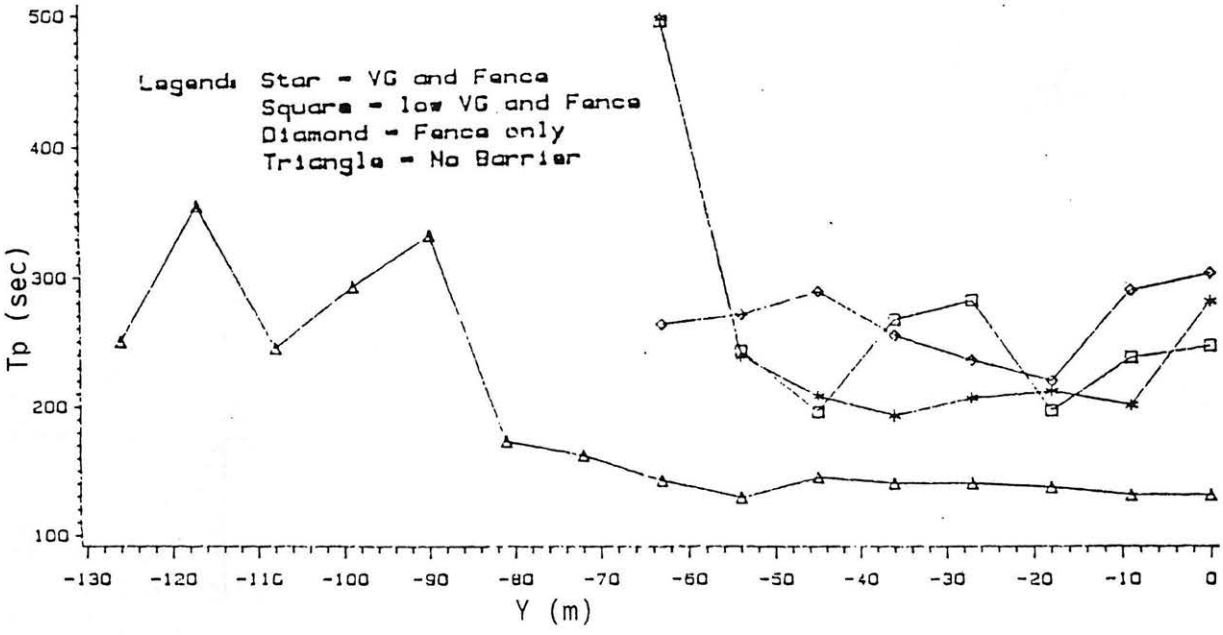

Figure 4.8-21 Peak Arrival Time vs Crosswind Distance at X = 15 m, V = 100 m^3, Q = 40 m^3/min LNG, Various Enclosure Arrangements

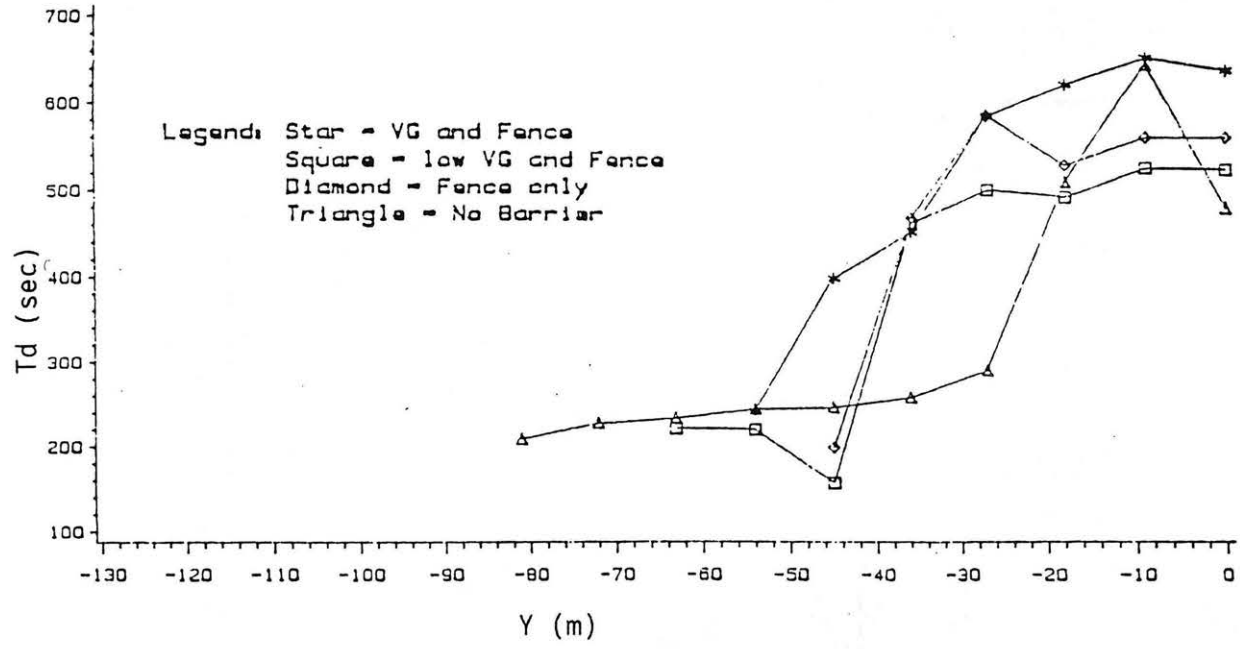

Figure 4.8-22 Departure Time vs Crosswind Distance at X = 15 m, V = 100 m^3, Q = 40 m^3/min LNG, Various Enclosure Arrangements

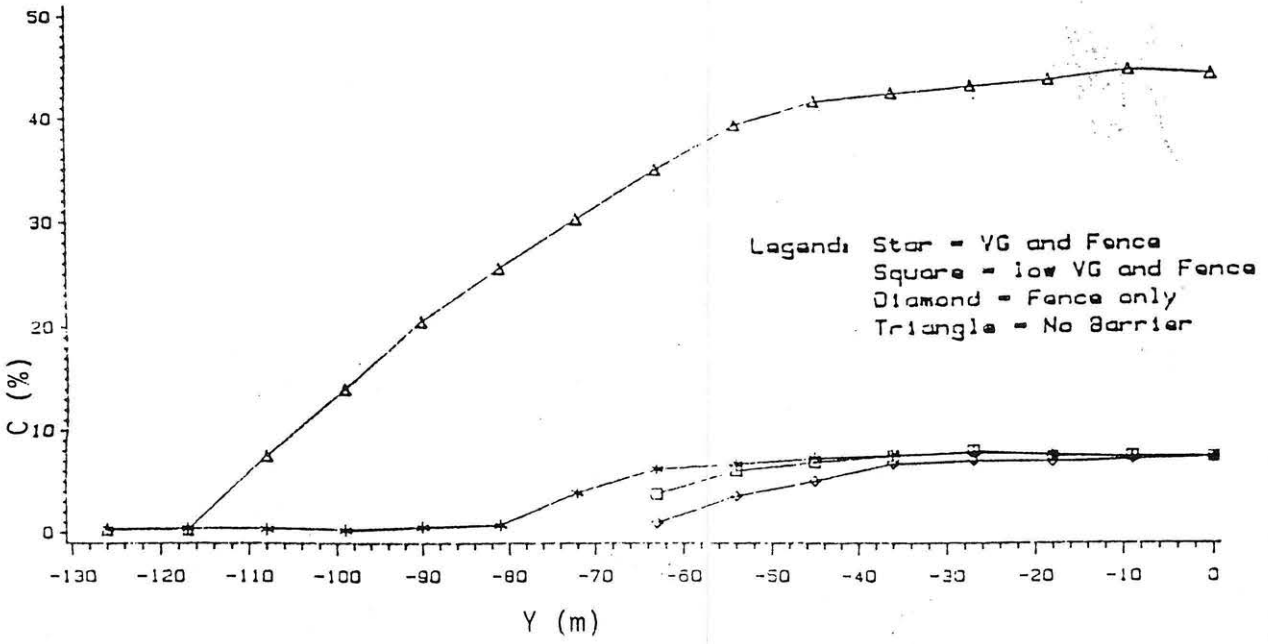

Figure 4.8-23 Peak Concentration vs Crosswind Distance at X = 75 m, V = 100 m^3, Q = 40 m^3/min LNG, Various Enclosure Arrangements

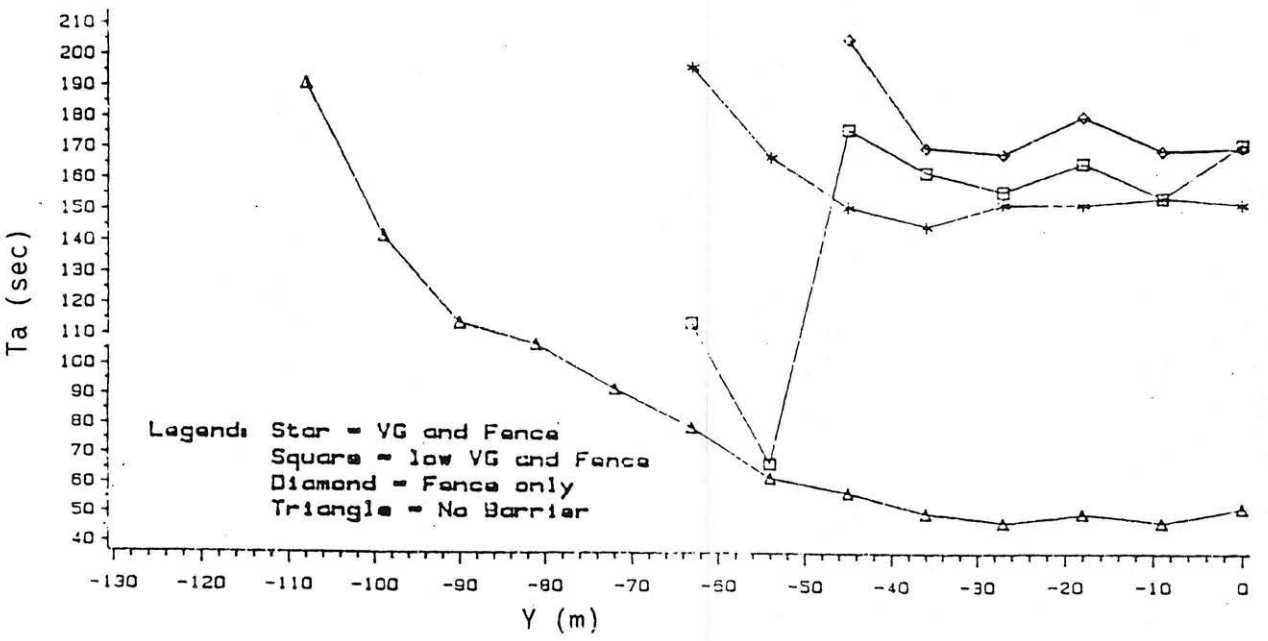

Figure 4.8-24 Arrival Time vs Crosswind Distance at X = 75 m, V = 100 m^3, Q = 40 m^3/min LNG, Various Enclosure Arrangements

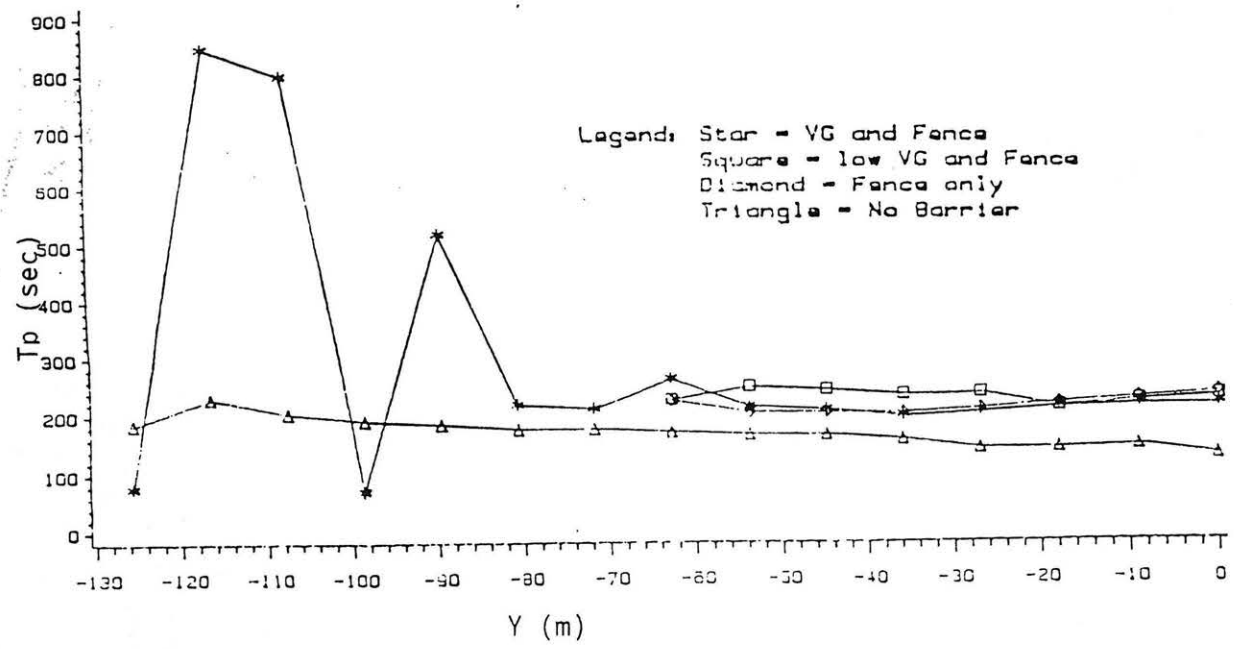

Figure 4.8-25 Peak Arrival Time vs Crosswind Distance at X = 75 m, V = 100 m^3, Q = 40 m^3/min LNg, Various Enclosure Arrangements

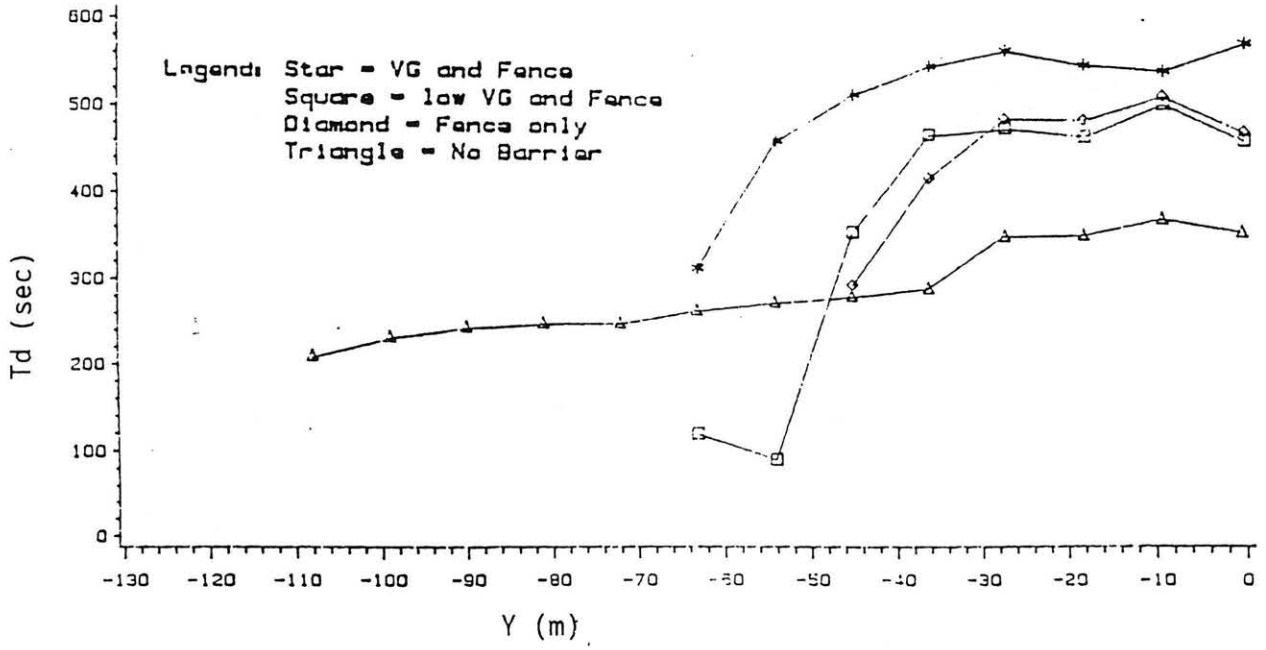

Figure 4.8-26 Departure Time vs Crosswind Distance at X = 75 m, V = 100 m^3, Q = 40 m^3/min LNG, Various Enclosure Arrangements

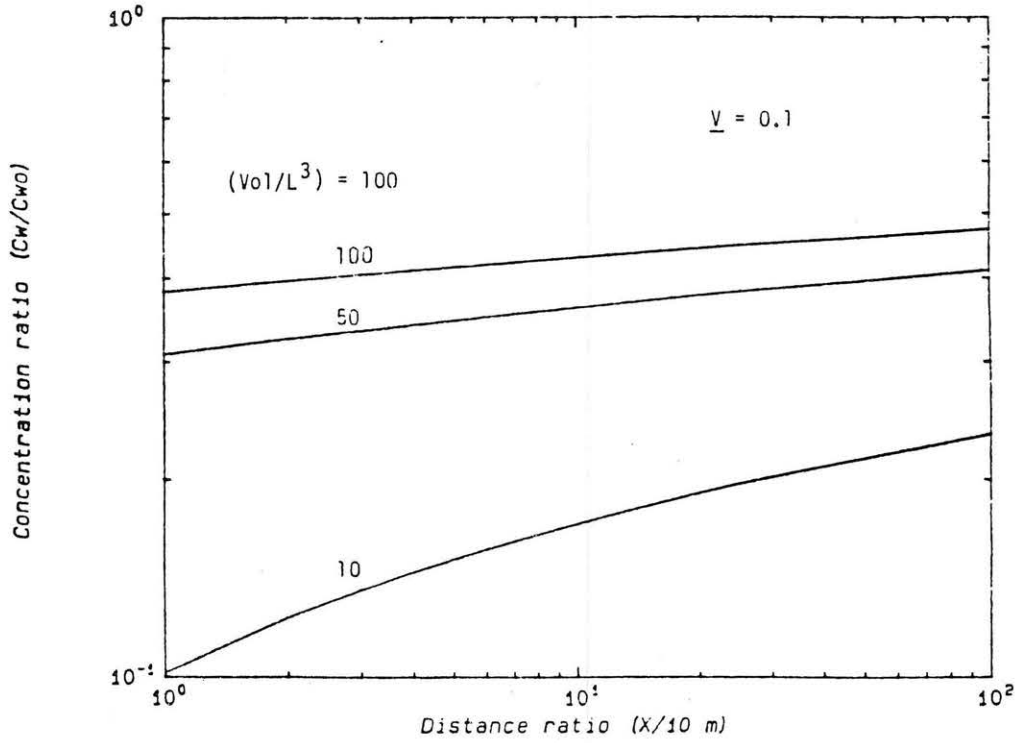

Figure 4.8-27 Peak Concentration Ratio vs. Downwind Distance, Volume Flux Ratio = 0.1, Total Volume Ratio = 10, 50 and 100, Predicted by ANOVA Relation

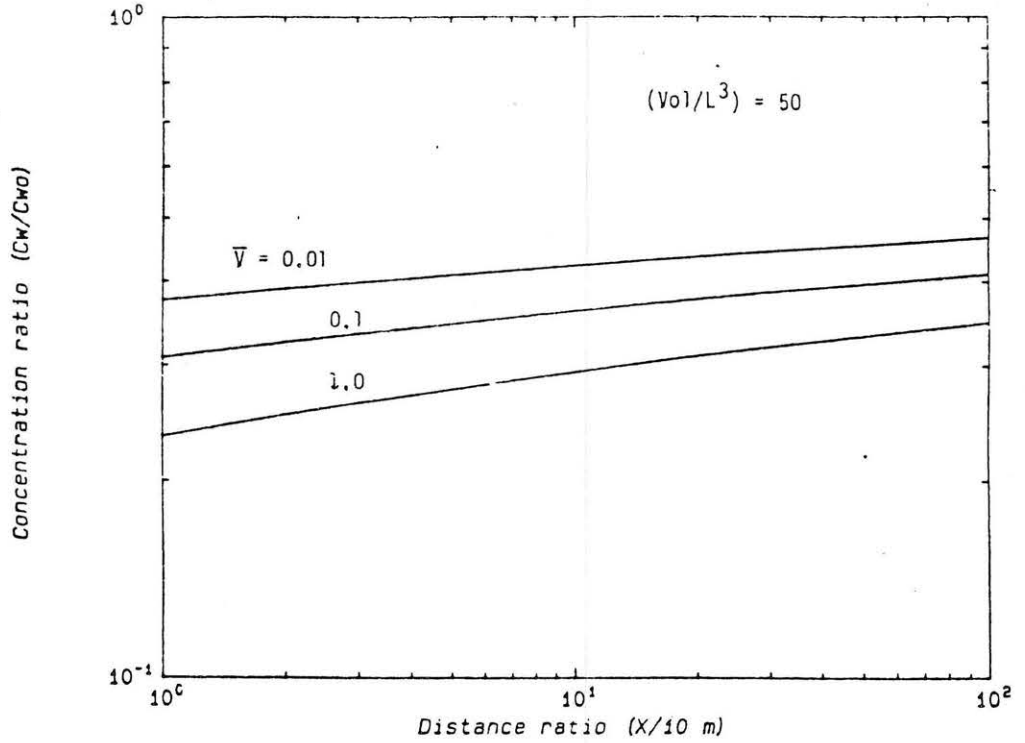

Figure 4.8-28 Peak Concentration Ratio vs. Downwind Distance, Total Volume Ratio = 50, Volume Flux Ratio = 0.01, 0.1 and 1.0, Predicted by ANOVA Relation

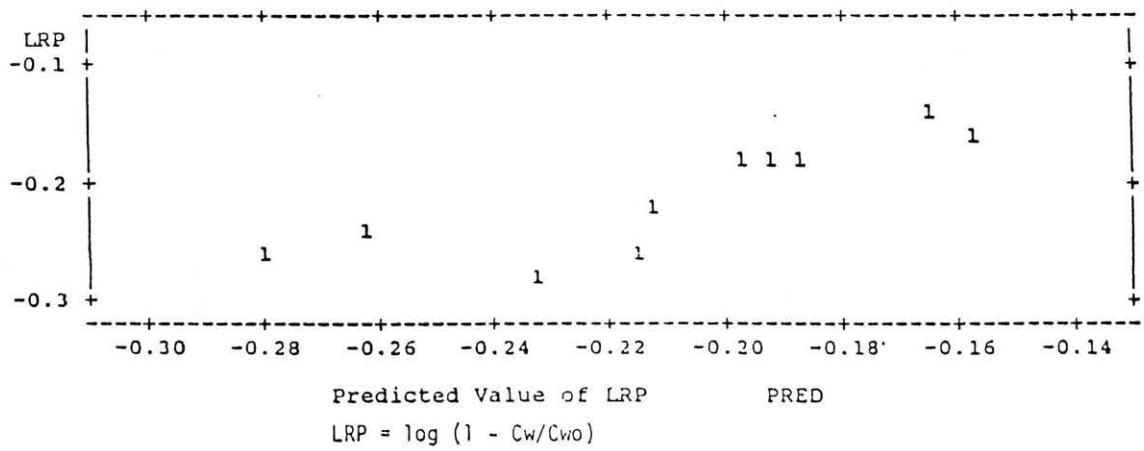

Figure 4.8-29 Measured vs Predicted Values of the Logarithmic Ratio in Concentrations with and without Vapor Fence for Falcon Test Series

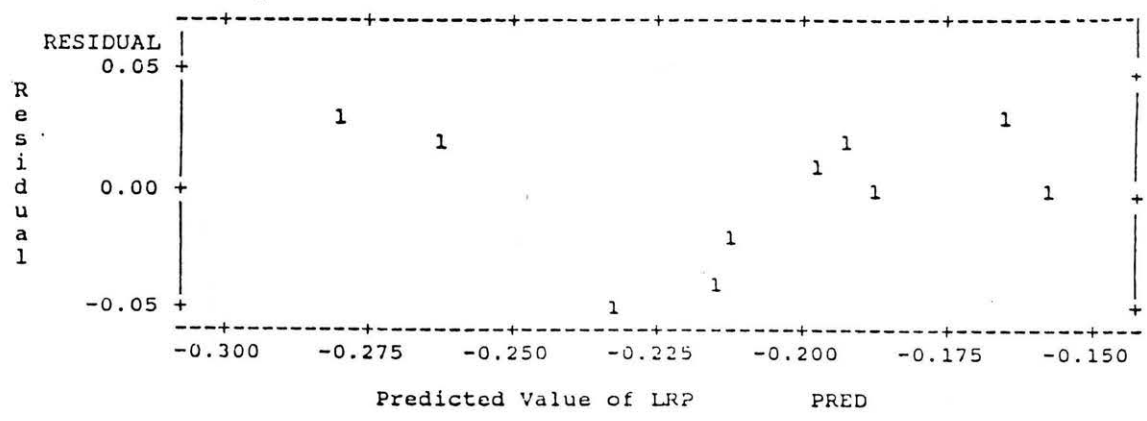

Figure 4.8-30 Residual vs Predicted values of the Logarithmic Ratio in Concentrations with and without Vapor Fence for Falcon Test Series

4.9 "Wind Tunnel Modeling of Density Current Interaction with Surface Obstacles," Koenig and Schatzmann, 1986

Experiment Configuration:

The data of Koenig and Schatzmann (1986) are unique in that they display the potential for some obstructions to reduce spread, inhibit mixing and increase surface concentrations. To validate their simulation approach and instrumentation methodology they also recreated the conditions of Thorney Island Trial No. 20 at model scales. Trial No. 20 released 2000 cubic meters of dense gas instantaneously from a collapsing tank. Fifty meters downwind of the tank the flow was obstructed by a 5 m tall semicircular fence. Koenig and Schatzmann used an aspirated hot-wire katherometer to measure concentration time series. They replicated each measurement several times to establish mean, rms, and peak concentration values.

Koenig and Schatzmann determined that the largest concentrations would occur downwind when the approach wind speed equaled the characteristic gravity spread of the source cloud. Hence, they performed most tests at their characteristic speed, i.e., Ucc = characteristic speed for continuous releases or Uci = characteristic speed for instantaneous releases, and U = 0 for calm conditions. Their study was planned to determine the influence of industrial complex and urban obstructions on the transport and dispersion of a hazardous gas cloud. They released both instantaneous cylindrical volumes (generated in a similar manner to the Thorney Island trials) and continuous area sources of dense gas. They considered the effects of undistorted and distorted simulant gas specific gravity on the cloud behavior.

Their final report discusses nine obstruction scenarios, and the authors provided additional time-series data to Colorado State for the purpose of this review. The situations considered include:

Thorney Island Trial No. 20 An instantaneous release of 2000 cubic meters of dense gas (Specific gravity 1.41 or 4.18) placed 50 m upwind of a 5 m high semicircular solid fence,

Test H1 An infinite height wall oriented in the streamwise direction to one side of a release point,

Test H2 A finite height wall oriented in the streamwise direction to one side of a release point,

Test H3 A street canyon of finite width and infinite height oriented in the streamwise direction,

Test H4 A street canyon of finite width and finite height oriented in the streamwise direction,

Test H9 A street canyon of finite width and infinite height oriented at 45 degrees to the streamwise direction,

Test H6 A street canyon intersection of finite width and infinite height with one street oriented in the streamwise direction, and

Test H8 A ditch or depressed roadway oriented perpendicular to the streamwise direction and downwind from the release point.

Measurements were taken both along the wind and transverse to the wind to evaluate cloud asymmetries.

Results of Comparison:

Figures 4.9-1 to 4.9-4 display the influence of a 5 m fence upon peak concentration ratios and cloud times during the simulated Thorney Island Trial 20 experiment. Data from trials using both distorted and undistorted density scaling are shown. (Distorted scaling refers to the practice of using an exaggerated model gas density while adjusting the model wind speed upward to maintain Froude number equality.) Field data from Trials 20 and 16 are also compared on the same figures as dotted lines. Since the laboratory data points are average values from several realizations, the difference between the dotted and solid lines reveal the deviations observed when a single experimental realization is considered.

Figures 4.9-5 to 4.9-13 examine the influence of the obstacles described above on instantaneous gas clouds, and Figures 4.9-14 to 4.9-23 examine the influence of the same obstacles on plumes released continuously from a similar size area source. The downwind distance, x, is scaled by a characteristic length, $L_{ci} = (\text{Volume})^{1/3}$, for instantaneous spills and by a second characteristic length, $L_{cc} = (Q/g(SG - 1))^{1/5}$, for continuous releases.

Figures 4.9-5 and 4.9-14 consider the effect of an infinite height wall under calm conditions upon the two spill types. Transverse concentrations are only slightly perturbed, but along wall concentrations are increased by a factor of about 2 to 3 due to cloud reflection. Figures 4.9-6 and 4.9-15 consider the effect of infinite and finite height walls on the longitudinal distribution of concentrations along the wall. Concentrations may be increased from 1.5 to 2 times. Transverse to an infinite wall downstream concentrations may be increased by factors from 2 to 4 as the plume reflects laterally, but the effect of a finite height wall is less, see Figures 4.9-7 and 4.9-16.

Figures 4.9-8 and 4.9-17 reveal the effect of constraining cloud dispersion within a street canyon. For an instantaneous plume the concentrations are increased by factors of 2 to 4 for both finite and infinite height walls, but for a continuous plume the gas escapes over the finite height wall and the peak concentration ratio decreases toward 1 with downstream distance.

When the canyon is oriented at 45° as shown in Figures 4.9-9 and 4.9-18 concentrations are often greater along the upwind side of the canyon than along the downstream side of the canyon. Although the

instantaneous source produced peak ratios greater than 1, the continuous source produced peak ratios less than one along both canyon walls.

Given a crosswind intersection in the canyon, and a spill in the middle of the intersection, Figures 4.9-10 and 4.9-19 show that longitudinal concentration ratios increase for the windless case, but the peak ratio remains the same or decreases with wind. Figures 4.9-11 and 4.9-20 show the variation of concentrations in the cross street. Again concentration ratios increase for the windless case, but fall toward zero with winds.

When a ditch or depressed roadway crosses the plume path as noted in Figures 4.9-12 and 4.9-21 the ditch decreases the transverse concentrations for both calm and windy situations. This occurs because the ditch traps a substantial part of the plume and diverts it along the ditch axis for a calm situation and introduces additional turbulence in the windy situation, see Figures 4.9-13 and 4.9-22.

As noted on the final Figure 4.9-23 even a three-fold increase in continuous source strength does not change the effect of a ditch on the dispersing cloud.

Conclusions:

The data set prepared by Koenig and Schatzmann demonstrates that some obstacle arrangements act to increase concentrations rather than reduce them. Urban areas and industrial complexes abound with narrow street canyons between tall buildings, walls, ditches, and intersections. Such configurations may multiply concentration hazards by factors ranging from 2 to 8. In addition the barriers may delay dispersion, and cause the hazard to persist for longer times. A cross-wind ditch acts effectively to reduce downwind concentrations and delay cloud transit times.

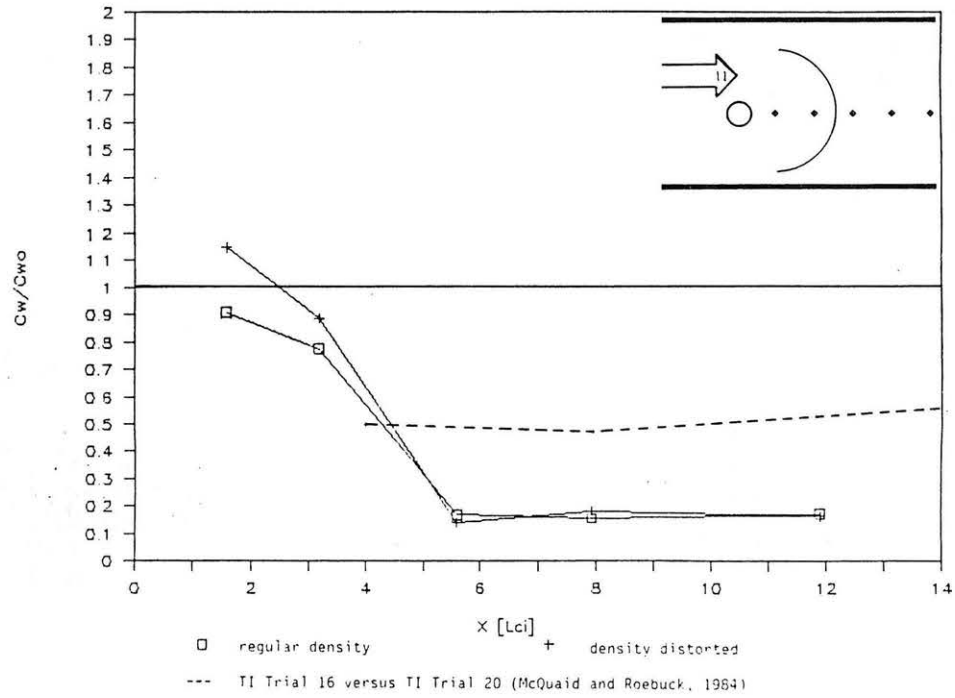

Figure 4.9-1 Peak Concentration Ratio vs. Downwind Distance, Thorney Island Trial 20 Model Simulation

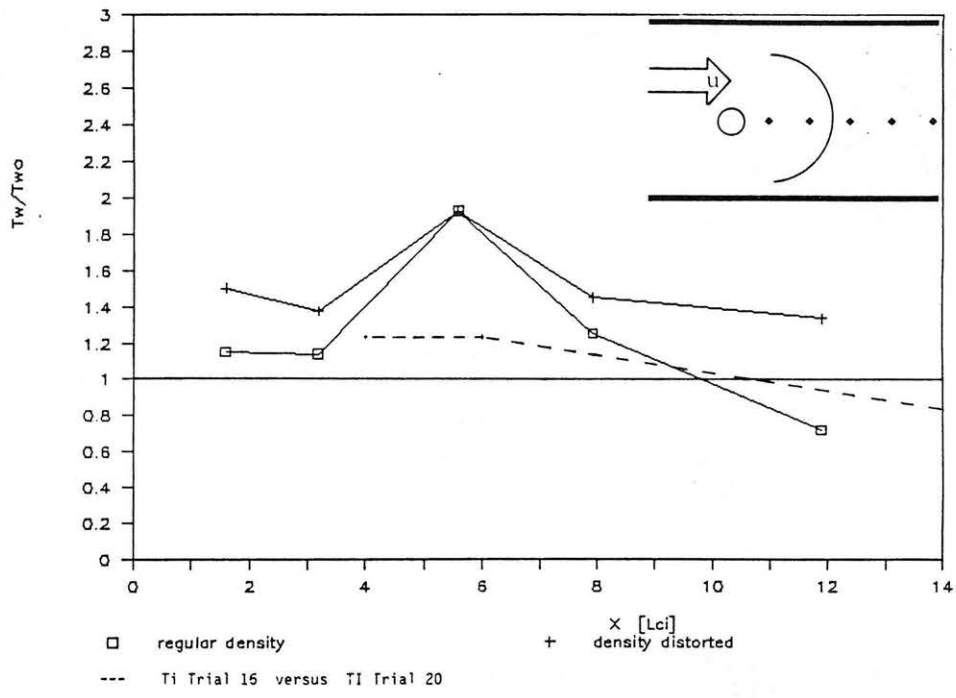

Figure 4.9-2 Arrival Time Ratio vs. Downwind Distance, Thorney Island Trial 20 Model Simulation

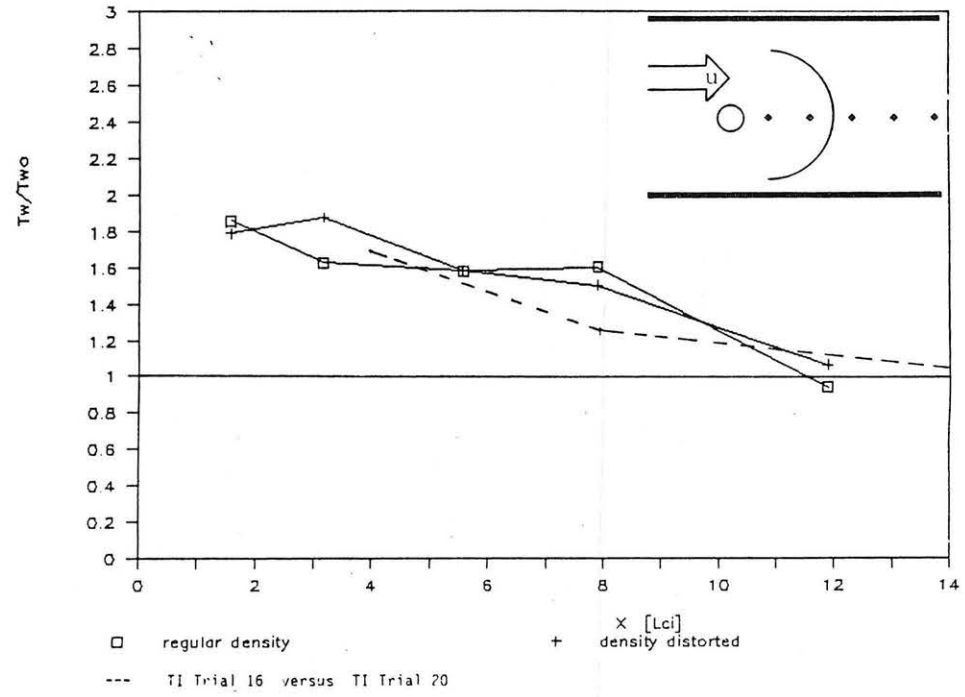

Figure 4.9-3 Peak Arrival Time Ratio vs. Downwind Distance, Thorney Island Trial 20 Model Simulation

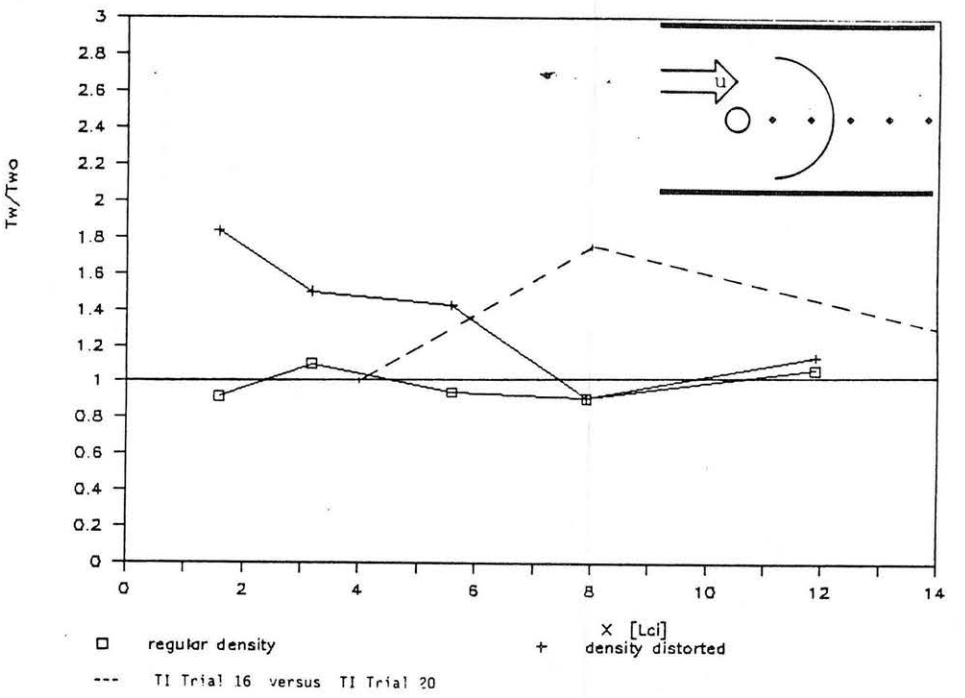

Figure 4.9-4 Departure Time Ratio vs. Downwind Distance, Thorney Island Trial 20 Model Simulation

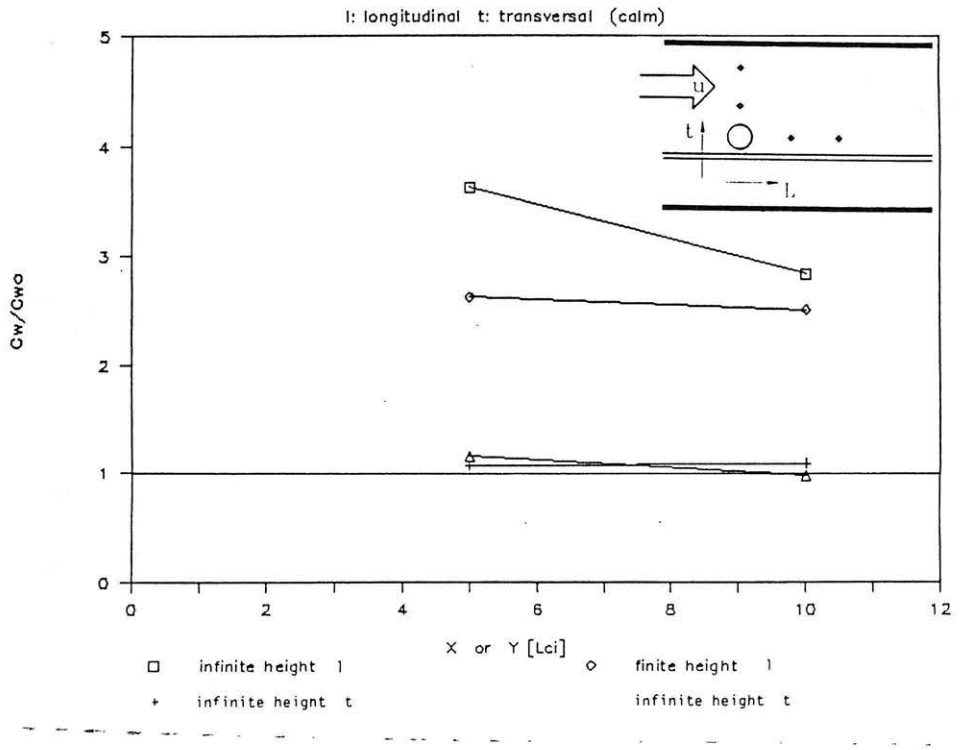

Figure 4.9-5 Peak Concentration Ratio vs. Downwind or Transverse Distance, Finite and Infinite Walls, Calm Conditions, Instantaneous Spill

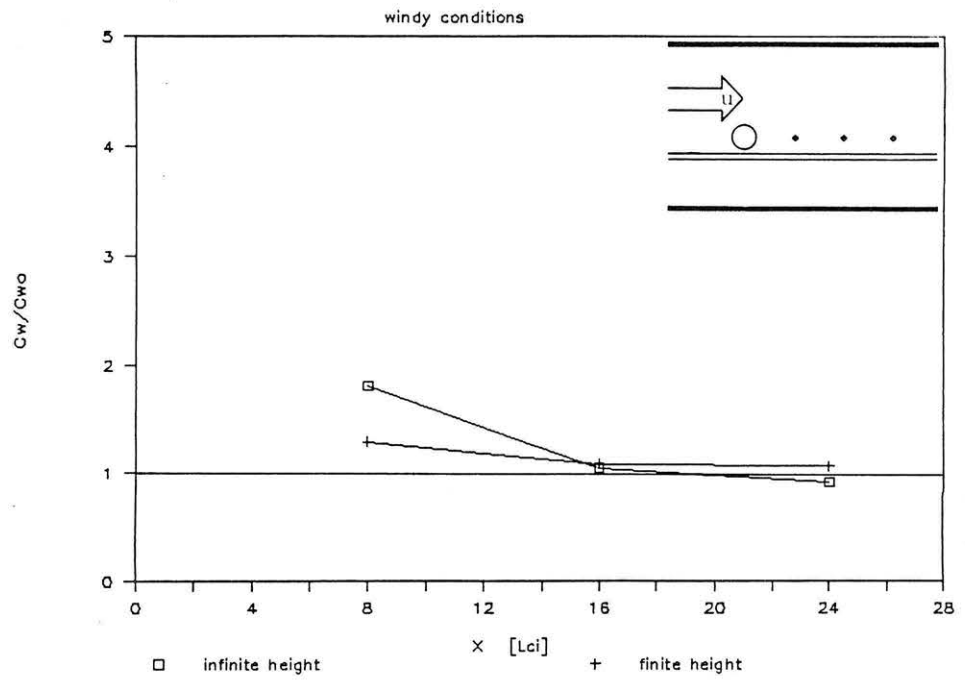

Figure 4.9-6 Peak Concentration Ratio vs. Downwind Distance, Finite and Infinite Walls, Windy Conditions, Instantaneous Spill

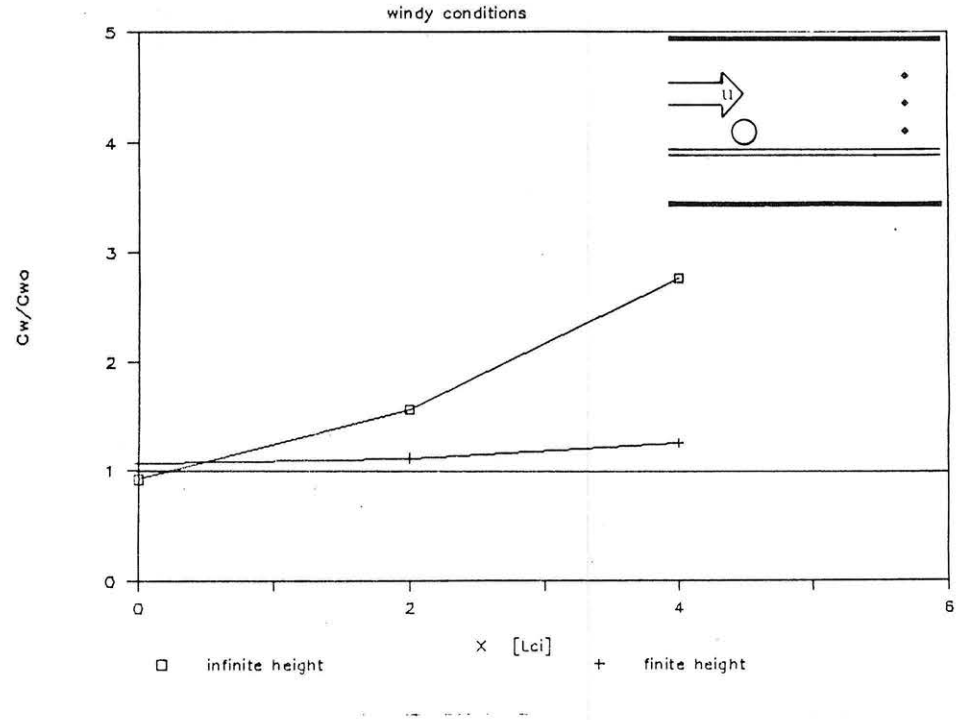

Figure 4.9-7 Peak Concentration Ratio vs. Transverse Distance, Finite and Infinite Walls, Windy Conditions, Instantaneous Spill

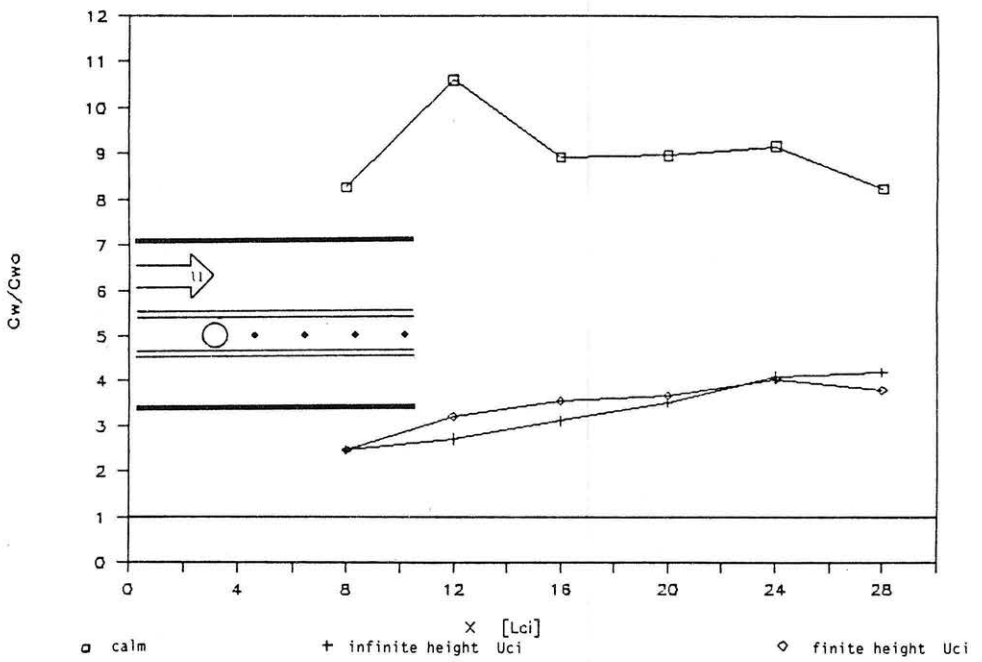

Figure 4.9-8 Peak Concentration Ratio vs. Downwind Distance, Finite and Infinite Canyon Walls, Instantaneous Spill

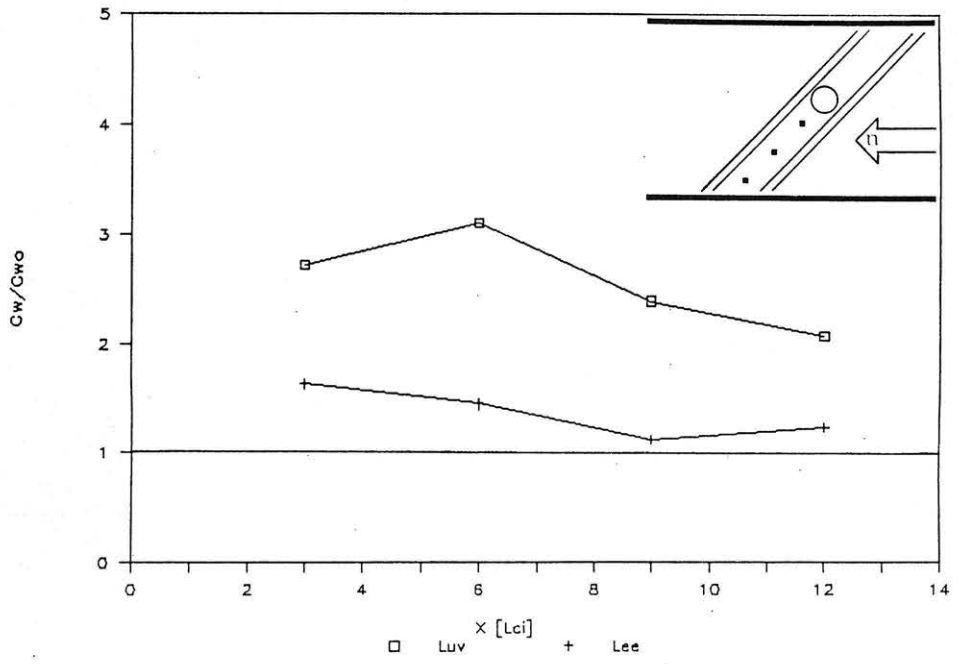

Figure 4.9-9 Peak Concentration Ratio vs. Downwind Distance, Infinite Canyon Walls, 45° Orientation, Instantaneous Spill

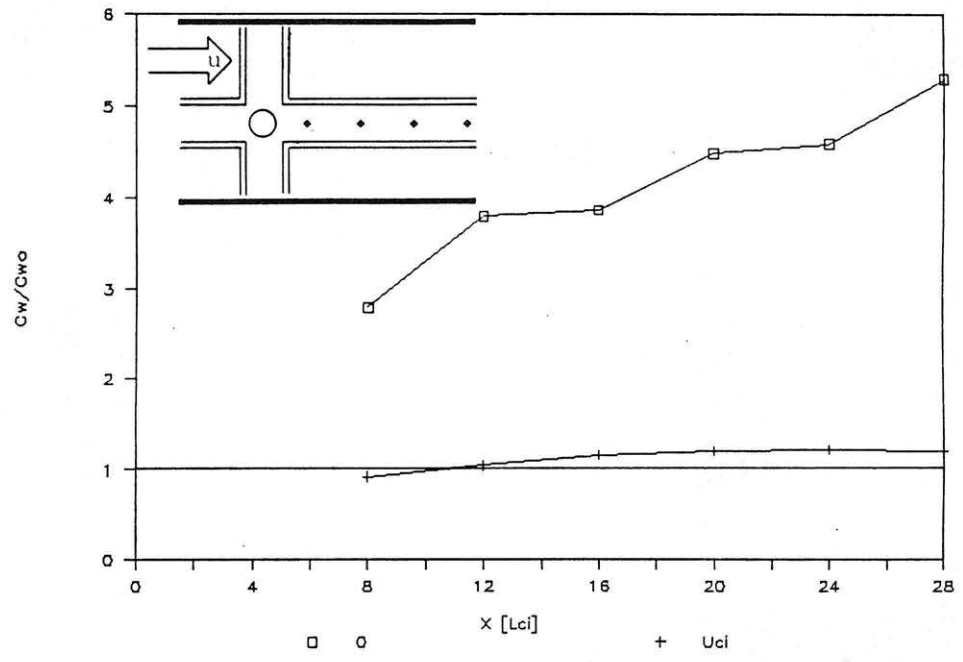

Figure 4.9-10 Peak Concentration Ratio vs. Downwind Distance, Canyon Intersection, Instantaneous Spill

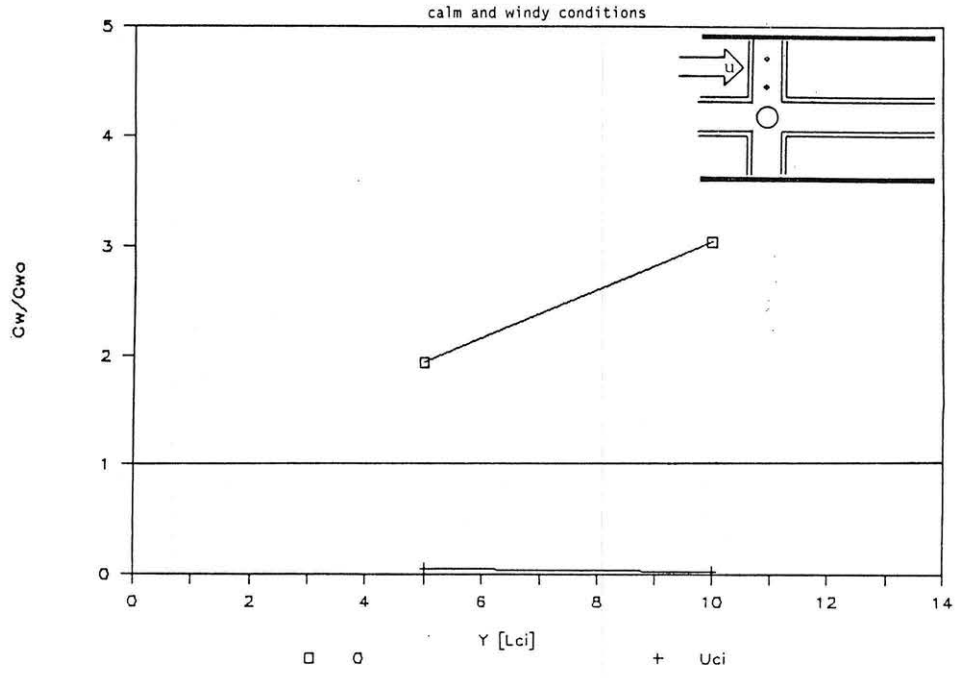

Figure 4.9-11 Peak Concentration Ratio vs. Transverse Distance, Canyon Intersection, Instantaneous Spill

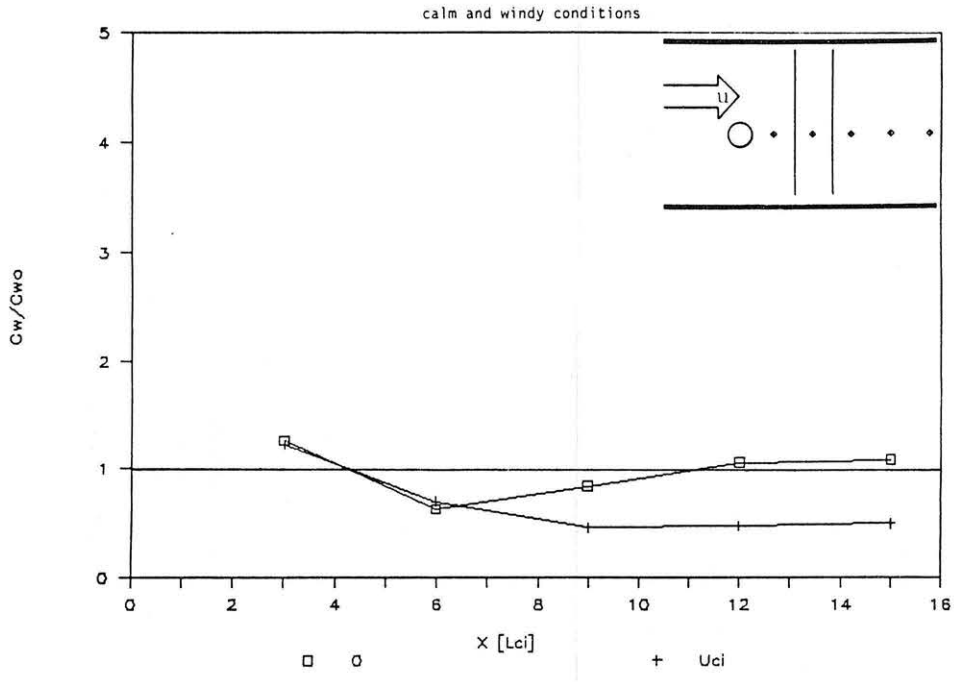

Figure 4.9-12 Peak Concentration Ratio vs. Downwind Distance, Crosswind Ditch, Instantaneous Spill

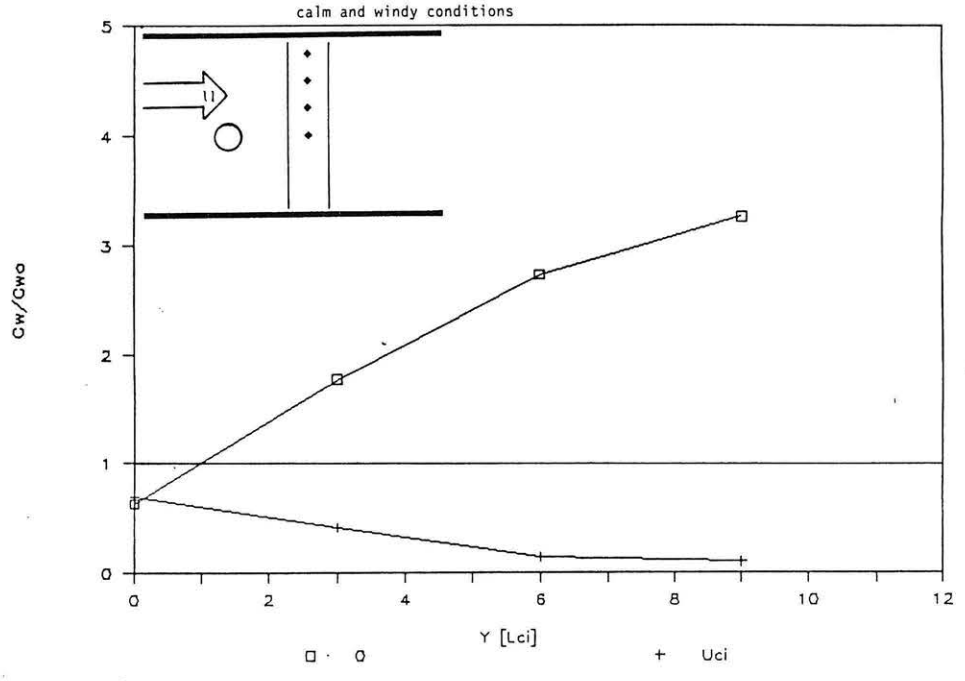

Figure 4.9-13 Peak Concentration Ratio vs. Transverse Distance, Crosswind Ditch, Instantaneous Spill

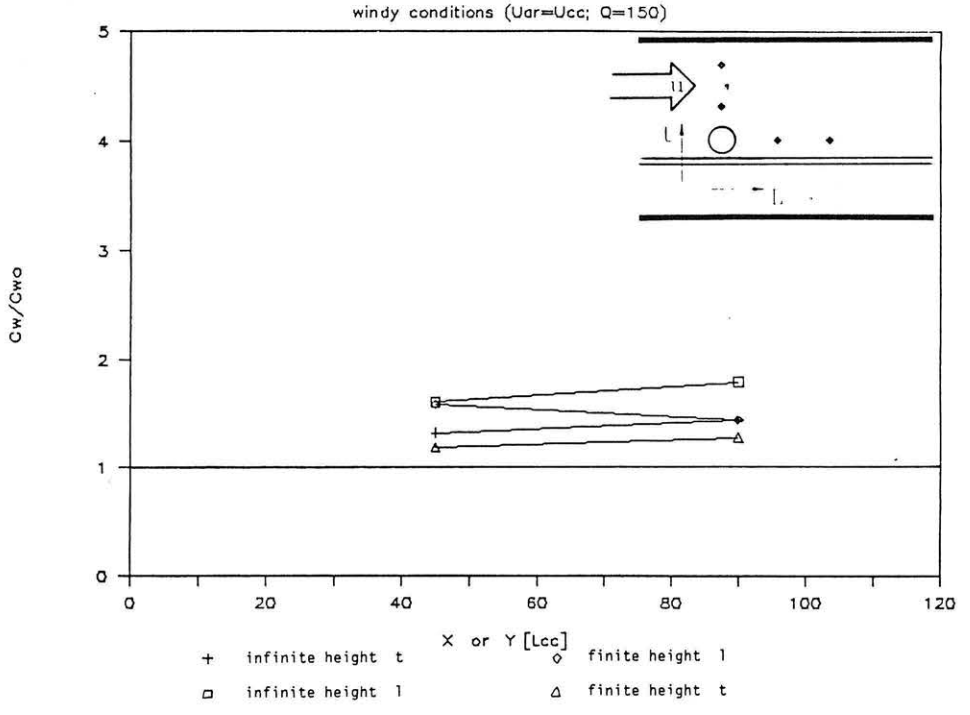

Figure 4.9-14 Peak Concentration Ratio vs. Downwind or Transverse Distance, Finite and Infinite Walls, Calm Conditions, Continuous Spill

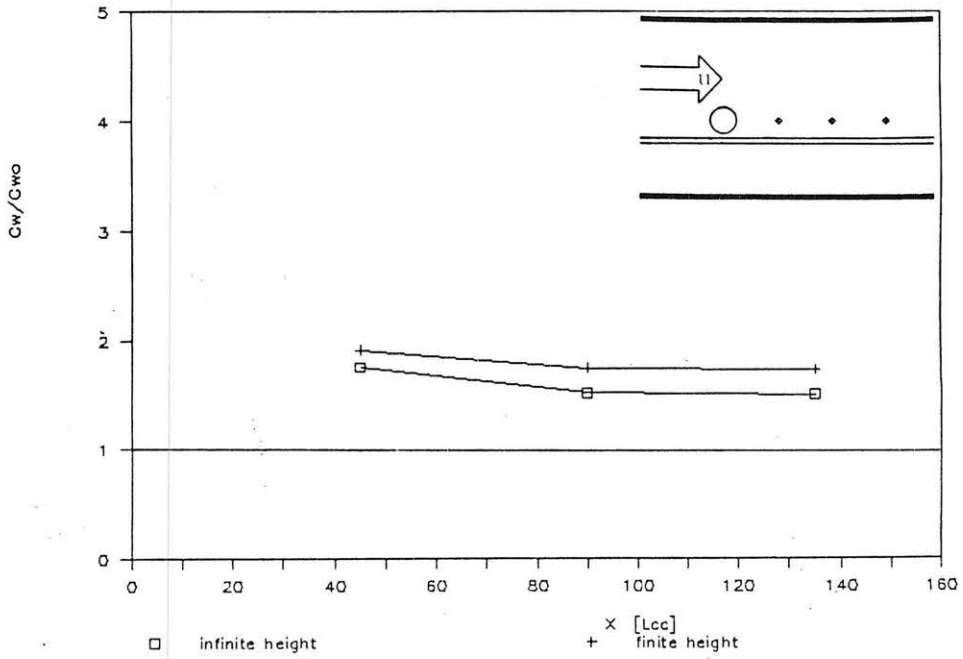

Figure 4.9-15 Peak Concentration Ratio vs. Downwind Distance, Finite and Infinite Walls, Windy Conditions, Continuous Spill

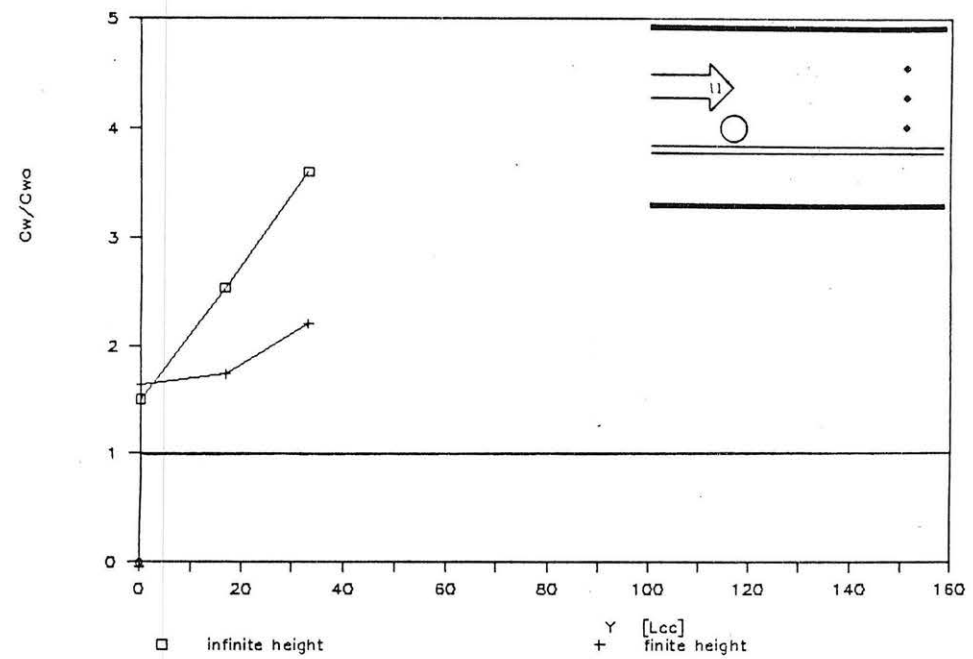

Figure 4.9-16 Peak Concentration Ratio vs. Transverse Distance, Finite and Infinite Walls, Windy Conditions, Continuous Spill

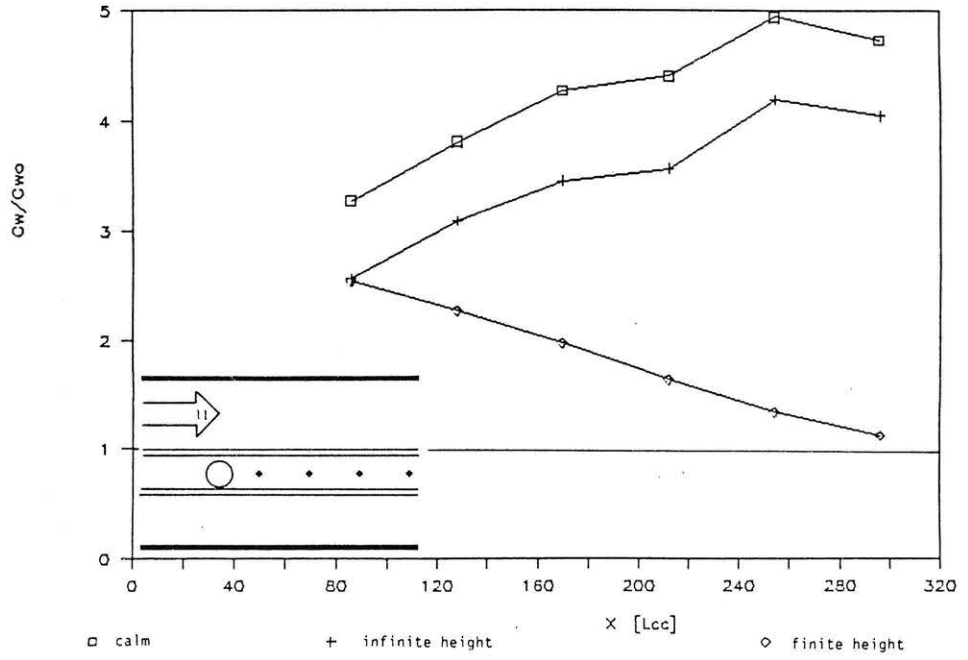

Figure 4.9-17 Peak Concentration Ratio vs. Downwind Distance, Finite and Infinite Canyon Walls, Continuous Spill

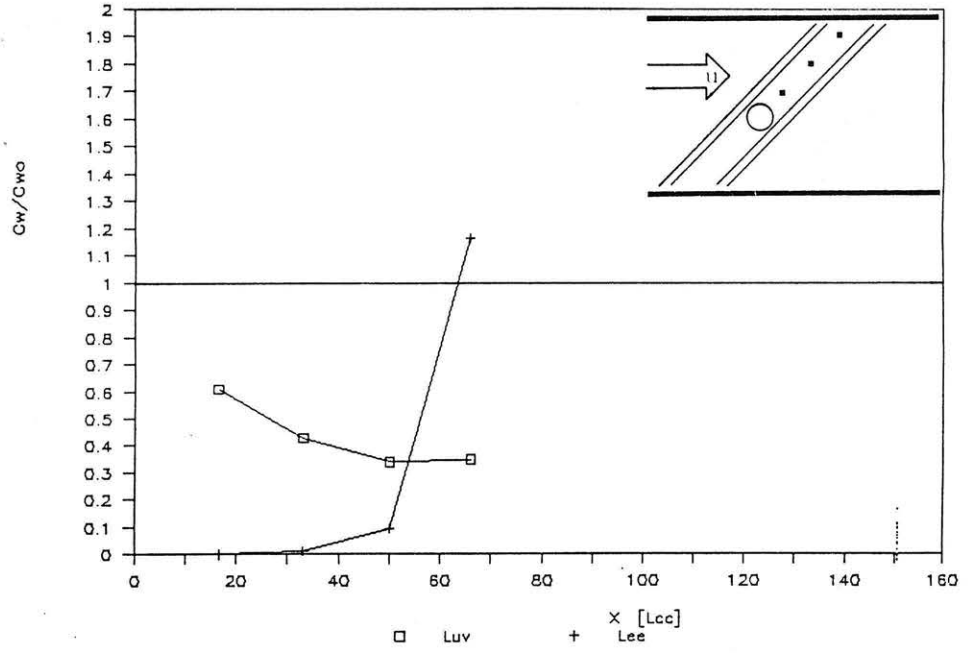

Figure 4.9-18 Peak Concentration Ratio vs. Downwind Distance, Infinite Canyon Walls, 45° Orientation, Continuous Spill

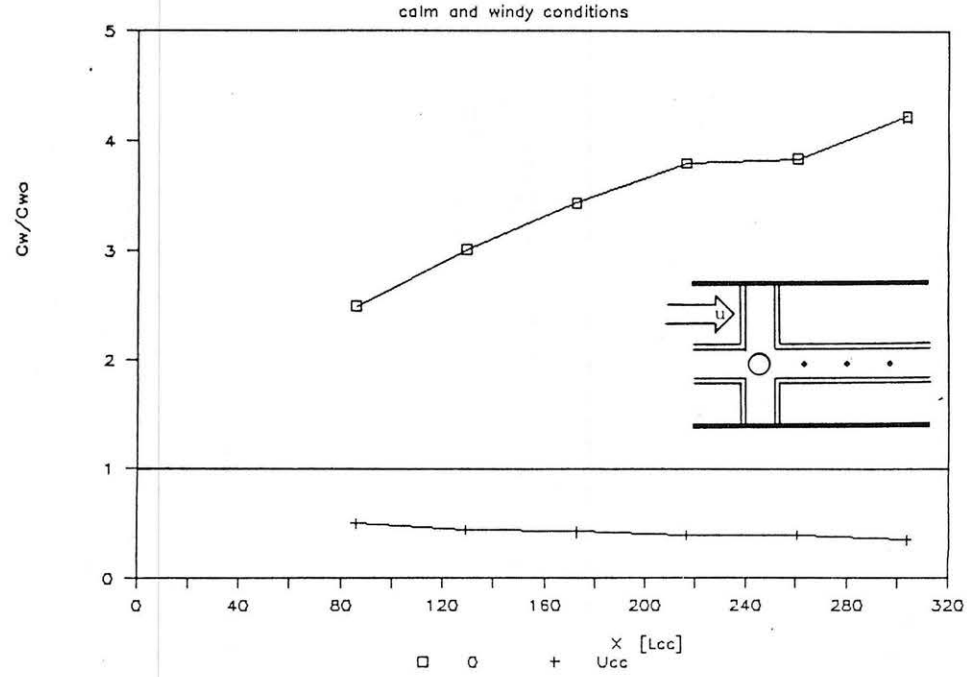

Figure 4.9-19 Peak Concentration Ratio vs. Downwind Distance, Canyon Intersection, Continuous Spill

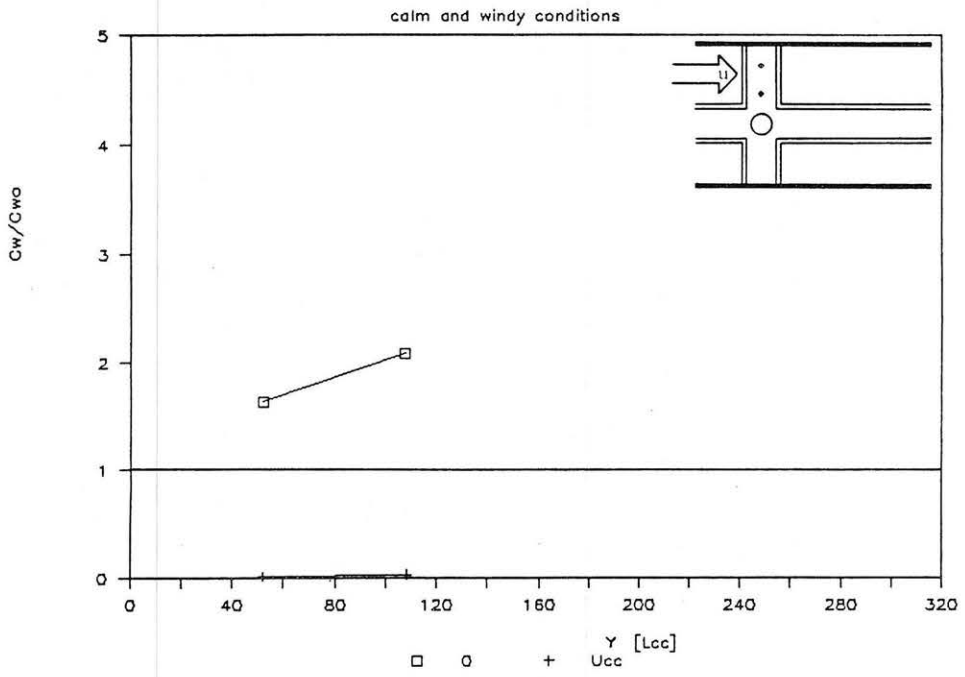

Figure 4.9-20 Peak Concentration Ratio vs. Transverse Distance, Canyon Intersection, Continuous Spill

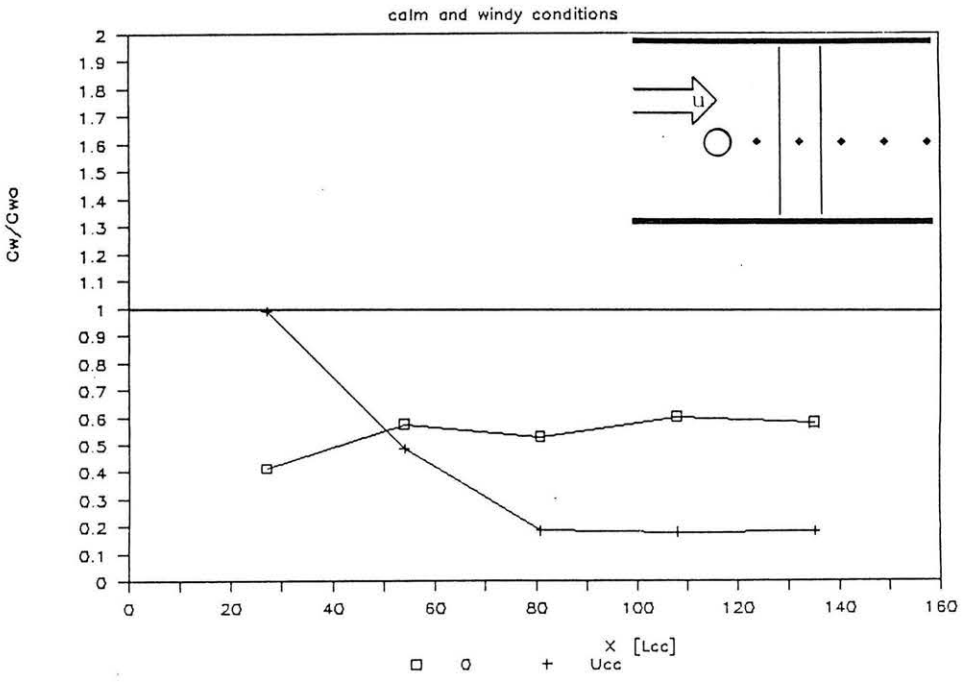

Figure 4.9-21 Peak Concentration Ratio vs. Downwind Distance, Crosswind Ditch, Continuous Spill, Q = 150 l/h

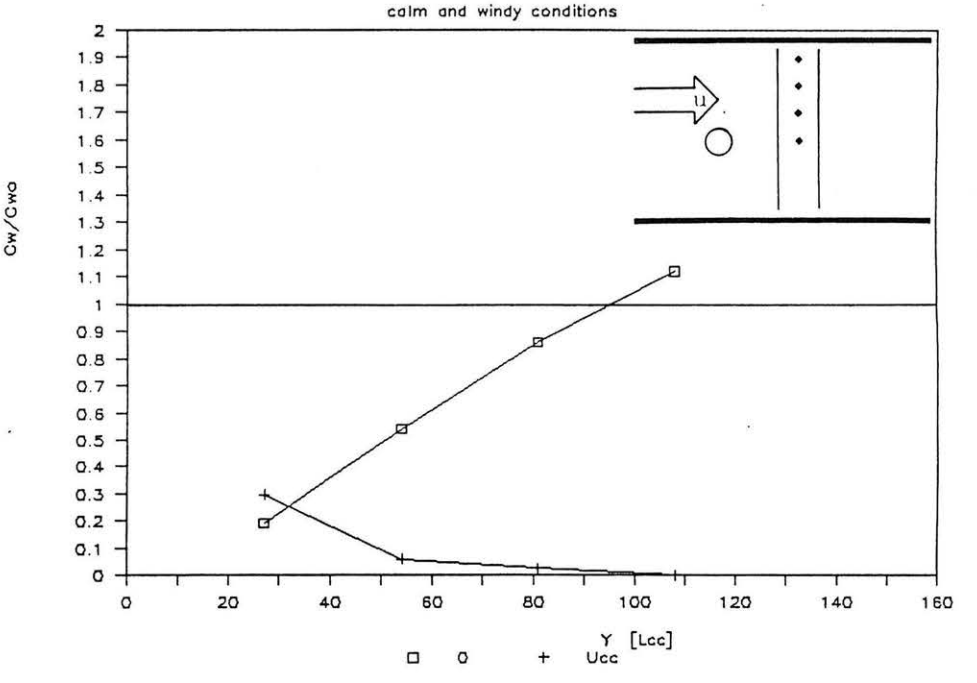

Figure 4.9-22 Peak Concentration Ratio vs. Transverse Distance, Crosswind Ditch, Continuous Spill, Q = 150 l/h

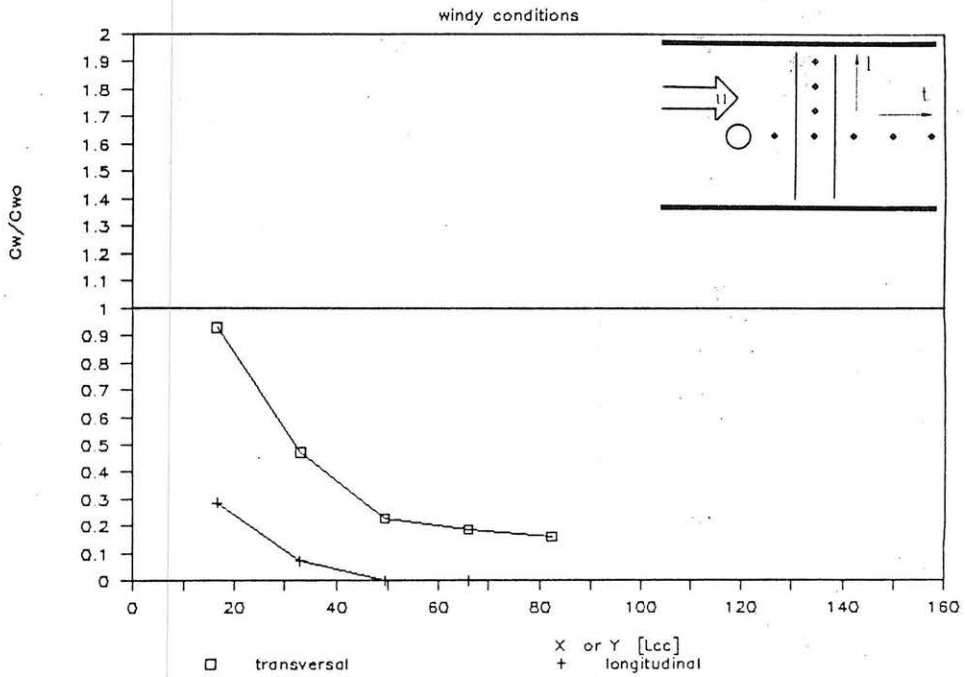

Figure 4.9-23 Peak Concentration Ratio vs. Downwind Distance, Crosswind Ditch, Continuous Spill Q = 500 l/h

5..0 EVALUATION OF NUMERICAL MODELS PROPOSED FOR WATER SPRAY AND VAPOR BARRIER DILUTION EFFECTS

As proposed in Chapter 2.4 two existing numerical models were equipped with entrainment algorithms which allow for the enhanced dilution caused by water spray curtains and vapor barrier fences. A continuous source box model (DENS6) created by Meroney (Andriev et al., 1983) was previously modified to incorporate the presence of an idealized water-spray curtain (SPRAY6A, SPRAY6B, Meroney and Neff, 1985). During this study the box model was modified further to facilitate sensitivity analysis of HF/water spray arrangements (SPRAY62), and additional subroutines were prepared to examine the behavior of HF/vapor fence arrangements (FENC62). Another version was prepared to include the effects of HF reduction by water/HF reaction and deposition (SPRAY65). These models have been compared against sets of selected data using the entrainment models described in Chapter 2.4.

A depth-averaged or slab type model developed by Meroney (DENS23, Meroney and Lohmeyer, 1982; Meroney, 1984; Meroney, 1985) was previously modified to incorporate the presence of an idealized water-spray curtain (SPRAY21, Meroney and Neff, 1985). During this study the slab model was modified further to facilitate sensitivity analysis of HF/water spray arrangements and include the effect of HF removal by deposition (SPRAY23), and additional subroutines were prepared to examine the behavior of HF/vapor fence arrangements (FENCE23). These models were used to evaluate the influence of barriers upon arrival, peak concentration, and departure time ratios.

5.1. Comparison of Numerical Models with Goldfish Trials Data

Blewitt, Yohn, and Ermak (1987b) compared the box model SLAB developed by Ermak et al. (1985) and the slab model DEGADIS developed by Havens and Spicer (1985) against Goldfish Trials No. 1, 2, and 3. A transient version of SLAB predicted experimental data within a factor of two. Averaging time ambiguities in the DEGADIS model led to difficulties in the interpretation of the predictions. The authors remained uncertain as to the value of these particular models when extrapolated to an industrial setting to accurately predict low concentrations in the far-field region. Nonetheless, such models provide a framework within which to examine the viability of various mitigation devices.

DENS62 predictions of Goldfish Trials No. 1, 2 and 3 were calculated using an ideal gas with molecular weight equal to 20, source temperatures of 20°, 20°, and 10° K, respectively, and molar specific heat capacities of 0.83, 0.83 and 0.9 times that of air, respectively. As noted in Chapter 2.2 these values are necessary to reproduce the HF density behavior predicted by the Schotte equations. A value for surface rougheness over the desert area of 0.005 m was assumed for all calculations presented here. Figures 5.1-1, 4, and 5 compare centerline concentration decay of the HF plume with measured values and the SLAB predictions by Blewitt et al. (1987b). The comparison Figure 5.1-6 shows

that these predictions reproduce measurements in the near-field within 50% and in the far-field within 20%.

Lateral plume concentrations at the 300 and 1000 meter distances downwind of the source for Goldfish Trial No. 1 are shown in Figures 5.1-2 & 3. Lateral concentration distributions were calculated from the predicted peak concentration and plume width incorporated into an algebraic relation suggested by Meroney (1984). The model does not predict concentrations reach the 8 meter height; hence, comparisons are not provided at this level.

The HF was released as a horizontal jet during the Goldfish trials. Intense mixing occurred near the source, which resulted in rapid dilution to cloud densities below 2.0 kg/cubic meter. The use of a pure HF source or a diluted HF gas to initiate the model has little effect upon initial plume dynamics since the model conserves buoyancy. Reduction in initial source density is compensated for by an increase in effective source volume. Comparisons were made between calculations for a pure HF and a dilute HF source (mass ratio = 4) for Goldfish Trial No. 1. These conditions produced less than 10% differences in concentrations, densities, plume dimensions and temperatures at distances farther than 100 m downwind.

The DENS62, SPRAY62, FENC62 model series seem to predict the Goldfish Trials adequately; hence, the programs were used to evaluate barrier behavior.

5.2 Calibration of the Vapor Barrier Fence Entrainment Model

Data from the pre-Falcon model tests performed by Neff and Meroney (1986) were used to calibrate the vapor barrier fence entrainment model proposed in Chapter 2.4. The behavior of the peak concentration ratios downwind of the 9.4 m fence during continuous spills of LNG simulant were slightly different when an upwind vortex generator was installed. In the absence of such upwind generators the peak concentration ratio reaches a minimum at about 75 meters downwind of the spill point, and then it increases linearly further downwind. Since the numerical model does not include the effect of an upwind vortex generator Run No. 5 (9.4 m fence enclosure alone) was selected to compare with Run No. 10 (no enclosure). These two tests simulated a liquid spill rate of 40 cubic meters/min for 2.5 minutes onto a water pond. The gas was assumed to flash immediately into a gas released over the 44 m x 44 m area of the water pond. Wind speeds simulated equaled 3.5 m/sec at a 2 meter height. Simulant concentrations were converted to equivalent LNG vapor concentrations.

Figure 5.2-1 compares the results of calculations by FENC62 when the coefficient C_D = 0.1. The source center was assumed to be about 60 m upwind of the fence to allow for the 88 m total longitudinal length of the fence enclosure and its tendency to move the virtual source upwind. Centerline measurements were used to negate the 3-dimensional effects of the enclosure corners. Model measurements at distances 15, 75, 200, and 400 meters downwind of the fence (or 75, 135, 260, and 460 meters from the

virtual source) are plotted on the figure. Variations in virtual distance between 60 and 44 m, and variations in the entrainment coefficient over a two-fold range did not significantly improve agreement. Best agreement occurred for Trial No. 10 data when the initial source width without a fence was set to 44 meters. A small dike existed about the model water spray pond, which may have inhibited lateral spread at the source.

Calculations of the peak concentration ratio from the numerical results at various downwind distances reproduce the minimum in the ratio noted at the 75 meter measurement station. Given a spill not constrained laterally at the source the numerical program predicts that peak concentration ratios may even exceed one near the source. Such a behavior was noted during the Thorney Island tests near the fence (See Chapter 4.6).

5.3 Calibration of the Vapor Removal Model

Blewitt et al (1987c) discuss the removal of HF by water sprays measured during Goldfish Trials No. 4, 5, and 6. Measurements of centerline concentrations were made with and without the water sprays on at 300 and 1000 m. Deposition measurements suggested that the water sprays removed 10-25%, 44%, and 47% of the HF during Trials 4, 5, and 6, respectively. The water spray systems were designed to produce small droplets to enhance chemical reactions, rather than strong dilution. SPRAY23 was used to predict cloud concentrations with the reduction mode on but water spray entrainment set to zero.

Figures 5.3-1 and 5.3-2 compare program predictions of cloud concentrations against measured values for Goldfish Trials No. 1 and 3.

The Appendix discusses the additional reduction in plume concentrations which may occur as a result of increased air entrainment induced by the water spray curtains.

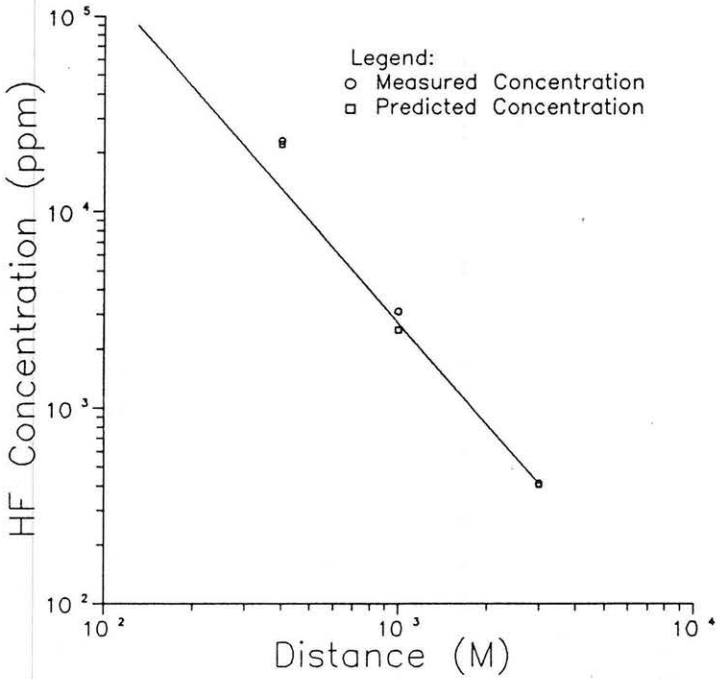

Fig. 5.1-1 Comparison of Observed, SLAB and DENS62 Predicted Plume Centerline Concentrations for Goldfish Test No. 1

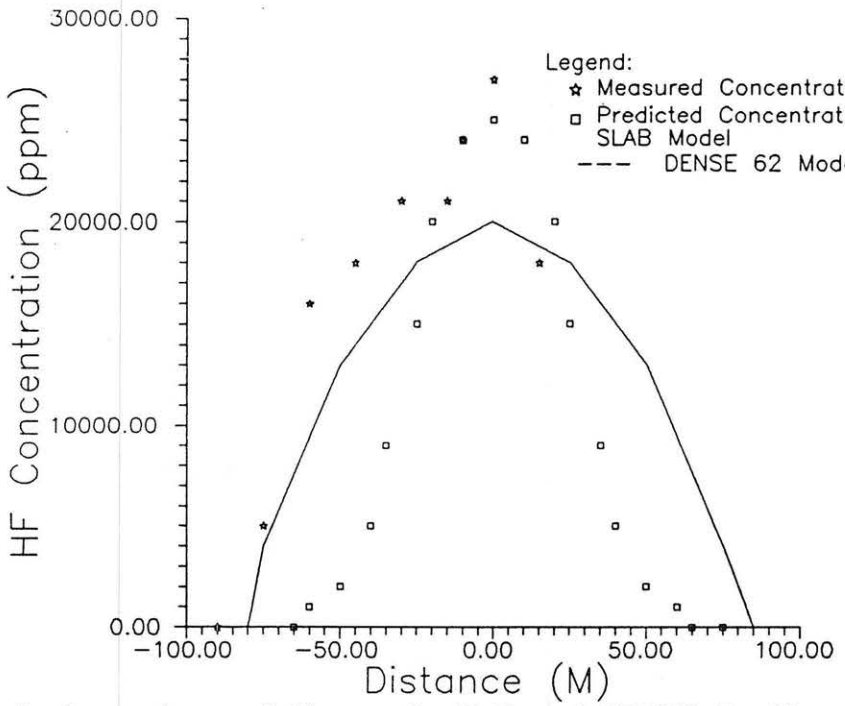

Fig. 5.1-2 Comparison of Observed, SLAB and DENS62 Predicted Crosswind Concentrations at 300 m for Goldfish Test No. 1

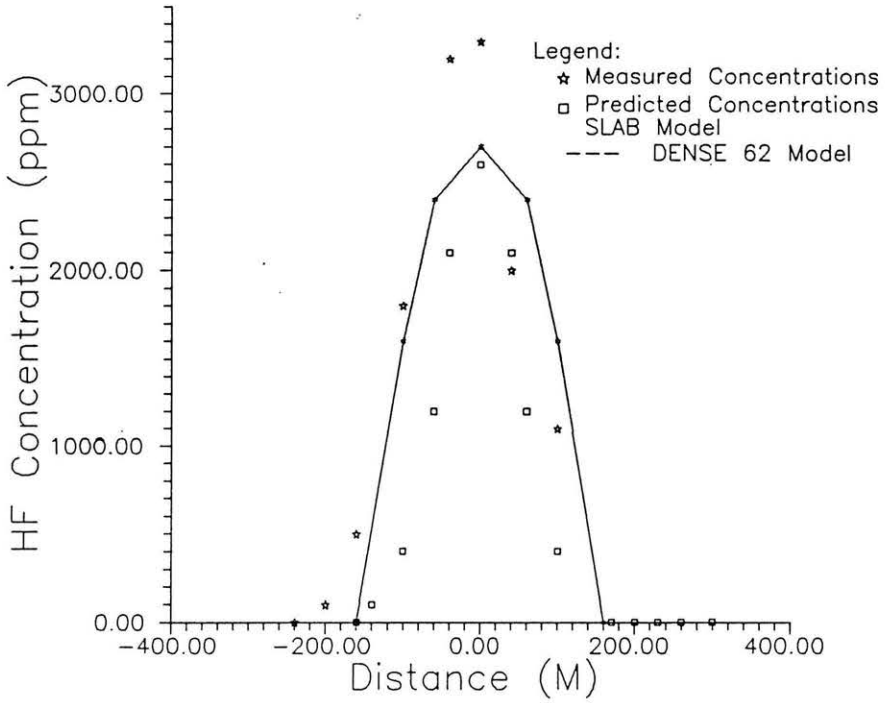

Fig. 5.1-3 Comparison of Observed, SLAB and DENS62 Predicted Crosswind Concentrations at 1000 m for Goldfish Test No. 1

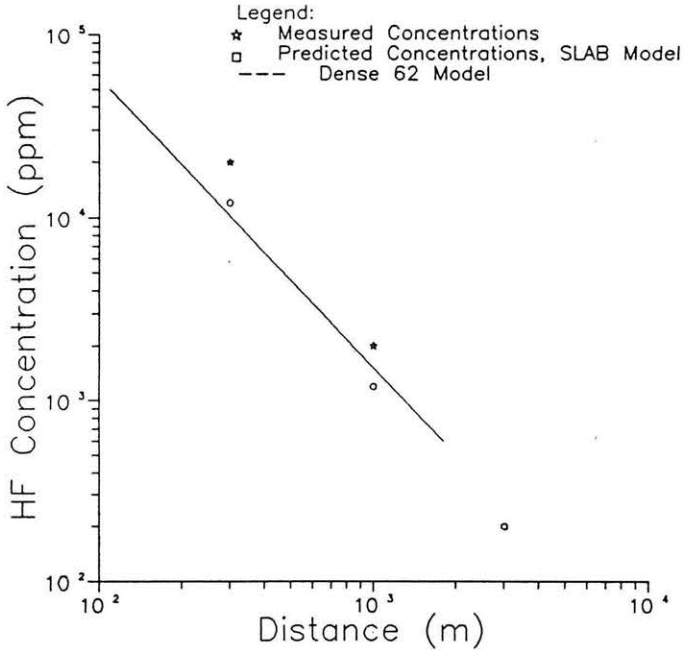

Fig. 5.1-4 Comparison of Observed, SLAB and DENS62 Predicted Plume Centerline Concentrations for Goldfish Test No. 2

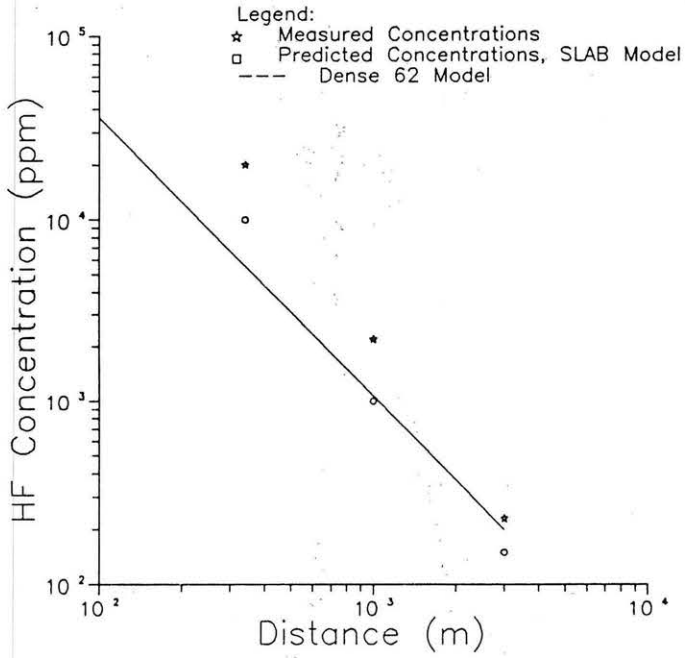

Fig. 5.1-5 Comparison of Observed, SLAB and DENS62 Predicted Plume Centerline Concentrations for Goldfish Test No. 3

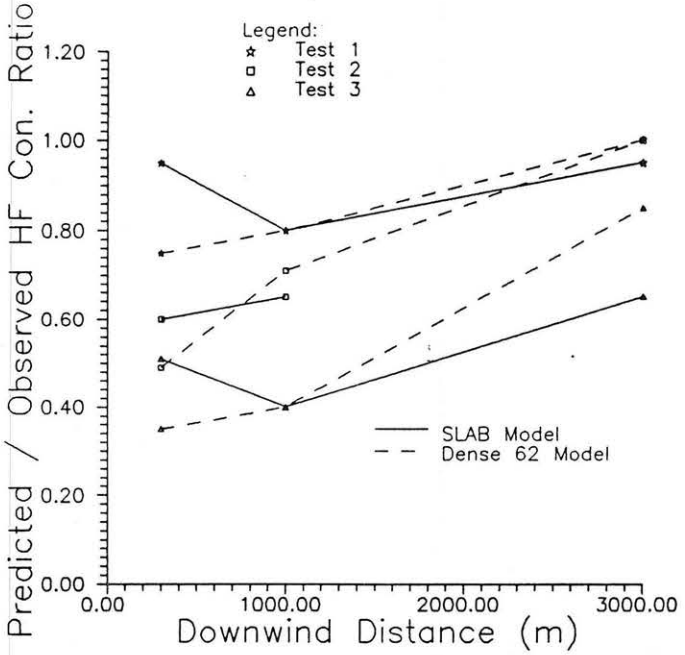

Fig. 5.1-6 Comparison of Ratios of Observed to SLAB and DENS62 Predicted Plume Centerline Concentrations for Goldfish Tests No. 1, 2, and 3

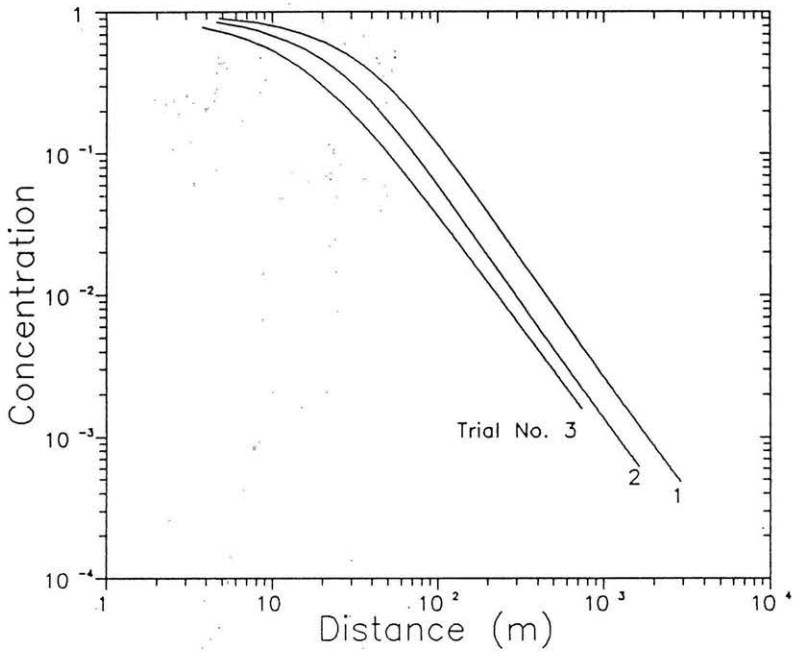

Fig. 5.1-7 Predicted Plume Centerline Concentrations for Goldfish Tests Nos. 1, 2, and 3 by DENS62

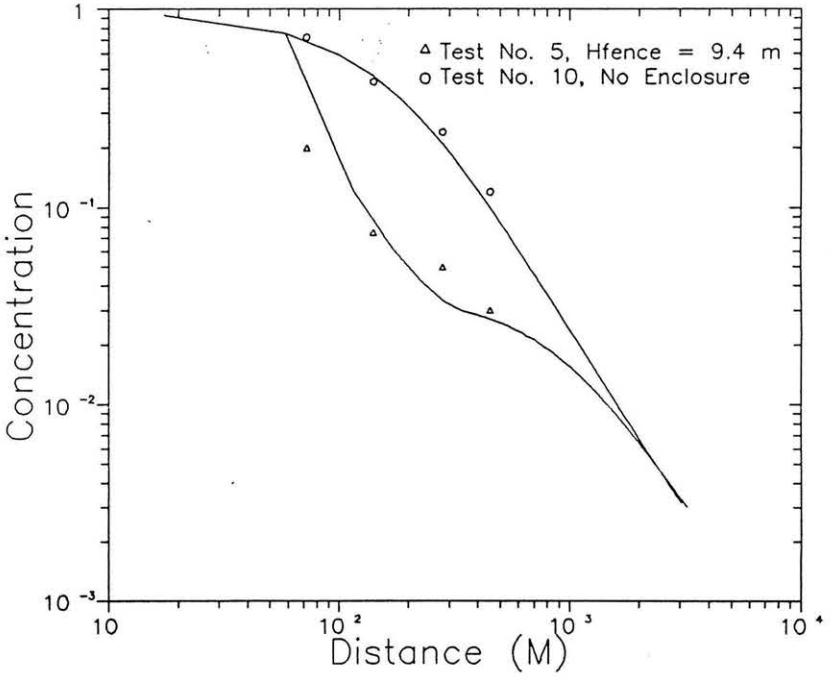

Fig. 5.2-1 Comparison of Observed and FENC62 Predicted Plume Centerline Concentrations for Goldfish Test No. 1

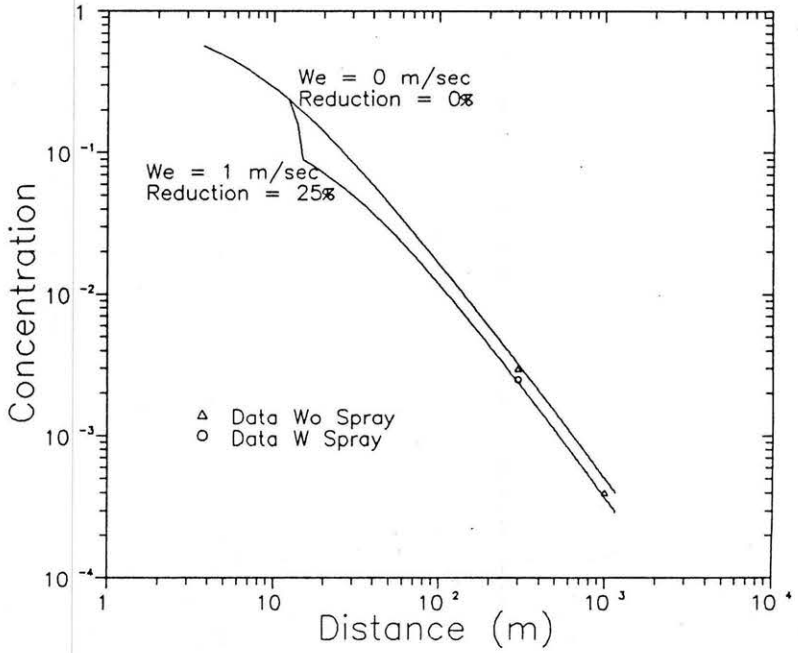

Fig. 5.3-1 Comparison of Observed and SPRAY65 Predicted Plume Centerline Concentrations for Goldfish Test No. 4

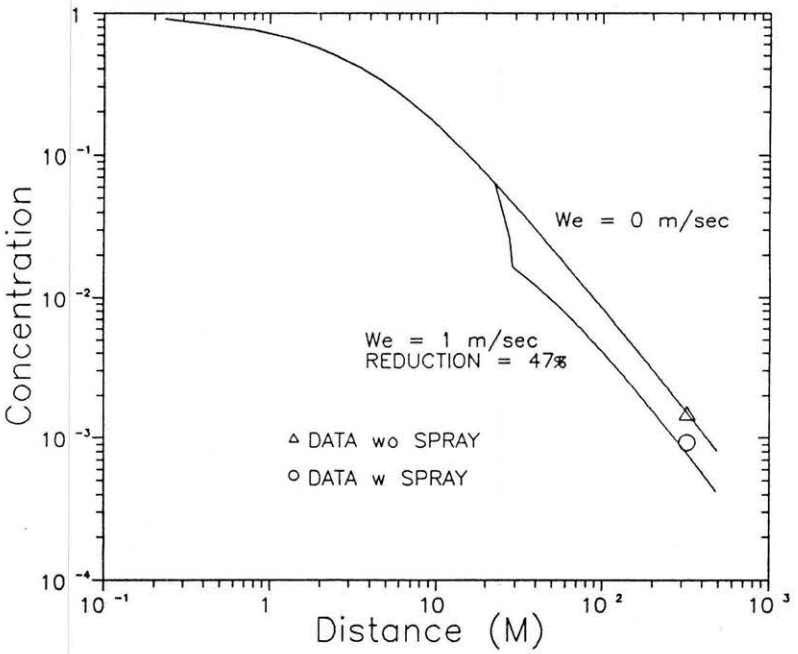

Fig. 5.3-2 Comparison of Observed and SPRAY65 Predicted Plume Centerline Concentrations for Goldfish Test No. 6

6.0 PREDICTION OF HYDROGEN FLUORIDE DILUTION

The conditions selected for design variations are equivalent to those observed during Test No. 1 of the Goldfish Trials performed at the DOE Liquefied Gaseous Fuels Test Facility by Blewitt et al. (1987). The HF source was assumed to arise from a 7 meter wide source at a rate of 469.2 gallons/min of liquid HF (28.33 kg/sec or 2.325 cubic meters/sec of gas). (This source configuration was also used by Blewitt et al. in their numerical calculations.) The ambient air temperature was set at 310° K, the wind speed of 5.6 m/sec at two meters was assumed to produce a friction velocity of 0.374 m/sec over a surface roughness of 0.005 meters. The source gas molecular weight was set at 20 and the source temperature was set to 20° K to reproduce the density mixture behavior predicted by Schotte for such conditions.

The Goldfish Test No. 1 conditions were chosen for barrier sensitivity tests because they relate to an actual HF release, even though the observed surface roughness is not typical of a refinery or chemical complex setting. The larger background turbulence levels associated with a "rough-boundary" refinery area will reduce the downwind distance over which vapor-barrier or water spray dilution significantly influence centerline concentration magnitudes. (The reader should consult the results of work in progress by Petersen and Radcliff of CPP for the American Petroleum Institute which examines the influence of roughness on dense plume dispersion.) Water spray removal of HF will not be affected by variations in surface roughness. The Goldfish HF Trials were designed to examine hypothetical release scenarios being evaluated by industry.

The humidity and the surface heat transfer in the models were set to zero so that adiabatic entrainment of air would reproduce the density mixture behavior predicted by Schotte. The molar specific heat capacity of the source gas was chosen to be 0.83 times that of air.

In DENS62, SPRAY62, and FENC62 the increments of downwind distance are automatically determined by various buoyancy scaling criteria and the need to maintain numerical stability. Thus, fence and spray locations varied somewhat when different wind speeds were investigated; however these variations were still small compared to the total plume trajectory examined.

In SPRAY23 and FENC23 only 100 longitudinal grid locations are available; hence, a nested set of calculations were performed as the cloud advected out of the initial calculation domain. The primary adjustment made was to the source size and source velocity. As the grid expands the effective source area increases and the source velocity decreases proportionately (the Flux Froude number and Volume Flux ratio are kept constant); thus, some irregularities are noted at locations where the grids overlap.

6.1 Goldfish Trial No. 1 with Vapor Barrier Fences

No tests were actually carried out during the Goldfish Trials in the presence of vapor barrier fences; however, calculations to show the effect of hypothetical fences are interesting. These calculations are representative of the entrainment resulting from straight sharp-edged fences, where separation occurs at a the fence top. Fences are assumed to be transverse to the wind direction. The effect of barrier height and wind speed are examined below. Calculations were performed with the fence entrainment model discussed in Chapters 2.4 and 5.4 and an entrainment coefficient $C_D = 0.1$.

Effects of Fence Location

The effects of fence location were determined to be similar to that of water spray curtain location. Fences are more effective in terms of initial dilution, when they are placed nearer the source. Fence dilution effects did not persist beyond 1000 m, when the fence was placed less than 400 m downwind of the source.

Effects of Fence Height

The fence entrainment model permits the entrainment velocity to increase with fence height velocity. Since wind profiles increase with height, then the dilution rate should increase with fence height. The FENC62 model assumes that a logarithmic velocity profile exists, such that wind speed is determined by surface roughness and friction velocity. Figure 6.1-1 displays a set of curves for fence heights ranging from 3 to 12 meters. The entrainment velocity does not turn off abruptly like the water spray model, but decreases linearly out to a distance of 30 fence heights. The resulting displacement of the concentration profile is cusp shaped rather than triangular, and the dilution effect is small after about 200 fence heights.

The effect of fence height on cloud height is displayed in Figure 6.1-2. The cloud height approaches the cloud height in the absence of a barrier after 1000 meters or about 200 fence heights.

Effects of Wind Speed

Increased wind speeds result in larger entrainment rates, but this is compensated by the tendency for the plume to pass through the fence wake more quickly. Given a constant fence height of 3 meters located 100 meters downwind of the source, Figure 6.1-3 and 4 suggests that, for a range of wind speeds varying from 1 to 8 m/sec, the increased entrainment and shortened time in the wake balance out to produce no net change in dilution rate. Plume height also remains constant. These calculations agree with other experiences in building aerodynamics where it is found that perturbation of gas plumes by obstacles seems to be velocity independent. Concentrations decay at higher wind speeds inversely with the speed, but this is an independent effect of source dilution by the ambient wind, not an effect of a fence.

Cloud height downwind of an obstacle is expected to be independent of wind speed, since a sharp edged geometry will produce similar streamline patterns over a range of velocities. Figure 6.1-4 suggests that the perturbation produced by a fence is constant, but the model fails to allow for a constant height wake region.

6.2 Goldfish Trial No. 1 with Water Sprays

As noted in Chapter 5.3 water spray curtain tests were performed during the Goldfish Trials No. 4, 5, and 6. These tests included chemical reactions between the HF and the water spray and subsequent deposition of the HF on the ground. Goldfish Trial No. 1 conditions are used below to examine the effect of various spray placement and water spray reduction and entrainment rate alternatives. The influence of added air entrainment induced by the water spray curtains is discussed in the Appendix.

Water Spray Effects on HF Reduction

SPRAY65 was used to predict the joint effects of water spray dilution and deposition on an HF cloud. Figure 6.2-1 displays the effect of placing a single spray which produces 80% deposition at 100m followed by a second spray of similar strength at 300 m. Notice that spray deposition produces a parallel shift of the concentration decay curve. A second spray produces a second shift of equivalent width. The decrease in concentration persists at all subsequent downstream distances.

Figure 6.2-2 depicts the effect of joint dilution and depletion. In this case it is assumed that $(w_e)_{spray}$ = 6 m/sec and HF reduction is again 80%. Reductions in plume concentration produced by the water spray alone do not persist, but combined dilution and reduction produce large local reductions and concentration followed by a shift in the concentration curve downward.

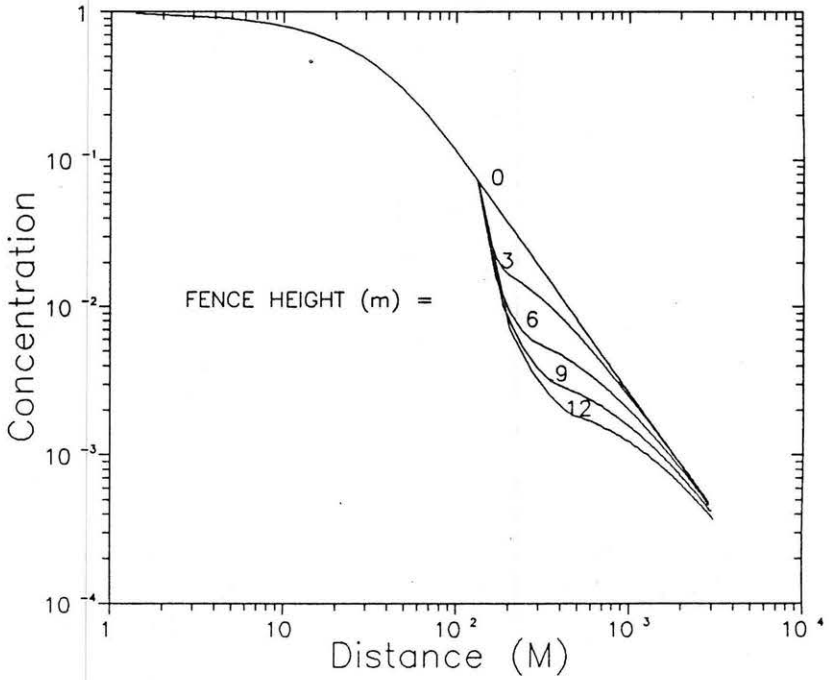

Fig. 6.1-1 FENC62 Predicted Plume Centerline Concentrations for Goldfish Test No. 1, Fence heights = 0, 3, 6, 9 and 12 m at X = 100m

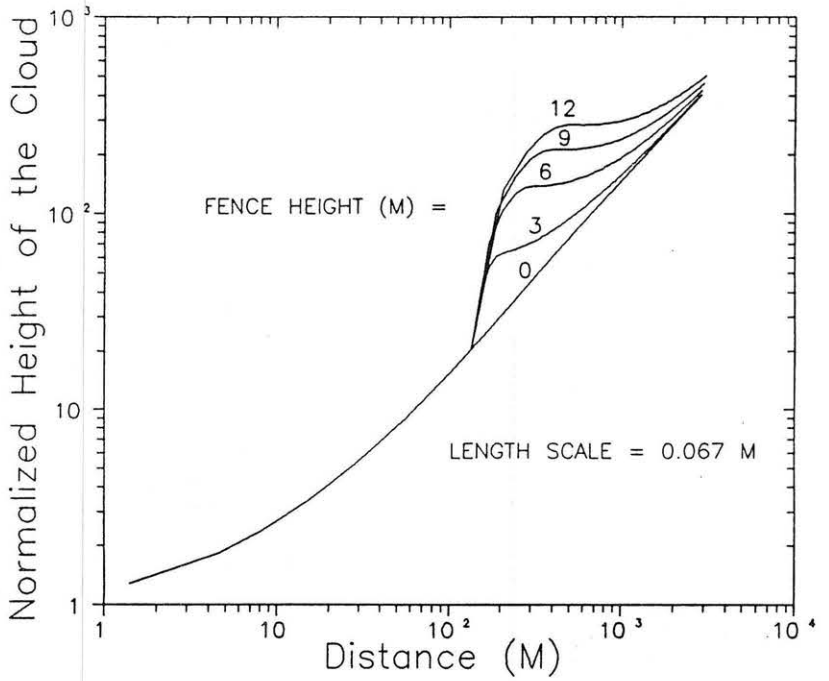

Fig. 6.1-2 FENC62 Predicted Plume Heights for Goldfish Test No. 1, Fence Heights = 0, 3, 6, 9 and 12 m at X = 100 m

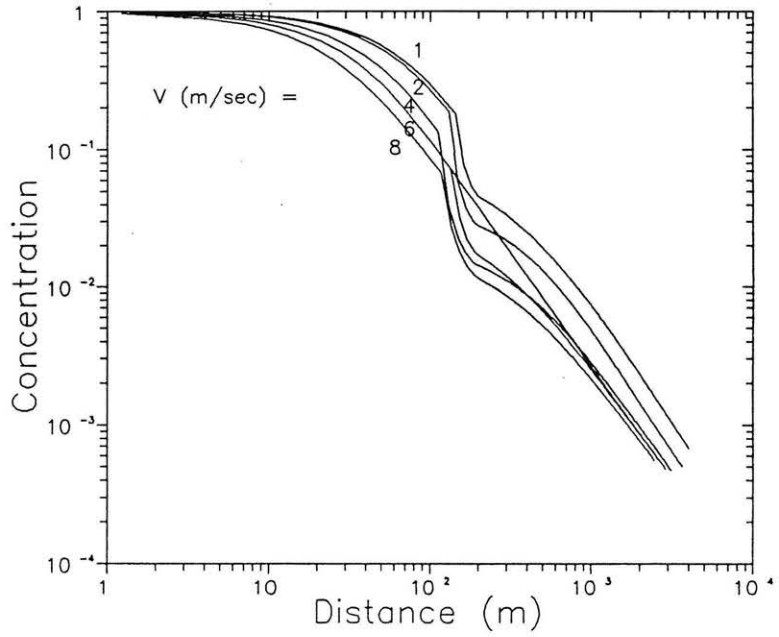

Fig. 6.1-3 FENC62 Predicted Plume Centerline Concentrations for Goldfish Test No. 1, Fence Height = 3m, X = 100 m, U = 1, 2, 4, 6, and 8 m/sec

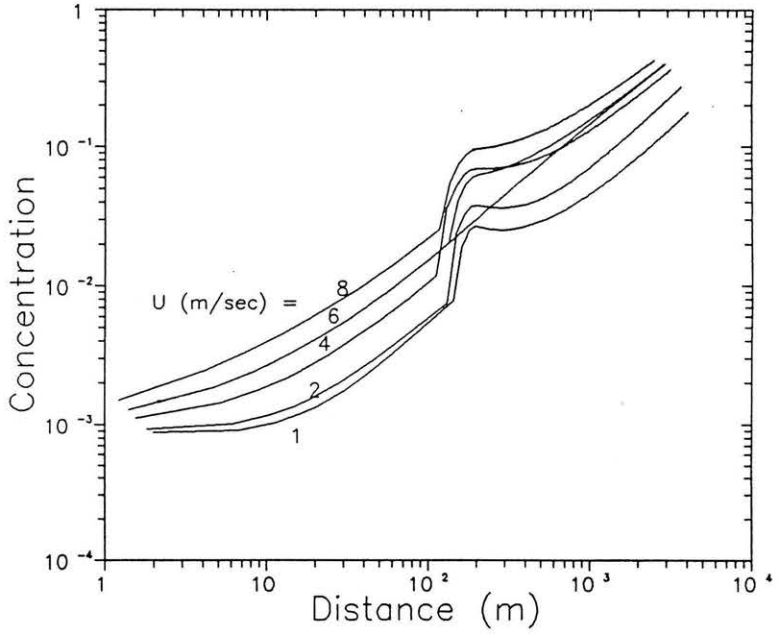

Fig. 6.1-4 FENC62 Predicted Plume Heights for Goldfish Test No. 1, Fence Height = 3 m, X = 100 m, U = 1, 2, 4, 6, and 8 m/sec

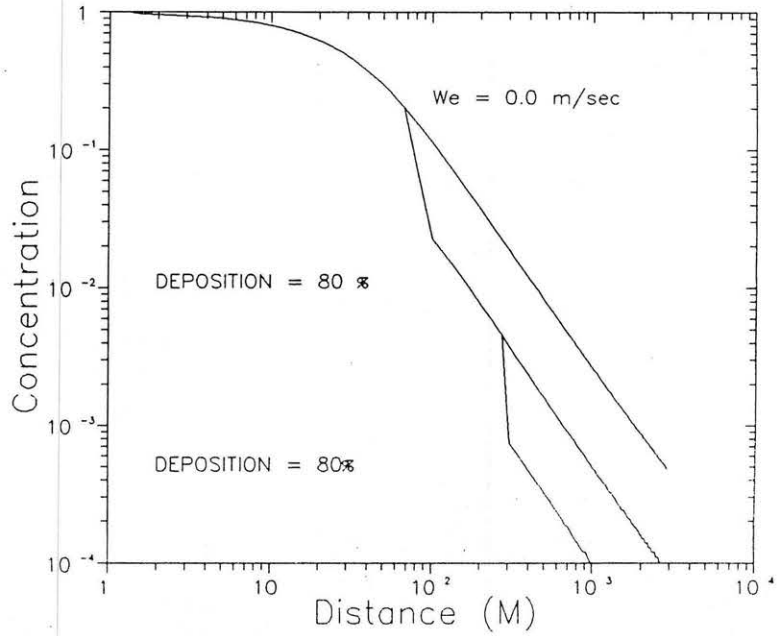

Fig. 6.2-1 SPRAY65 Predicted Plume Centerline Concentrations for Goldfish Test No. 1, 80% HF Removal by Water Spray at X = 100 m and X = 300 m

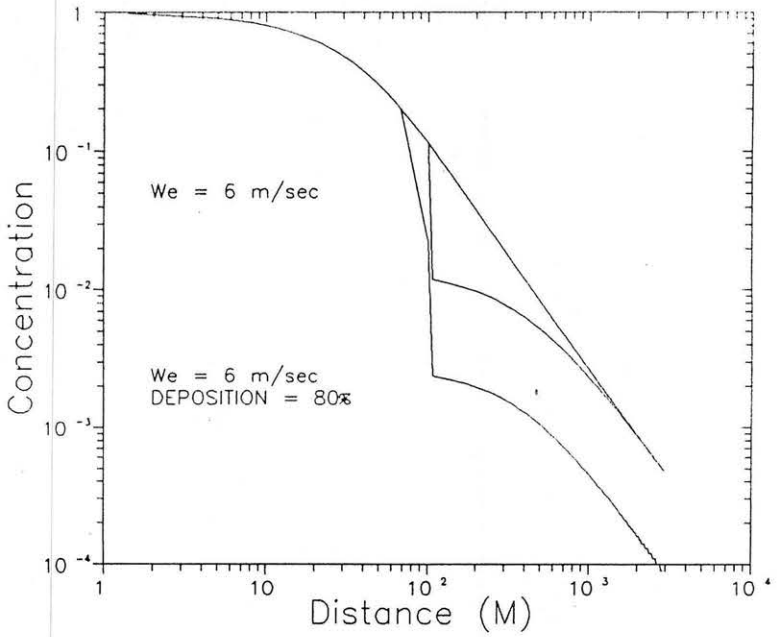

Fig. 6.2-2 SPRAY65 predicted plume centerline concentrations for Goldfish Test No. 1, 80% HF removal and W_e = 6 m/sec by a water spray at X = 100 m.

7.0 REMARKS ABOUT LABORATORY SIMULATION OF A HYDROGEN FLUORIDE SPILL

Measurements of the behavior of simulated hydrogen fluoride gas clouds dispersing over small-scale models placed in meteorological wind tunnels provide an opportunity to evaluate relative merits of various mitigation techniques and the associated hazards of the gas cloud in a controlled environment. Two systems at different geometric scales will exhibit similitude if a one to one correspondence exists in space and time between fluid particle kinematics (locations, velocities, accelerations and rotations) caused by fluid particle dynamics (pressures, gravity, Coriolis forces, viscous forces, etc.), when properly scaled by characteristic scales of fluid properties, force, length and time. To achieve this similarity, however, is not trivial. The specification of dimensionless parameters which guarantee similarity has historically been the subject of much discussion and debate.

The capabilities and limitations of physical modeling techniques for dense gas clouds were summarized by Meroney (1986a), and a formal set of guidelines were proposed by Meroney (1986b) to assure credible physical modeling for the prediction of behavior of dense gas clouds. This section discusses the specific range of HF spill conditions suitable for credible modeling, the need for special corrections applied to measured model concentrations, and the potential for modeling the reactive character of an HF cloud.

7.1 Wind Tunnel Performance Envelope for HF Spills

The viability of a given simulation scenario is not only a function of the governing flow physics but the availability of a suitable simulation facility and the measurement instrumentation to be employed. It is appropriate, therefore, to suggest bounds for the range of field situations which can reasonably be treated by physical modeling.

The major practical limitations of accurate wind tunnel simulation of HF cloud dispersion are (1) operational constraints, particularly the inability of most facilities to obtain a steady wind profile, or to accurately simulate atmospheric turbulence at the lowest wind speeds of interest, and (2) Reynolds number constraints (as yet somewhat ill-defined) associated with the proper scaling of the mixing turbulence and the frontal velocities. When these considerations are combined with estimates of the restraint to plume expansion by wind tunnel side walls, these considerations permit the development of performance envelopes for particular wind tunnel facilities.

Different performance envelopes result depending upon whether experimental focus is placed upon the behavior of pure HF and its associated high initial specific gravity (circa 10-14) or pre-diluted HF found in the region following jet mixing and its associated low specific gravity (circa 1.3). Two envelopes are considered below, one appropriate to the simulation of pure HF using an SF_6 simulant, and one appropriate to the simulation of dilute HF after it is mixed to a mass ratio of lbm

air/lbm HF equal to 5.0. In the latter case it is assumed that the simulant gas has a specific gravity equal to 1.29.

It is instructive to consider the operational constraints on meteorological wind tunnels to determine those field situations which may be exactly simulated or only marginally simulated. Operational limitations used to construct Figures 7.1-1 and 7.1-2 include:

1. Most large wind tunnels are unable to function satisfactorily at very low wind speeds (< 0.1 m/sec). At low wind speeds the wind tunnels become sensitive to small disturbances, both external and internal, which lead to unrealistic perturbation of the mean flow.

2. The associated inability to maintain large Reynolds number.

   a. When the characteristic obstacle Reynolds number ($Re = UL_c/\nu$) falls below 3300, wake turbulence no longer remains similar to field conditions. Figure 7.1-1 and 7.1-2 consider the limiting effect of a prototype obstacle ten meters tall.

   b. When the wall roughness Reynolds number ($Re_* = u_*Z_o/\nu$) falls below 2.5, the near-wall region will not behave in a fully turbulent manner. This turbulence level will govern HF mixing in the far-field region. Since HF vapor is hazardous at ppm levels, the correct simulation of this parameter is more critical than for flammable gases where cloud mixing drops below the flammability limit in the near-field region. Figures 7.1-1 and 7.1-2 show a curve presuming the field roughness length is 10 centimeters.

3. A minimum spatial resolution for concentration measurements of 2.0 mm is likely in the laboratory. Minimum pertinent vertical resolution required in the field to define vertical concentration profiles may be 0.25 m for a shallow HF cloud.

4. Mixing rates associated with molecular diffusion exaggerate dilution at low wind speeds. Molecular dispersion becomes significant for unobstructed flows (or after water spray or vapor barrier turbulence has diminished) when the Peclet/Richardson number ratio, Pe/Ri, is less than 1500, or Pe_*/Ri_* is less than 0.2. This effect may be particularly important for HF predictions, since the error produces concentrations which are too low.

5. Lateral interference with a spreading dense plume by wind tunnel walls. Interaction conditions may be calculated using the spread formula proposed and tested against laboratory and field spills by Britter (1980). Since the constraint this effect produces would be typically smaller than Reynolds number limitations for most meteorological wind tunnels (> 2 m wide), this curve is not shown on Figures 7.1-1 or 7.1-2.

6. Meteorological wind tunnels typically produce turbulent eddies no larger than the simulated boundary layer thickness. This results in model turbulent integral scales near 2 to 3 m, but atmospheric turbulence which dominates mixing in the far-field region supports ground level integral scales near 100 m. Thus, models with length scale ratios (LSR) smaller than about 33 should not be used in most meteorological wind tunnels.

Prototype velocities (U_p) plotted on Figures 7.1-1 and 7.1-2 are related to Length Scale Ratios (LSR) through equality of the Froude number parameter introduced in Chapter 4.0. An HF cloud has a source specific gravity near 10, and the densest isothermal simulant used in the laboratory is SF_6 with a specific gravity equal to 5.1. Thus increased laboratory wind speeds through distorted scaling of density is not possible, indeed model wind speeds are required significantly lower than for simulation of LNG, propane, chlorine, or other hazardous gases.

The final region for reliable simulation of HF dispersion down to ppm levels lies in a triangle between the Re* > 2.5 line and the Min Integral Scale line. Accurate scaling of far-field dispersion at prototype wind speeds below 5 m/sec or with model LSR above 100 is unlikely. Near field simulation of the influence of vapor barriers and water spray curtains is likely down to prototype wind speeds of 2 m/sec and model scales below 150. The quantitative penalty for working outside these envelopes is not very well defined. Many of the laboratory experiments discussed in Chapter 4.0 fall in the region to the right of the minimum wind speed criteria and below the minimum resolution criteria, but the experimentalists were focusing on near source plume behavior.

7.2 Conversion of Model Concentrations to HF Concentrations

The local molar concentrations, measured in the model and the prototype will be directly proportional to the actual number of moles released at the source. Most plume studies measure the concentration magnitudes at distances far downwind from the source; hence Snyder (1981) encourages analysts to evaluate source volume flux rates at ambient (not stack or source) temperatures. At long distances, the effect of volume flux ratio distortion and source gas temperature differences between a model and prototype are corrected by this approach. Unfortunately, correct simulation of the kinematics of dense plume motion and initial mixing near the source does require similarity of the volume flux ratio. Consideration of the molar concentrations, volume flux ratio effects, and source temperature distortions produces the following relation which relates prototype and model concentrations.

$$C_p = C_m/(C_m + (1 - C_m)(\underline{V}T_{amb}/T_s)_m/(\underline{V}T_{amb}/T_s)_p),$$

where $\underline{V} = Q/(U^*L_c^2)$ is the Volume Flux Ratio. Thus, whenever the Volume Flux Ratio is not simulated, or there are different source temperatures used in the model and prototype, the model concentrations must be corrected to field values. Of course this relation presumes that plume

kinematics and dynamics are correctly simulated in all other respects. Note that if $\underline{V}_m = \underline{V}_p$ and $(T_{amb}/T_s)_m = (T_{amb}/T_s)_p$, then $C_p = C_m$.

Assuming that the Volume Flux Ratio is exactly scaled between model and prototype and that an isothermal simulant at 300° K is used in the model, then for a pure HF gas released at the effective source temperature of 20° K, low prototype concentrations will be about 15 times larger than model measurements. Figure 7.2-1 displays the nature of the concentration correction over a wide range of molar concentrations. Given a model concentration measurement system accurate to 1 ppm, then 15 ppm HF levels can be predicted in the field; however, if the instrument is reliable to say 100 ppm, then only 1500 ppm HF levels can be predicted in the field.

Fortunately, an alternative approach which simulates plume behavior after it has diluted to the minimum temperature levels may be satisfactory. In this case concentration corrections may be quite small (See Figure 7.2-1). The only drawback to this procedure is the absence in the laboratory model of some source dynamics very close to the release point.

7.3 Potential for Laboratory Simulation of a Reactive Hydrogen Fluoride Plume

Water spray/HF measurements by Allied Corporation reported by Blewitt et al. (1987c) suggest that water sprays might remove 78% or more of the HF from a plume through chemical reaction and deposition. It would be desirable to simultaneously model the removal and dilution influence of water spray curtains and fences in a wind tunnel. Unfortunately, it is likely that the reaction rate response times, the heat transfer convection and conduction time constants, and the time constants associated with turbulent mixing will be mismatched during the typical model experiment. This has been found to be the case during model tests of the dilution of cryogenic gas clouds (See Andriev et al., 1983). Buitjles (1981) performed exploratory model tests with a NO plume and a tunnel flooded with ozone, O_3. The gas interaction involves a first-order chemical reaction; however, the measurements were not very extensive, and application of the technique seems limited.

The chemical reaction that occurs between HF gas and water requires large surface areas. Thus droplet sizes recommended in field experiments were less than 500 micrometers but larger than 100 micrometers to permit gravitational settling. To maintain an equivalent surface area ratio during model tests droplets at a length scale ratio of 100 must be less than 5 micrometers, but then little deposition would occur in the model experiment.

One must conclude that a study of a chemically reactive cloud in the wind engineering laboratory should be a subject for basic research and is not suitable for an environmental impact analysis at this time.

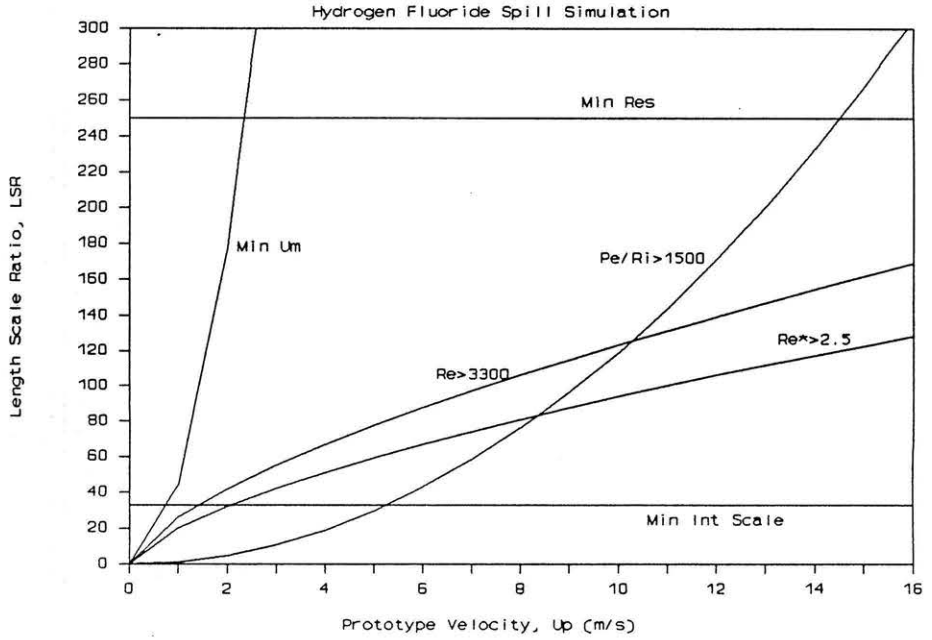

Fig. 7.1-1a Performance Envelope for Simulation of HF Spills in Meteorological Wind Tunnels, S.G. = 1.29

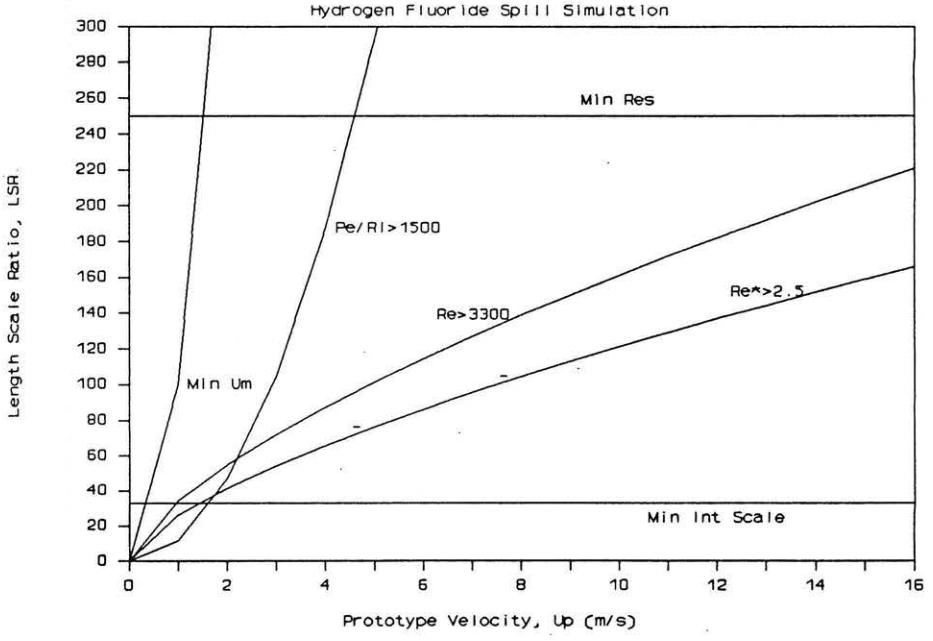

Fig. 7.1-1b Performance Envelope for Simulation of HF Spills in Meteorological Wind Tunnels, S.G. = 5.05

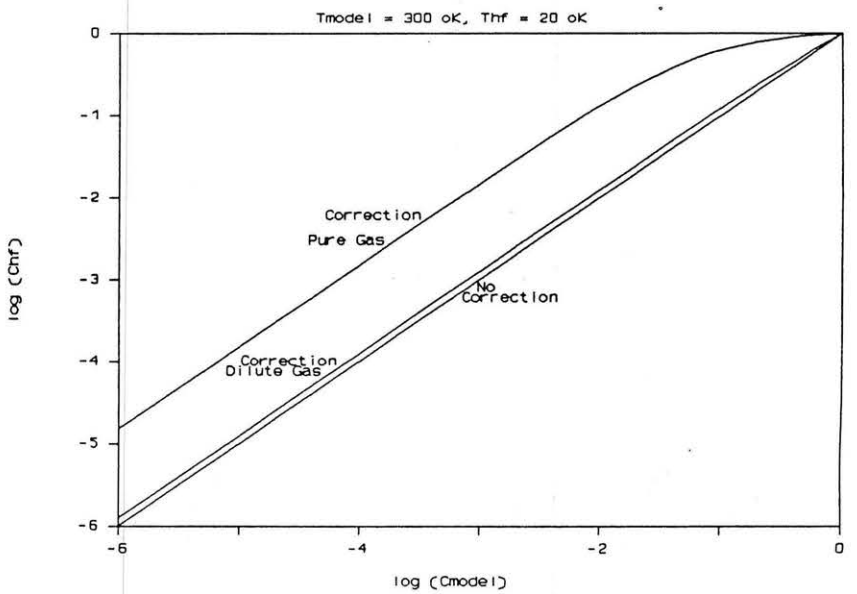

Fig. 7.1-2 Conversion of Model Concentrations to HF Concentrations, Corrections for Pure Gas and Dilute Gas Model Scenarios .

8.0 CONCLUSIONS

Accidental releases of Hydrogen Fluoride (HF) can result in initially dense gas clouds that will typically contain a mixture of gases, aerosols and droplets which can be transported significant distances before lower hazard levels of HF concentration are reached. The potential for hazard mitigation through the use of containment fences, vapor barriers or water-spray curtains to hold-up or delay a gas cloud expansion, elevate plume trajectories downwind of barriers, and enhance cloud dilution or remove HF gas from a cloud by deposition were considered in this report. Previous related field and laboratory experiments were analyzed to estimate the effectiveness of barrier devices. Conclusions drawn from these analysis and review follow.

8.1 Dilution Performance of Vapor Barriers in the Near-field Region

Eleven data sets from field and laboratory experiments dealing with the influence of vapor barrier fences and water spray curtains on the dispersion of dense gas clouds were examined. Tests were paired into sets of data which reflected the dilution of the cloud with and without the barriers present. Peak concentration ratios, cloud arrival time ratios, peak arrival time ratios, and departure time ratios were calculated for each test pair. Consideration of the regions immediately downwind from the fences and sprays (distances less than 300 m downwind of the barriers) reveals that:

Vapor Barrier Fences:

@ Concentrations directly downwind of a vapor fence may be slightly higher or lower than for plumes released in the absence of the fence. The concentrations then diminish to a minimum peak concentration ratio dependent upon source strength, spill volume, wind speed and fence height.

@ An additional fence or vortex generator located upwind of the source tends to reduce the likelihood of an increased concentration ratio directly downwind of the downwind fence.

@ Additional dilution occurs downwind of the fence as the turbulence produced by the shear at the top of the fence persists for about 30 fence heights.

@ A fence tall enough to hold up a dense gas cloud will produce a broader cloud immediately downwind of the barrier; thus concentrations to the sides of the cloud centerline will actually increase substantially above values found in the absence of the barrier.

@ Given comparable spill situations the decrease in concentration ratio is not strongly dependent upon Froude number magnitude or wind speed. ANOVA calculations suggest the most important variables are spill volume, and spill rate.

@ The peak concentration ratio is not significantly influenced by wind speed. Although the turbulence levels at fence top are expected to increase with wind speed, the cloud residence time in the fence wake decreases with increasing wind speed. The net effect is minimal variation in fence performance with wind speed.

@ Taller fences are more effective than shorter fences. The top of tall fences are at levels where higher wind speeds act. Taller fences also have longer wake regions.

@ Cloud arrival time, peak arrival time, and departure time ratios often increase directly downwind of a fence because lower winds in the wake advect the cloud more slowly. However, farther downwind the cloud arrives earlier because once the cloud leaves the wake region it is transported downwind with the greater depth averaged velocities associated with the increased cloud height. As the cloud height asymptotes to the no-fence conditions even farther downwind no change in arrival time will be observed.

Water Spray Curtains: Removal Charactersitics

@ Concentrations in a gas cloud will decrease abruptly as a result of chemical reaction and removal processes associated with HF and water spray interaction, even when accelerated entrainment associated with the water spray curtain is not considered. The removal efficiency will be a function of water/HF volume ratios, water droplet sizes and cloud concentrations.

Water Spray Curtains: Dilution Characteristics

@ Concentrations in a gas cloud will decrease abruptly by factors ranging from 2 to 80 depending upon barrier location, wind speed, water spray intensity, and spray/cloud intercept area.

@ Water spray curtains are more effective at low wind speeds. Given a constant curtain entrainment velocity, the dilution performance varies inversely with wind speed.

@ Water spray curtains are more effective closer to the source. As the water curtain is placed further downwind the dilution rate decreases; however for constant wind speed, water spray intensity, and intercept area the resultant concentrations downwind of the curtain are about equal.

@ A strategic combination of droplet size, spray pattern, and nozzle orientation can improve curtain performance by a factor of 2 to 5.

@ Cloud height directly downwind of a water spray curtain will increase proportional to the dilution obtained in the curtain.

@ Turbulence and mixing motions generated by the spray curtain do not appear to persist downwind of the curtain location.

8.2 Dilution Performance of Vapor Barriers in the Far-field Region

HF is hazardous at ppm levels. Thus, far-field concentrations are of interest in evaluating mitigation strategies. Most laboratory and field experiments were originally constructed to consider the behavior of flammable gases; hence, measurements were only taken at distances out to 1000 m downwind or less. Consideration of the regions modestly far downwind of barriers and spray curtains (300 m to 1000 m) reveals that:

Vapor Barrier Fences:

@ Entrainment levels return to pre-fence levels at distances greater than 30 to 50 fence heights downwind of the fence location. After that point the concentrations asymptote to levels found in the absence of the fence or barrier about 2000 m downwind of fences placed between 10 and 100 meters downwind of the spill site.

@ Again peak concentrations measured during the experiments did not generally fall below 10,000 ppm of simulant or 150,000 ppm HF over the measurement domain. The one exception was data from the unperturbed Goldfish HF Trials where peak concentrations as low as 200 ppm HF were measured at 3000 m downwind of the spill site. Again it appears that plausible height fences (5 to 10 m) would produce dilutions that would asymptote to levels found in the absence of the fence 2000 m downwind.

Water Spray Curtains: Removal Characteristics

@ The reduction in HF cloud concentrations induced by water spray/cloud deposition processes persists at all downwind distances.

Water Spray Curtains: Dilution Characteristics

@ Vertical entrainment rates return to pre-curtain values just downwind of the curtain location; hence, concentrations initially decay with distance at a rate lower than that found without spray curtains. The concentration levels asymptote to unperturbed plume levels about 2000 m downwind of curtains placed between 10 and 100 meters downwind of the spill site.

@ Peak concentrations measured during the experiments did not drop below 10,000 ppm of simulant or 150,000 ppm HF over the measurement domain. It appears, however, that intersection of the original plume concentrations and the perturbed plume concentrations would occur about 1000 m downwind at levels near these values.

@ In the far-field, but before the cloud asymptotes to no-curtain sizes, cloud arrival time, peak arrival time, and departure time ratios are less than without curtains. Again this is associated with higher depth-averaged velocities which advect the deeper clouds faster.

8.3 Vertical Concentration Distributions

Vertical concentration distributions were available from the data taken during the pre-Falcon Trials vapor barrier tests (Chapter 4.8) and the water spray curtain tests (Chapter 4.5).

Close to the fence ($x/H < 2$) during the pre-Falcon Trials elevated concentration maximums occurred as the plume flowed over the fence. However, at all other downwind distances the maximum occurred at ground level. Vertical concentrations indicated a well mixed plume existed to heights above the measurement domain. Vertical concentration profiles measured without a fence present displayed the characteristic of shallow plumes decaying exponentially with height observed for dense gas clouds.

At elevated heights the cloud arrived and departed earlier for the enclosure cases than for the unperturbed situation.

Water spray curtain measurements produced very similar shape plumes to the fence scenarios; however, no elevated maximum occurred near the curtain.

8.4 ANOVA Regression Model

The ANOVA multilinear regression model was only applied to the pre-Falcon data set, since this data was the most complete, reliable, and comprehensive available.

The ANOVA procedure was applied to the logarithmic version of a simple power law formulae, i.e.

$$(1 - C_w/C_{wo}) = A*Fr^a*\underline{V}^b*(Vol/L_c^3)^c*(H/L_c)^d*(x/L_c)^e,$$

where A, a, b, c, d, and e are constants to be determined by the ANOVA procedure. Since the peak concentration ratios were prepared from comparable data pairs, it was quickly found that inclusion of the Froude number term did not reduce variance significantly. The dominant terms were volume spill rate and total volume spilled. The optimum relation found was:

$$C_w/C_{wo} = 1 - 1.55*\underline{V}^{0.051}*(Vol/L_c^3)^{-0.163}*(H/L_c)^{0.04}*(x/L_c)^{-0.035}.$$

This expression applies only to a spill completely surrounded by a fence enclosure of aspect ratio 2 to 1 with wind flowing along the longitudinal dimension of the enclosure. The method is also limited to the data range near to that used to determine the coefficients.

8.5 Proposed Entrainment Models

Given a box or depth-integrated type numerical model simple expressions to account for the increased entrainment associated with water spray curtains or fence barriers may be used with confidence. These models do not account for chemical reactions, deposition, gravity current reflection, rapid flow speed up through a porous barrier, or the presence of a hydraulic jump downwind of a barrier. Both the initial dilution and post-barrier concentration decay are predicted well. The essence of the entrainment models are:

Fence entrainment model:

$$(w_e)_{fence} = 0.1\ U(H)(1 - P)(1 - (x - x_f)/(30\ H)),$$

where U(H) is the wind speed at fence height, P is fence porosity, H is fence height, x is distance downwind of the spill point, x_f is the fence location. Note that $(w_e)_{fence}$ exceeds background entrainment rates only to 30H downwind of the fence, after which it is set to zero.

The entrainment velocities above should be added to the values available calculated for entrainment from turbulence in the background atmospheric flow.

Water spray entrainment model:

$$(w_e)_{spray} = \frac{Q_s(T_{amb}/T_s)(1 - C_{spray}/C_{no\ spray})}{C_{spray}N(\pi * d_g^2/4)},$$

where Q_s is HF source strength, N is the total number of spray nozzles, and d_g is the spray intercept diameter with the cloud. This equation does somewhat presume the answer desired; however, other expressions related to the dynamics of the water spray nozzles themselves are available (Moodie, 1985).

8.6 Laboratory Simulation of a Hydrogen Fluoride Spill

The capabilities and limitations of physical modeling techniques for HF gas clouds were reviewed. Performance envelopes were constructed to illustrate the constraints of facilitiy size and gravity spreading. The following conclusions were made:

- @ Laboratory simulation of a pure HF release with an isothermal simulant is not recommended. Reliable simulations would be limited to prototype wind speeds greater than 5 m/sec at scales less than 1:100. Model concentrations must be adjusted upward by a factor of 15 in the far downwind regions.

- @ Laboratory simulation of a pre-diluted HF cloud can be accomplished. Reliable simulations should be possible at all

distances for prototype wind speeds greater than 5 m/sec at scales less than 1:100.

@ Reliable simulations of pre-diluted HF clouds should be possible in the near-field of barriers and sprays for prototype winds speeds greater than 2 m/sec and at scales less than 1:150. The quantitative penalty for working outside these ranges is not well defined.

@ The laboratory simulation of a water spray curtain and a reactive hydrogen fluoride plume cannot be recommended without further basic research. Basic studies of how reactive plumes disperse in the presence of humidity, reactants, turbulence, and compressibility effects should be supported.

REFERENCES

Abramovich, G.N. (1963), The Theory of Turbulent Jets, The M.I.T. Press, Cambridge, Mass, 671 pp.

Allwine, D.J., Meroney, R.N. and Peterka, J.A. (1979), "Rancho Seco Building Wake Effects on Atmospheric Diffusion: Simulation in a Meteorological Wind Tunnel," Technical Report for U.S. Nuclear Regulatory Commission.

Andreiev, G., Meroney, R. N., and Neff, D. E. (1983), "Heat Transfer Effects During Cold Dense Gas Dispersion," for Gas Research Institute, GRI Report GRI 83/0082, CER83-84DEN-RNM3.

Blackmore, D.R., Herman, M.N., and Woodward, J.L. (1982), "Heavy gas dispersion models," J. Haz. Mat., Vol. 6, pp. 107-128.

Blewitt, D.N., Yohn, J.F., Koopman, R.P., and Brown, T.C. (1987a), "Conduct of Anhydrous Hydrofluoric Acid Spill Experiments," Proceedings of International Conference on Vapor Cloud Modeling, CCPS, Cambridge, MA, 2-4 November, pp. 1-38.

Blewitt, D.N., Yohn, J.F., and Ermak, D.L. (1987b), "An Evaluation of SLAB and DEGADIS Heavy Gas Dispersion Models Using the HF Spill Test Data," Proceedings of International Conference on Vapor Cloud Modeling, CCPS, Cambridge, MA, 2-4 November, pp. 56-80.

Blewitt, D.N., Yohn, J.F., Koopman, R.P., Brown, T.C., and Hague, W.J. (1987c), "Effectiveness of Water Sprays on Mitigating Anhydrous Hydrofluoric Acid Releases," Proceedings of International Conference on Vapor Cloud Modeling, CCPS, Cambridge, MA, 2-4 November, pp. 155-180.

Bodurtha, F.T. (1980), Industrial Explosion Prevention and Protection, McGraw-Hill Book Company, New York, 167 pp.

Bouwmeester, R.J.B., Meroney, R. N., and Kothari, K.M. (1979), "Algorithm to Estimate Field Concentrations in the Wake of a Power Plant Complex Under Nonsteady Meteorological Conditions from Wind-tunnel Experiments," Journal of Applied Meteorology, Vol. 30, pp. 92-101.

Brenchley, D.L. (1981), "Assessment of Research and Development (R&D) Needs in Ammonia Safety and Environmental Control," U.S. D.O.E. Contract DE-AC06-76RLO 1830, Pacific Northwest Laboratory, Battelle Memorial Institute Report PNL-4006.

Briggs, G.A. and Binkowski, (1986), "Research on Diffusion in Atmospheric Boundary Layers: A Position Paper on Status and Needs," Atmospheric Sciences Research Laboratory, U.S. E.P.A., Research Triangle Park, North Carolina, 227 pp.

Britter, R.E. (1980), "The ground level extent of a negatively buoyant plume in a turbulent boundary layer," Atmos. Envir., Vol. 9, pp. 779-785.

Britter, R.E. (1982), "Special Topics on Dispersion of Dense Gases," Report on Contract No. 1200/01.01, Research and Laboratory Services Division, Health and Safety Executive, Sheffield, U.K., 100 pp.

Builtjes, P.J.H. (1980), "The modelling of a chemically reacting plume in a windtunnel," Extended abstract for 3rd Symposium on Turbulent Shear Flows, Univ. of California, Davis, September 1981, 8 pp.

Coast Guard (1974), "CHRIS: Hazard Assessment Handbook," Department of Transportation, Report COMDTINST MI6465.13 (old CG-446-3).

Crum, J.M. (1986), "Accidental Release Case Histories and Credible Scenarios," Joint EPA/DOE Workshop on Determination of Atmospheric Dilution for Emergency Preparedness, 15-17 October 1986, Raleigh/Durham, North Carolina, 23 pp.

Davenport, J.A. (1977), "A Survey of Vapor Cloud Incidents," Chemical Engineering Progress, September, pp. 54-63.

Davies, M.E. and Inman, P.N. (1986), "Wind Tunnel Modelling of the Thorney Island Heavy Gas Dispersion Trials," Gas Research Institute Contract No. 5084-252-1016, British Maritime Technology, U.K.

DeSteese, J.G. (1982), " Assessment of Research and Development (R&D) Needs in LPG Safety and Environmental Control," U.S. D.O.E. Contract DE-AC06-76RLO 1830, Pacific Northwest Laboratory, Battelle Memorial Institute Report PNL-3991.

Diener, R. (1988) Personal Communication, EXXON Schotte Model, EXXON Research and Engineering Company, Florham Park, N.J.

Ermak, D.L., Chan, S.T., Morgan, D.L., and Morris, L.K. (1982), "A comparison of dense-gas dispersion model simulations with Burro series LNG spill test results," J. Haz. Mat., Vol. 6, pp. 129-160.

Griffiths, R.F. and Kaiser, G.D. (1979), "The Accidental Release of Anhydrous Ammonia to the Atmosphere - A Systematic Study of Factors Influencing Cloud Density and Dispersion," Safety and Reliability Directorate Report SRD R 154, United Kingdom Atomic Energy Authority, Wigshaw Lane, Culcheth Warrington, 36 pp.

Hague, W.J. (1988), Personal Communication, Schotte Model Calculations, Allied Corporation, Morristown, N.J.

Hardee, H.C. and Lee, D.O. (1975), "Expansion of Clouds from Pressurized Liquids," Accid. Anal. & Prev., Vol. 7, pp. 91-102.

Hartwig, S. and Flothmann, D. (1980), "Open and controversial problems in the development of models for the dispersion of a heavy gas," Heavy Gas and Risk Assessment, S. Hartwig (ed.), Battelle-Institut e.V., Frankfurt am Main, BRD, p. 1-14.

Hatcher, R.V., Meroney, R.N., Peterka, J.A. and Kothari, K. (1977), "Dispersion in the Wake of a Model Industrial Complex," Technical Report for U.S. Nuclear Regulatory Commission.

Havens, J.A. and Spicer, T.O. (1985), "Development of an Atmospheric Dispersion Model for Heavier-than-Air Gas Mixtures," Report No. CG-D-22-85 for the U.S. Coast Guard by the Chem. Eng. Dept., University of Arkansas, Fayetteville, Ark., Three volumes.

Heskestad, G., Kung, H.C., and Todtenkopf, N.F. (1976), "Air Entrainment into Water Sprays and Spray Curtains, American Society of Mechanical Engineers Paper 76-WA/FE-40, 11 pp., plus Erratum, 18 January, 1977, 4 pp.

Heskestad, G., Meroney, R.N., Kothari, K.M., and Neff, D.E. (1983), "Effectiveness of Water Spray Curtains in Dispersing LNG Vapor Clouds," Proceedings of the American Gas Association Transmission Conference, {a[er 93-T-60. 1-4 May, Seattle, Washington, pp. T-169 to T-183.

Heskestad, G. (1985), "Dispersal of LNG Vapor Clouds with Water Spray Curtains: Phase 2B-Extended Wind Tunnel Experiments," Gas Research Institute, Report GRI-85/0031, 106 pp.

Hirst, W.J.S. (1986), "Combustion of Large-Scale Releases of Pressurized Liquid Propane," Heavy Gas and Risk Assessment - III, S. Hartwing (ed.) Battele-Institut e.V.m Frankfurt am Main, BRD, pp. 267-286.

Jagger, S.F. and Edmondson, J.N. (198-), "Discharge of Dense Gases from Relief Valves - A Method for Calculating Safe Discharge Velocities to Allow for Different Weather Conditions," I. Chem. E. Symposium Series No. 85, U.K., 15 pp.

Jagger, S.F. and Kaiser, G.D. (1980), "The Accidental Release of Dense Flammable and Toxic Gases from Pressurized Containment - Transition from Pressure Driven to Gravity Driven Phase," Proceedings of 11th NATO/CCMS ITM on Air Pollution MOdeling and Its Applications, Amsterdam, 24-27 November, 13 pp.

Kaiser, G.D. and Griffiths, R.F. (1982), "The Accidental Release of Anhydrous Ammonia to the Atmosphere: A Systematic Study of Factors Influencing Cloud Density and Dispersion," Journal of the A.P.C.A., Vol. 32, No. 1, pp. 66-71.

Kaiser, G.D. and Walker, B.C. (1978), "Releases of Anhydrous Ammonia from Pressurized Containers - The Importance of Denser-than-air Mixtures," Atmospheric Environment, Vol. 12, pp. 2289-2300.

Koenig, G. and Schatzmann, M. (1986), "Experimentelle Untersuchung des Einfluesses von Gebaudeformationen af die Ausbreitung Schwerer Gases," BMFT-Forschunsvorhaben RGB 8324, Meteorologisches Institut,Universitat Hamburg, 110 pp.

Koenig, G. and Schatzmann, M. (1986), "Wind Tunnel Modeling of Density Current Interaction with Surface Obstacles," Int. Symposium on Buoyant Flows, National University of Athens, 9 pp.

Kothari, K. and Meroney, R.N. and Peterka, J.A. (1979), "Nuclear Power Plant Building Wake Effects on Atmospheric Diffusion: Simulation in Wind Tunnel," Technical Report for Electric Power Research Institute, EPRI NP-1891.

Kothari, K. M. and Meroney, R. N. (1980), "Dispersion of Vapor from LNG Spills at Green Point Energy Center: Simulation in a Wind Tunnel," Brooklyn Union Gas Company, New York, CER79-80KMK-RNM9.

Kothari, K. M. and Meroney, R. N. (1981), "Dispersion of Vapor From LNG Spills at Energy Terminal Service Corporation: Simulation in a Wind Tunnel, ETSC, Newark, New Jersey, CER80-81KMK-RNM59.

Kothari, K. M. and Meroney, R. N. (1981), "LNG Plume Interaction with Surface Obstacles," for Gas Research Institute, GRI Report GRI 80/0095, CER81-82KMK-RNM22.

Kothari, K. M. and Meroney, R. N. (1982), "Accelerated Dilution of Liquefied Natural Gas Plumes with Fences and Vortex Generators," for Gas Research Institute, GRI Report GRI 81/0074, CER81-82KMK-RNM79.

Kothari, K. M. and Meroney, R. N. (1986), "Liquefied Natural Gas (LNG) Plume Interaction with Surface Obstacles," ASME Paper No. 84-WA/HT-77, ASME J. of Heat Transfer, Vol. 108, No. 2., CEP83-84KMK-RNM20.

McQuaid, J. (1975), "Air Entrainment into Bounded Axisymmetric Sprays," Proc. Inst. Mech. Eng., Vol. 189, pp. 197-202.

McQuaid, J. (1977), "The Design of Water Spray Barriers for Chemical Plants," 2nd International Loss Prevention Symposium, Heidelberg, DECHEMA, Frankfurt, pp. 511-518.

McQuaid, J. (1982), "Future Directions of Dense-gas Dispersion Research," J. of Hazardous Materials, Vol. 6, pp. 231-247.

McQuaid, J. and Fitzpatrick, R.D. (1981), "The Uses and Limitations of Water-Spray Barriers," Northwestern Brach Symposium Papers 1981, No. 5, Institution of Chemical Engineers, Manchester, U.K., pp. 1.1-1.13.

McQuaid, J. and Roebuck, (1984), "Large Scale Field Trials on Dense Vapor Dispersion - Final Report to Sponsors on Heavy Gas Dispersion Trials at Thorney Island 1982-1984," Health and SAfety Executive, Sheffield, U.K.

Meroney, R.N. (1980), "Wind-tunnel experiments on dense gas dispersion," J. of Hazardous Materials, Vol. 6, Nos. 1 & 2, pp. 85-106.

Meroney, R.N. (1980), "Physical Simulation of Dispersion in Complex Terrain and Valley Drainage Flow Situations", Proceedings 11th NATO/CCMS International Technical Meeting on Air Pollution Modeling and Its Applications, Amsterdam, the Netherlands, 25-28 November 1980, 21 pp.

Meroney, R.N. (1982), "Building Aerodynamics", Chapter 11 from Engineering Meteorology, (ed. E.Plate), Elsevier Publishing Company, New York.

Meroney, R. N. (1982), "Wind-Tunnel Experiments on Dense Gas Dispersion," Dense Gas Dispersion, R. E. Britter and R. F. Griffiths, eds., Elsevier Scientific Pub. Co., 1982.

Meroney, R. N. (1984a), " Transient Characteristics of Dense Gas Dispersion; Part I: A Depth-Averaged Numerical Model," J. of Hazardous Materials, Vol. 9, pp. 139-157.

Meroney, R. N. (1984b), "Transient Characteristics of Dense Gas Dispersion; Part II: Numerical Experiments on Dense Cloud Physics," J. of Hazardous Materials, Vol. 9, pp. 159-170.

Meroney, R.N., Bowen, A.J., Lindley, D. and Pearse, J.R. (1978), "Wind Characteristics over Complex Terrain: Laboratory Simulation and Field Measurements at Rakaia Gorge", New Zealand, U.S. Dept. of Energy Report RLO/2438-77/2, 219 pp.

Meroney, R. N., Cermak, J. E., and Neff, D. E. (1976), "Wind Tunnel Study of the Negatively Buoyant Plume Due to an LNG Spill," Prepared for R & D Associates, Marina del Rey, California, CER76-77RNM-JEC-DEN22.

Meroney, R. N. and Kothari, K. M. (1980), "Building Effects on the National Transonic Facility Exhaust Plume," NASA, Langley Research Center Contract NASI-15925, CER79-80KMK-RNM35.

Meroney, R. N., Kothari, K. M., Neff, D. E., and Andreiev, G. (1983), "Model Study of Liquefied Natural Gas Vapor Cloud Dispersion with Water Spray Curtains," for Factory Mutual Research Corporation, CER82-83RNM-KMK-DEN-GA41.

Meroney, R. N. and Lohmeyer, A. (1982), "Gravity Spreading and Dispersion of Dense Gas Clouds Released Suddenly into a Turbulent Boundary Layer," for Gas Research Institute, GRI Report 82/0025, CER82-83RNM-AL-7.

Meroney, R. N. and Lohmeyer, A. (1984), "Prediction of Propane Cloud Dispersion by a Wind-Tunnel-Data Calibrated Box Model," J. of Hazardous Materials, Vol. 8, pp. 205-221.

Meroney, R. N., Lohmeyer, A., and Plate, E. J. (1981), "Model investigations of the Spreading of Heavy Gases Released from an Instantaneous Source at the Ground," Air Pollution Modeling and Its Application, C. De Wispelaere, ed., Plenum Publishing Co., pp. 433-448.

Meroney, R. N. and Neff, D. E. (1985), "Numerical Assessment of Water Spray Barriers for Dispersing Dense Gases," Atmospheric Environment, Vol. 31, pp. 233-247.

Meroney, R. N., Neff, D. E., Cermak, J. E., and Megahed, M. (1977), "Dispersion of Vapor from LNG Spills - Simulation in a Meteorological Wind Tunnel - Part II," Prepared for R & D Associates, Marina del Rey, California, CER76-77RNM-JEC-DEN-MM57.

Meroney, R. N., Neff, D. E., and Heskestad, G. (1984), "Wind-Tunnel Simulation of the U.K. Health and Safety Executive Water Spray Curtain Dense Gas Dispersion TEsts," J. of Boundary Layer Meteorology, Vol. 28, pp. 107-119

Moodie, K., Taylor, G. and Beckett, H. (1981), "Water Spray Barrier Trials: 181, Test Parameters and Concentration Data for Trials 35-48," Health and Safety Executive Report FM/15/81/3, Sheffield, U.K., 60 pp.

Neff, D. E. and Meroney, R. N. (1979), "Dispersion of Vapor from LNG Spills - Simulation in a Meteorological Wind Tunnel of Spills at China Lake Naval Weapons Center, California," U. S. Coast Guard, Department of Transportation, Contract DOT CG-75279-A, CER78-79DEN-RNM-1.

Neff, D. E. and Meroney, R. N. (1981), "The Behavior of LNG Vapor Clouds: Wind Tunnel Simulation of 40 m^3 LNG Spill Tests at China Lake Naval Weapons Center, California," for Gas Research Institute, GRI Report GRI 80/0094, CER81-82DEN-RNM-1

Neff, D. E. and Meroney, R. N. (1982), "The Behavior of LNG Vapor Clouds: Wind-Tunnel Tests on the Modeling Heavy Plume Dispersion," for Gas Research Institute, GRI Report GRI 80/0145, CER81-82DEN-RNM25.

Plate, E.J. and Baechlin, W. (1987), "Wind Tunnel Tests as Part of a Warning System for Accidental Gaseous Spills," Proceedings of 7th International Conference on Wind Engineering, Aachen, FRG, 6-10 July 1987, Vol. 3, pp. 239-249.

Puttock, J.S., Blackmore, D.R., and Colenbrander, G.W. (1982), "Field experiments on dense gas dispersion," J. Haz. Mat., Vol. 6, pp. 13-41.

Ricou, F.P. and Spalding, D.B. (1961), "Measurements of entrainment by axisymmetrical turbulent jets," J. of Fluid Mechanics, Vol. II, pp. 21-32.

Rottman, J.W. and Hunt, J.C.R. (1985), "The initial and gravity-spreading phases of heavy gas dispersion: Comparison of models with Phase I data,", J. Haz. Mat., Vol. 11, pp. 261-279.

Rottman, J.W., Simpson, J.E., Hunt, J.C.R., Britter, R.E. (1985), "Unsteady gravity current flows over obstacles: Some observations and analysis related to the Phase II trials," J. Haz. Mat., Vol. 11, pp. 325-340.

Saminy, M. (1983), "The Fluid Dynamics of Safety Valve Vent Stacks," ASME Paper 83-WA/FE-21, 7 pp.

Schotte, W. (1987), "Fog Formation of Hydrogen Fluoride in Air," Ind. Eng. Chem. Res., Vol. 26, pp. 300-306.

Shaw, P. and Briscoe, F. (1978), "Evaporation from Spills of Hazardous Liquids on Land and Water," Safety and Reliability Directorate Report SRD R 100, U.K. Atomic Energy Authority, 52 pp.

Snyder, W.H. (1981), "Guideline for Fluid Modeling of Atmospheric Diffusion," USEPA, Environmental Sciences Research Laboratory, Office of Research and Development, Research Triangle Park, NC, Report No. EPA600/8-81-009.

Wiekema, B.J. (1984), "Vapor Cloud Explosions - An Analysis Based on Accidents," Jour. of Hazardous Materials, Vol. 8, pp. 295-311.

Wilson, D.J. (1981), "Expansion and Plume Rise of Gas Jets from High Pressure Pipeline Ruptures," Research Report for Pollution Control Division, Alberta Environment, Canada, 61 pp.

APPENDIX: Numerical Simulation of Water Spray Dilution of Gas Plumes

A.1 Entrainment due to a water-spray barrier

The presence of a water spray barrier results in a local increase in entrainment rate. McQuaid and Fitzpatrick (1981) hypothesized a finite increase in local entrainment without specifying how the numbers would be related to nozzles used or their location; however, McQuaid (1975) derived a semi-empirical relationship for conical sprays which gives the rate of entrainment of air as a function of water flow, water pressure and size of spray. Of course, $(w_e)_{spray} = Q_e/A_i$, where Q_e is the flux of air entrained and A_i is the area of intersection between cloud and spray. Heskestad et al. (1976) also predicted a range of entrainment rates in terms of water flow, spray type, spray angle and distance from the nozzle. Values of entrainment rate velocity ranged from 5.0 to 34.0 m/sec when nozzle diameters ranged from 1 to 25 mm, spray angles ranged from 30 to 130°, and cloud intersection distance varied from 0.25 to 4.0 m.

Water spray entrainment can be included in the numerical models by either using a multiplicative factor with the normal entrainment rate, i.e.,

$$(w_e)_{total} = MR \times w_e,$$

or an additive factor, i.e.,

$$(w_e)_{total} = w_e + (w_e)_{spray}.$$

The additive factor approach must be considered more realistic; however, there are circumstances where a multiplicative methodology might be more convenient if shown to be nominally effective. The area of interaction, A_i, is specified by the downwind interval, S, over which the spray intersects the plume. To ensure good mixing, McQuaid (1977) suggested a minimum velocity of air in the spray of $(w_e)_{spray} > 6$ m/sec at the plane where the spray meets the gas. In a 3 m/sec wind, a typical level of entrainment due to shear mixing alone would be 0.2 m/sec; hence, the multiplicative factors will range from 25 to 170.

The interval of spray interaction, S, should relate to lateral nozzle separation, L_s, and impact circle diameter, d_g, by the equation

$$S = \pi * d_g^2/(4L_s).$$

The effective entrained air velocity may be estimated from actual field or laboratory data from

$$(w_e)_{spray} = \frac{Q_s(T_{amb}/T_s)(1 - C_{spray})/C_{no\ spray})}{C_{spray}N(\pi * d_g^2/4)},$$

where N is the total number of spray nozzles. Alternatively one must estimate entrainment velocities from methods proposed by McQuaid (1975) or Heskestad (1976).

These models for water spray interaction with dense gas clouds have been validated by comparison with extensive laboratory measurements (Meroney and Neff, 1985).

A.2 Calibration of the Water Spray Entrainment Model

In a paper by Meroney and Neff (1985) extensive comparisons were made of the water spray algorithms proposed in Chapter 2.4 and the laboratory water spray tests discussed in Chapter 4.5. As shown in Figures A.2-1, 2, and 3 the use of an additive specified water spray entrainment velocity over the intercept region of the gas cloud faithfully reproduces measurements. The comparisons were made over a 5-fold range of water spray intensity and a 2.5-fold range of wind speed. Note that increased wind speed tends to decrease the diluting effect of the water spray curtain. This result occurs because at higher wind speeds the gas cloud parcels spend a shorter time within the spray curtain.

An additive water spray entrainment factor which is proportional to water volume flow rate, droplet size, and spray angle will adequately predict the initial dilution of a gas cloud passing through a spray curtain. The numerical model also satisfactorily reproduces the post spray curtain concentration decay rates.

A.3 Goldfish Trial No. 1 with Water Sprays

As noted in Chapter 5.2 water spray curtain tests were performed during the Goldfish Trials No. 4, 5, and 6. These tests included chemical reactions between the HF and the water spray and subsequent deposition of the HF on the ground. Goldfish Trial No. 1 conditions are used below to examine the effect of various spray placement and water spray entrainment rate alternatives.

Effects of Spray Barrier Location

In these calculations, only the location of the spray curtain was changed: from 30 to 50 to 100 to 400 meters downwind of the spill center. A nominal spray entrainment rate of 6 m/sec was chosen for these calculations. Figure A.3-1 displays box model predictions. The post spray concentrations are very similar with slightly lower concentrations when the spray is further downwind. The magnitude of the reduction in concentrations when the barrier is farther from the source is not large and any advantage in final concentrations would be outweighed by the greatly increased water consumption as the spray curtain width increases over the wider plume. Note that none of the spray curtains manage to dilute the peak concentrations significantly beyond 1000 m, yet concentrations still exceed 2000 ppm, which is far above the TLV for HF.

Figure A.3-2 displays the effect of a water spray curtain on plume height when activated at various downwind distances. Near the source cloud height is increased 25-fold; whereas further downwind the same spray curtain only causes a 2.5-fold increase in height.

Effects of Spray Entrainment Rate

Calculations were performed for a ten-fold range of spray entrainment velocity. Given a constant spray location (100 m), wind speed (5.6 m/sec), and plume width, increased entrainment velocities result in proportional increases in dilution. As noted in Figure A.3-3 a fairly substantial entrainment rate of 10 m/sec will result in about a ten-fold dilution for these conditions.

Plume height also increases at a rate proportional to water spray entrainment velocity in Figure A.3-4.

Effects of Wind Speed

Increased wind speed advects the gas plume through the spray zone more quickly. Figures A.3-5 and 6 exhibit the marked effects of wind speed on dilution effectiveness. Given a constant water spray entrainment rate of 6 m/sec, then a plume moving slowly through the spray curtain at 1 m/sec will receive about 12.5 times more dilution than a plume traveling at 10 m/sec. Cloud height increases by the same ratio.

Water Spray Effects on Arrival, Peak Concentration and Departure Times

SPRAY23 was used to estimate the influence of a water spray barrier on the downwind arrival of a transient gas cloud. A base case of a spray curtain located 100 m downwind of the source operating with the Goldfish Test No. 1 atmospheric and spill conditions and a water spray entrainment velocity of 1 m/sec was considered. Cloud arrival and departure were determined by two separate techniques. In Figure A.3-7 the arrival and departure of the could based on cloud height are shown. The cloud is seen to arrive and depart in a wave like manner with a sudden rise and fall in height. Note that the cloud arrives and departs earlier in the presence of the water spray curtain. In Figure A.3-8 the arrival and departure times are based on the arrival and departure of the 10% of peak concentration levels. The peak arrival time was chosen to be when the local concentration reaches 90% of the maximum level. This value was chosen since the peak in the time trace was sometimes rather flat.

The decrease in arrival, peak arrival, and departure times result from the lofting of concentration to greater heights by the spray curtain. The raised portion of the cloud travels at greater velocities since the boundary layer permits wind velocity to increase with height. Downwind the cloud disperses downward to the ground resulting in shorter arrival, peak arrival, and departure times.

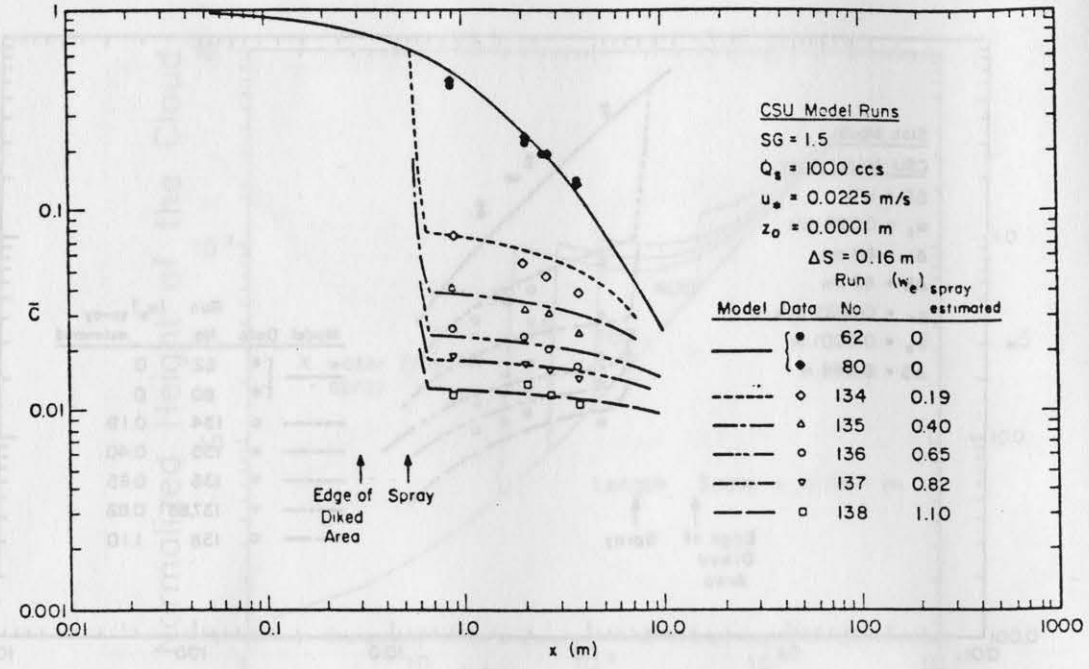

Fig. A.2-1 Comparison of Observed and SPRAY62 Predicted Plume Centerline Concentrations for Colorado State Water Spray Tests

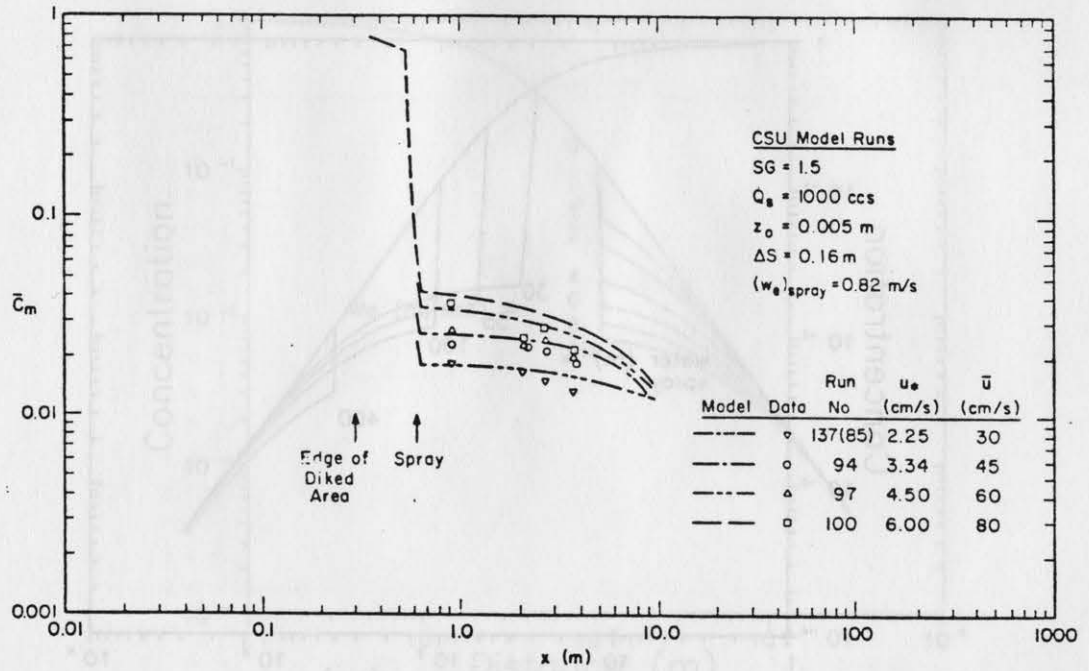

Fig. A.2-2 Comparison of Observed and SPRAY62 Predicted Plume Centerline Concentrations for Colorado State Water Spray Tests

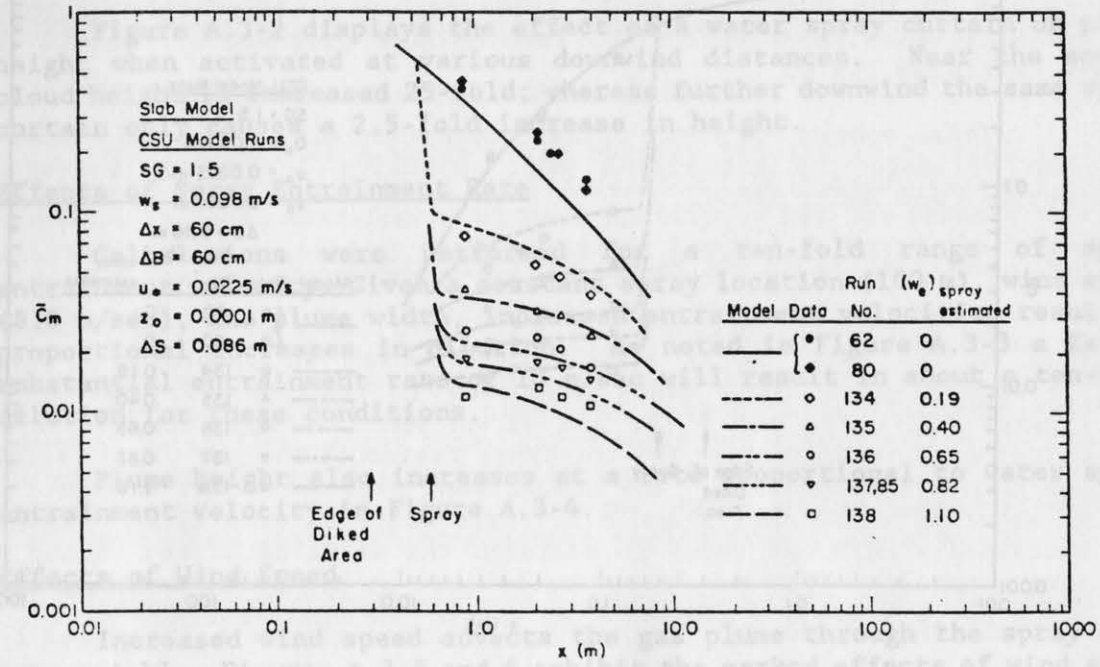

Fig. A.2-3 Comparison of Observed and SPRAY23 Predicted Plume Centerline Concentrations for Colorado State Water Spray Tests

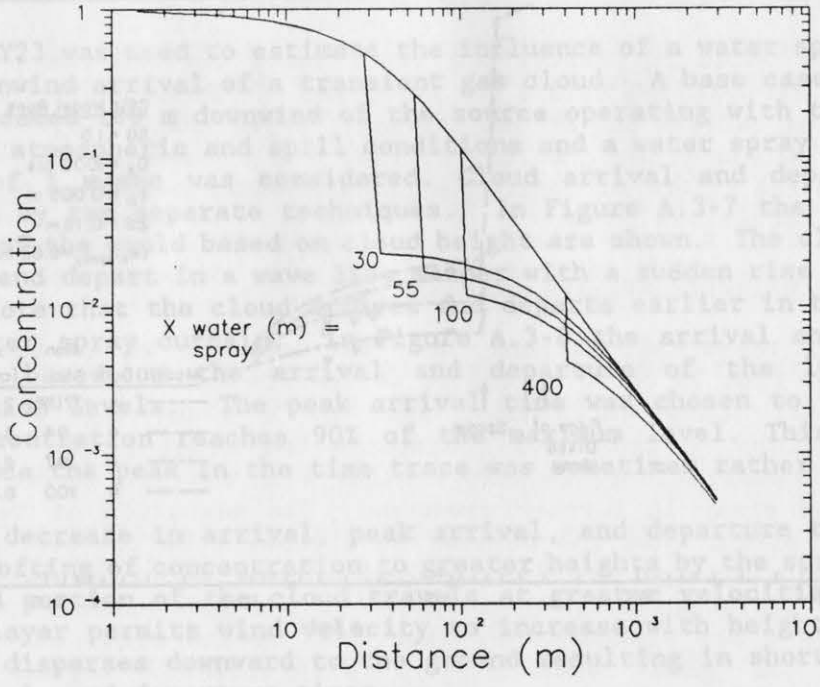

Fig. A.3-1 SPRAY62 Predicted Plume Centerline Concentrations for Goldfish Test No. 1 , Water Spray Placed at X_{spray} = 30, 55, 100, and 400 m

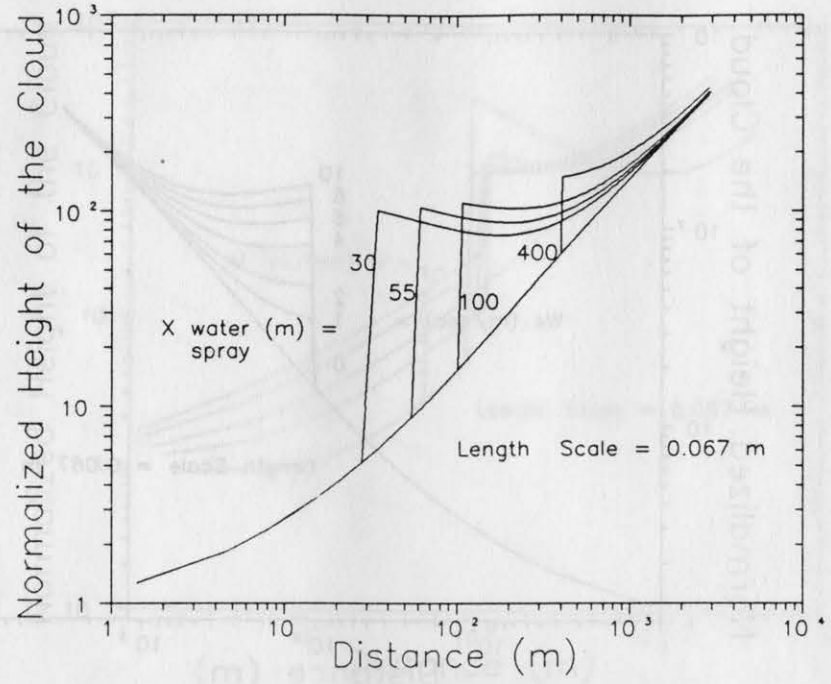

Fig. A.3-2 SPRAY 62 Predicted Plume Heights for Goldfish Test No. 1, Water Spray Placed at X_{spray} = 30, 55, 100, and 400 m

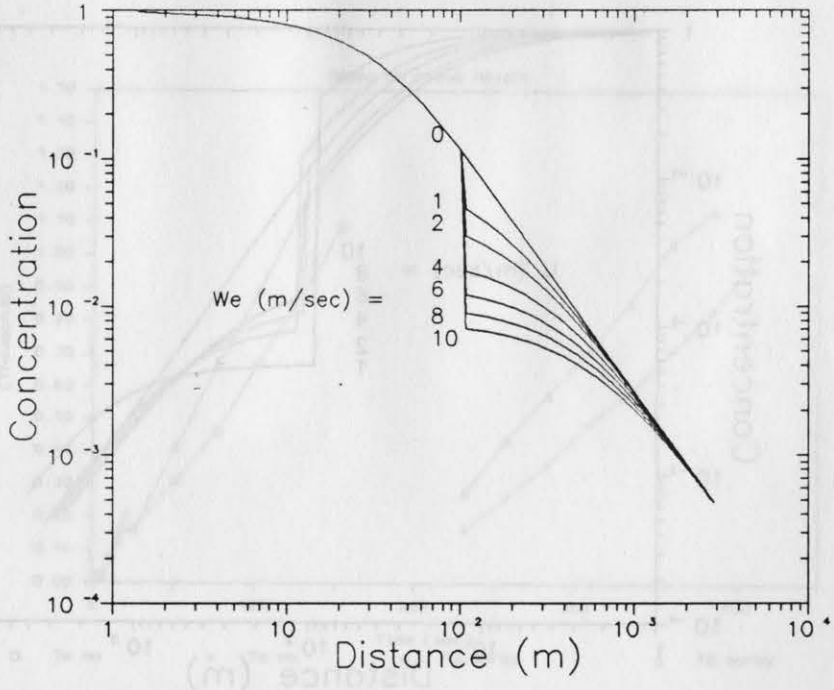

Fig. A.3-3 SPRAY62 Predicted Plume Centerline Concentrations for Goldfish Test No. 1 , X_{spray} = 100 m, w_e = 1, 2, 4, 6, 8, and 10 m/sec

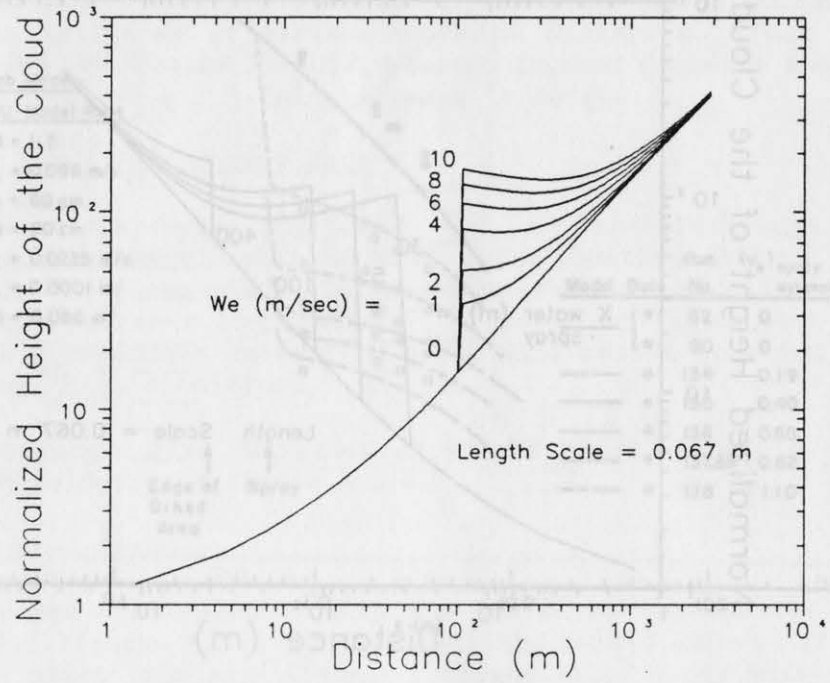

Fig. A.3-4 SPRAY62 Predicted Plume Heights for Goldfish Test No. 1, X_{spray} = 100 m, w_e = 1, 2, 4, 6, 8, and 10 m/sec

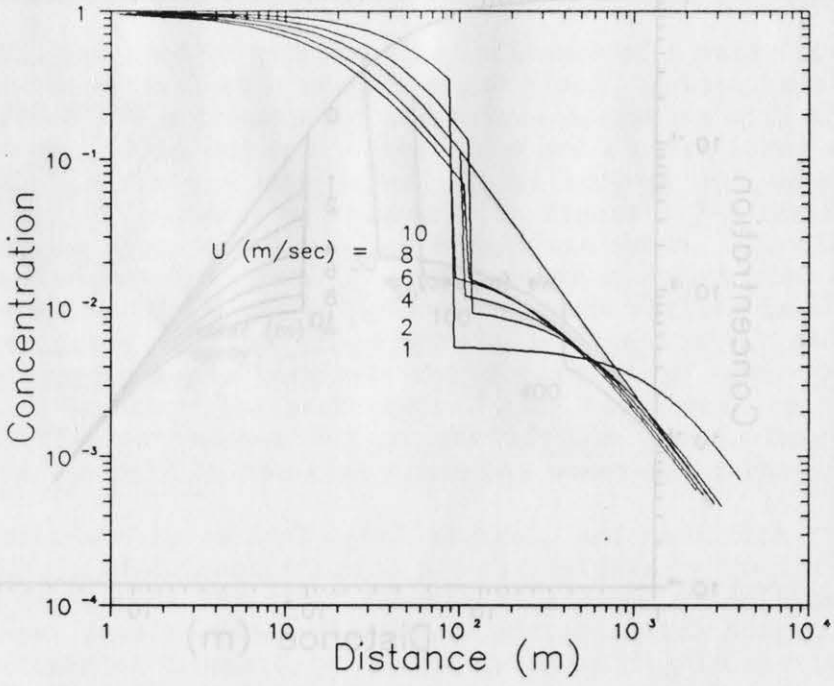

Fig. A.3-5 SPRAY62 Predicted Plume Centerline Concentrations for Goldfish Test No. 1 , X_{spray} = 100 m, w_e = 6 m/sec, U = 1, 2, 4, 6, 8, and 10 m/sec

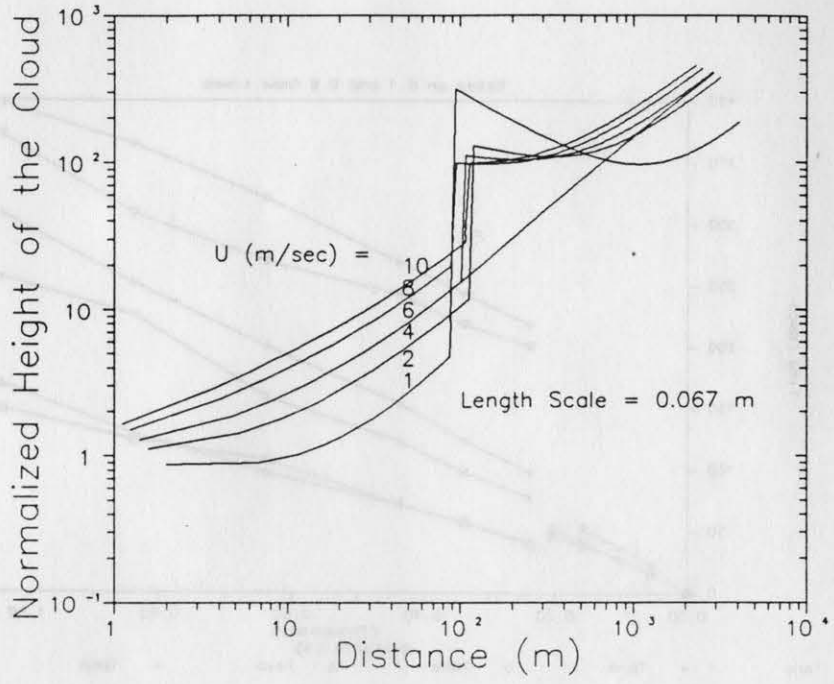

Fig. A.3-6 SPRAY62 Predicted Plume Heights for Goldfish Test No. 1 , X_{spray} = 100 m, w_e = 6 m/sec, U = 1, 2, 4, 5.6, 8, and 10 m/sec

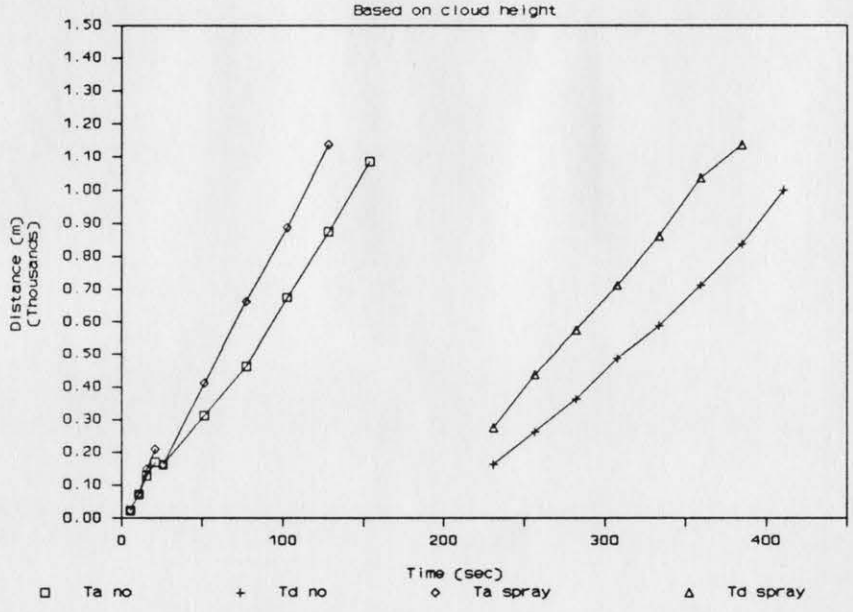

Fig. A.3-7 SPRAY23 Predicted Cloud Arrival and Cloud Departure Times for Goldfish Test No. 1, X_{spray} = 100 m (Based on predicted cloud heights)

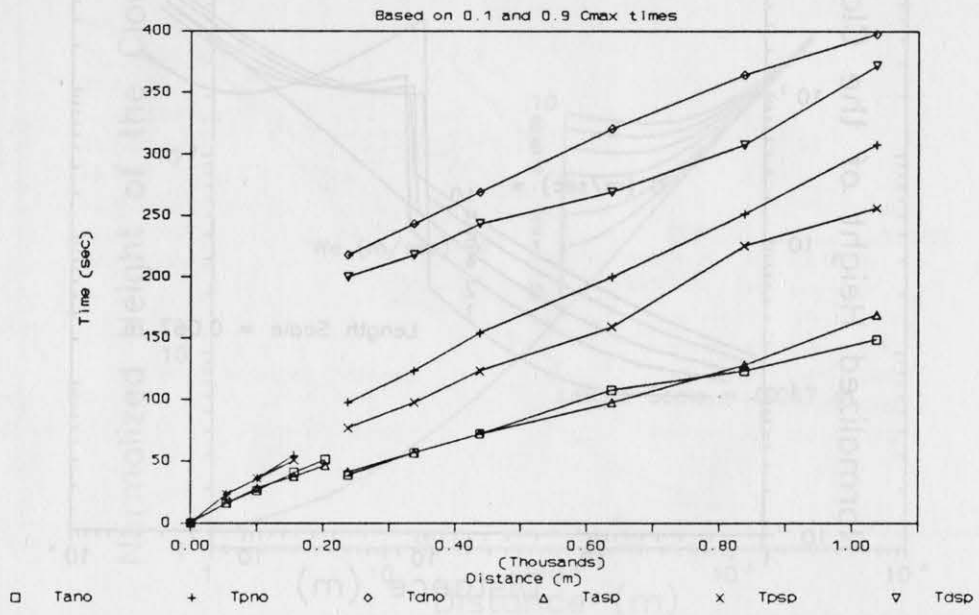

Fig. A.3-8 SPRAY23 Predicted Cloud Arrival and Cloud Departure Times for Goldfish Test No. 1, X_{spray} = 100 m (Based on predicted cloud concentrations)